AD_____

Award Number: DAMD17-00- 1-0344

TITLE: Ultrasonically-Induced Vaporization of Perfluorocarbon Droplets for Occlusion Therapy of Breast Cancer

PRINCIPAL INVESTIGATOR: Jeffrey B. Fowlkes, Ph.D.

CONTRACTING ORGANIZATION: Regents of the University of Michigan
Ann Arbor, MI 48109-1527

REPORT DATE: June 2004

TYPE OF REPORT: Final

PREPARED FOR: U.S. Army Medical Research and Materiel Command
Fort Detrick, Maryland 21702-5012

REPORT DOCUMENTATION PAGE

Form Approved
OMB No. 0704-0188

1. REPORT DATE *(DD-MM-YYYY)*	**2. REPORT TYPE**	**3. DATES COVERED** *(From - To)*
01-06-2004	Final	1 Jun 2000 - 31 May 2004

4. TITLE AND SUBTITLE
Ultrasonically-Induced Vaporization of Perfluorocarbon Droplets for Occlusion Therapy of Breast Cancer

5a. CONTRACT NUMBER

5b. GRANT NUMBER
DAMD17-00- 1-0344

5c. PROGRAM ELEMENT NUMBER

6. AUTHOR(S)
Jeffrey B. Fowlkes, Ph.D.

E-Mail: fowlkes@umich.edu

5d. PROJECT NUMBER

5e. TASK NUMBER

5f. WORK UNIT NUMBER

7. PERFORMING ORGANIZATION NAME(S) AND ADDRESS(ES)
Regents of the University of Michigan
Ann Arbor, MI 48109-1527

8. PERFORMING ORGANIZATION REPORT NUMBER

9. SPONSORING / MONITORING AGENCY NAME(S) AND ADDRESS(ES)
U.S. Army Medical Research and Materiel Command
Fort Detrick, Maryland 21702-5012

10. SPONSOR/MONITOR'S ACRONYM(S)

11. SPONSOR/MONITOR'S REPORT NUMBER(S)

12. DISTRIBUTION / AVAILABILITY STATEMENT
Approved for Public Release; Distribution Unlimited

13. SUPPLEMENTARY NOTES
Original contains color plates: ALL DTIC reproductions will be in black and white

14. ABSTRACT
A technique termed Acoustic Droplet Vaporization (ADV) has been developed in which ultrasound triggers small liquid droplets to form gas bubbles in arterial blood. The droplets are injected intravenously thus eliminating catheterization. Droplets vaporize into bubbles at the desired location in the body by applying ultrasound through the skin. Using renal occlusion as a model, blood flow following ADV in the renal artery was reduced by greater than 90% in the renal cortex and more than 60% in the medullary tissues. An average organ perfusion reduction of >70% was achieved using ADV. The studies performed represented the most extensive investigation of flow occlusion by ADV to date. The control kidney on the contralateral side showed a maximum decrease in regional blood flow of 18% relative to the pre- ADV baseline. Image-based hyper-echogenicity from ADV of IA injections was monitored for pproximately 90 minutes, and cortex perfusion was reduced by >60% of its original value for more than 1 hour. This could be enough time for the onset of cell death and possible tumor treatment via ischemic necrosis. Moreover, currently used radiofrequency tissue ablation-based tumor treatment could benefit from ADV due to the decreased heat loss via vascular cooling.

15. SUBJECT TERMS
Blood Flow Control, Occlusion, Hypoxia, Ultrasound Therapy, Non- Lead Optimization, ionizing Radiation, Localized Therapy, Minimally Invasive Therapy

16. SECURITY CLASSIFICATION OF:			**17. LIMITATION OF ABSTRACT**	**18. NUMBER OF PAGES**	**19a. NAME OF RESPONSIBLE PERSON**
a. REPORT	**b. ABSTRACT**	**c. THIS PAGE**			USAMRMC
U	U	U	UU	89	**19b. TELEPHONE NUMBER** *(include area code)*

Table of contents

Introduction

Occlusive therapy has been used in a number of applications involving the direct injection of material into arteries which either blocks blood flow at the injection site or immediately downstream. This has typically involved obtaining direct access to an artery such as using a catheter, which limits its application in breast cancer therapy. A unique process (**A**coustic **D**roplet **V**aporization), where ultrasound remotely triggers the vaporization of liquid droplets, has been developed during the course of this project. The droplets can be manufactured using albumin (from a variety of species) or lipids to form the stabilizing shell for the droplets. These droplets have been used in a series of experiments to evaluated the effects on blood flow. Results indicate that substantial reduction in blood flow can be achieved and some level of reduction persists for periods up to 90 minutes. A summary of the results from experiments is presented below following the developing the droplets through to their demonstration in an animal model. Details of many of these experiments are in the publications included in the appendix.

Scientific Summary

Methods Development for ADV

In order to understand the factors affecting the vaporization of droplets (Objective 2 of the original proposal), several parameter dependences of Acoustic Droplet Vaporization (ADV) have been studied. Some of these were intended to yield insight into the physical mechanism for ADV and to provide information on effective means of ADV for the future in vivo tests. Details of these experiments can be found in the thesis of Oliver Kripfgans, PhD completed in June 2002 and in the references in the appendix.

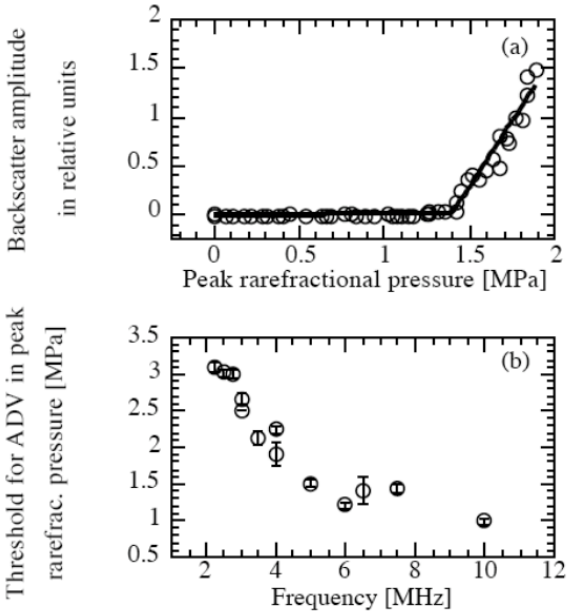

Figure 1 – (a) At 7.5 MHz the threshold for acoustic vaporization of droplets is approximately 1.5 MPa PRP. At lower pressures droplets rarely, if ever, boil into gas bubbles. Therefore ultrasonic images of the area to be treated can be taken at pressures below 1.5 MPa PRP. The threshold for ADV is a function of frequency; it rises with decreasing frequency (b). From Kripfgans et al.

Frequency Dependence of ADV

The center frequency (f) used for *in vivo* procedures is an important factor since the acoustic attenuation in most soft tissues is 0.5-0.7 dB/cm-MHz. These results are reported in detail in our

publication Kripfgans et al, 2002 included in the appendices. The trend for the threshold as a function of the driving frequency can be seen in Figure 1. As the center frequency of the transmitted tone burst increases from 2 to 10 MHz, the pressure necessary to phase transition droplets into gas bubbles decreases from 3 to 1 MPa peak negative pressure. This suggests a tradeoff for the use of frequencies and depth of the tissue to be treated. These results would suggest that there is additional impetus to apply the ADV methods at shallower depths within tissue. For future application in breast this may be an advantage given the relatively small distance required to reach points within the breast. However, breast tissue is highly heterogenous which can cause substantial aberration in acoustic beam formation.

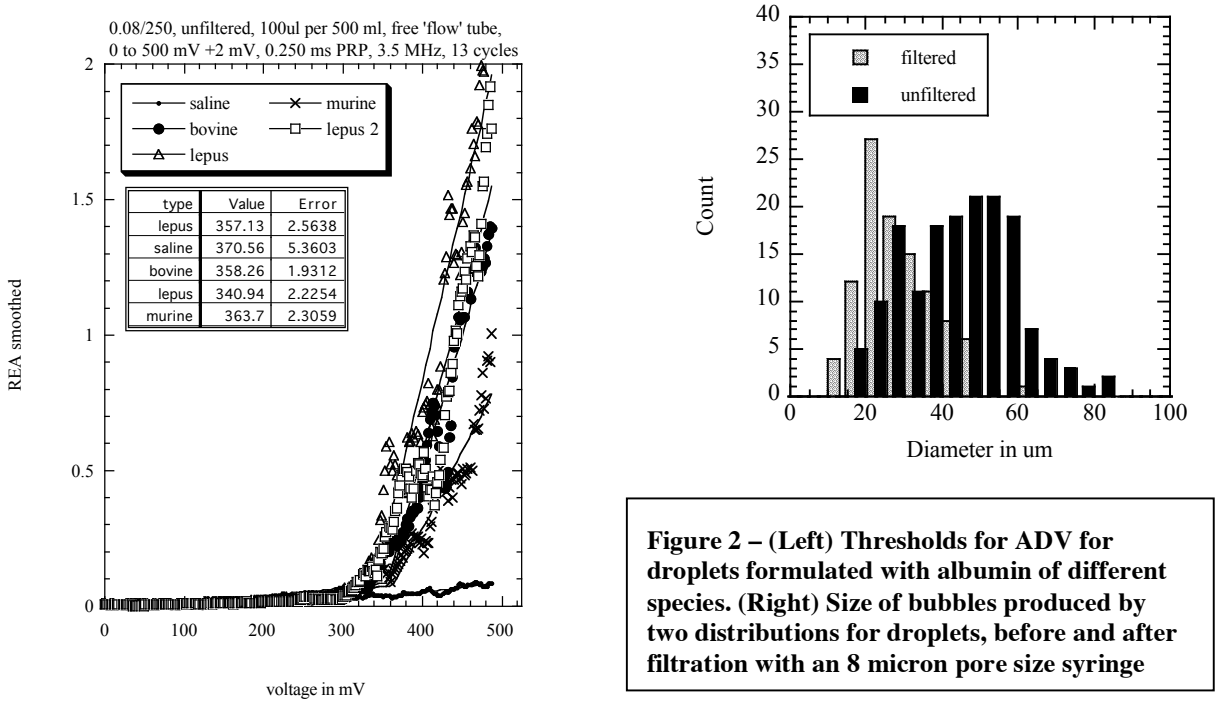

Figure 2 – (Left) Thresholds for ADV for droplets formulated with albumin of different species. (Right) Size of bubbles produced by two distributions for droplets, before and after filtration with an 8 micron pore size syringe

Albumin dependence of ADV

We determined that the formulation of droplets for ADV using the albumin of different species was possible. Dodecafluropentane (DDFP) emulsions could be made with lepus and murine albumin in addition to bovine and the acoustic pressure threshold for ADV of the three albumins is comparable (see Figure 2 Left). A reduction in yield by a factor of two for murine albumin compared to lepus looks like a drawback, but does not have to be for *in vivo* work, when accounting for the size of the treated animal. Also the droplets can be concentrated simply by gravity or centrifugation. In addition to albumin of differing species, a sham experiment using saline only has been performed and is also shown in figure 2. The slight positive slope in the data points is assumed to be an under compensation of the scattered ADV sound field into the receive beam of the imaging array. Finally we have also made droplets with lipid shells, which would allow for targeting of droplets based on binding receptors in the vasculature. Lipid shells provide the potential for targeting receptors within the vasculature. This concept would be pursued under separate sponsorship.

Size of ADV generated gas bubbles

A major factor in the design of droplets for ADV therapy is the size of the generated gas bubbles. On one hand, bubbles have to be sufficiently large to effectively block blood flow. Contrarily, large bubbles can produce undesired bioeffects since a single bubble could potentially cause damage when blocking large vessels, i.e. blood supply for a wider region. An *in vitro* experiment was performed where the size of the generated gas bubbles was recorded using a standard video system attached to a microscope and a strobe light to increase the effective video bandwidth. The size distribution histogram for the recorded gas bubbles is shown on the right graph in Figure 2. One can see that filtered and unfiltered droplets result in gas bubbles in the range from 10 to 50 um and 20 to 85 um, respectively. Details related to these measurements appear in Kripfgans et al, 2002.

Concentration-of-emulsion dependence of ADV

ADV of droplet emulsions at various emulsion concentrations was measured to identify a possible shift in pressure threshold for ADV. This is of interest for *in vivo* ADV when local concentration changes can be anticipated. A 10 MHz, 33 cycle tone burst was sent with a pulse repetition period of 1 ms. It can be seen from figure 3 that the highest concentration yields ~4x greater ultrasound amplitude due to bubble scattering than the lowest. Looking at Figure 4, the

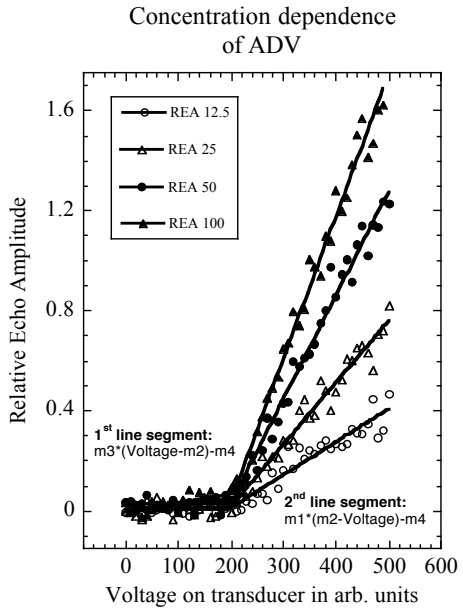

Figure 3 – Effect of droplet concentration on ultrasound echo amplitude from bubbles produced by ADV.

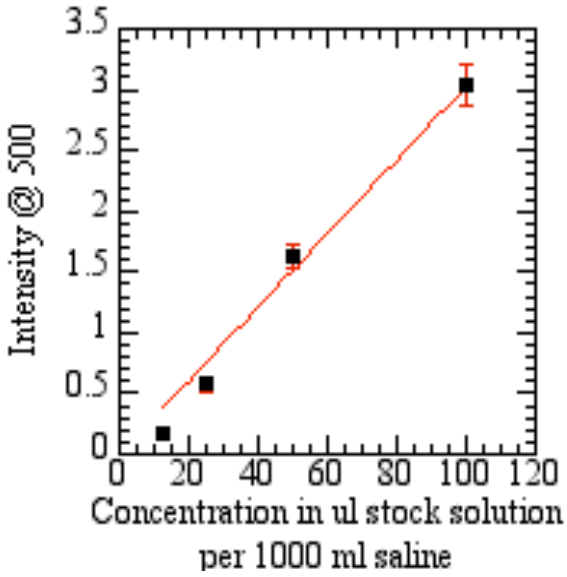

Figure 4 – Acoustic intensity from bubble scattering for ADV at 500 mV setting shown in Figure 4.

ultrasound intensity should scale linearly with droplet concentration if bubble production is in proportion to the number of droplets. The fit is indeed linear (R=0.991) although slightly low for the lower concentrations.

Pulse repetition frequency dependence of ADV

Another parameter, which could directly control ADV is the selected pulse repetition frequency (PRF). The PRF is the rate at which pulse are applied to the droplets during ADV. Several results related to this topic were provided in the 2001 Progress Report. These can be summarized as follows.

1. ADV echogenicity increases with increasing PRF. This effect eventually limits out with the conversion of all possible droplets in the ultrasound beam. Thus relatively high PRFs sufficient to expose droplets to multiple pulses would be required for complete conversion. This would affect the PRF needed *in vivo* to match blood flow rates and beam shape.
2. Besides the amplitude change, a change in threshold for ADV is observed as the PRF changes. The shift in threshold is very marginal but statistical and consistent. The threshold for ADV as a function of the pulse repetition period (inverse of the PRF) reaches a maximum and flattens at ~10 ms since this time is equivalent to the transit time of the fluid flow through the focus of the ADV transducer. Again this would be a possible effect *in vivo*.

Direct Observations of ADV

Using a high-speed camera system, the responses of individual droplets were observed at different acoustic pressures. An Imacon 468 high-speed video system (DRS Technologies, DRS Hadland, Inc. Cupertino, CA, USA) was used to optically image the process of ADV. Full-frame pictures of 576 by 385 pixels were taken with frame rates of 5-10 MHz. In streak mode the vertical central line of an image was captured at 57.6 MHz (17.4 ns per streak line). Since the ADV occurs at a micron scale, an optical microscope (JenaVAL, Carl Zeiss Jena GmbH, Jena, Germany) was connected to the video system (Figure 5A). In this way micrometer sized droplets were monitored at the full frame rate of 10 MHz with 0.46 um resolution. The light of a 2.5 kW Argon flash lamp was guided into the optical path as a source for the 100x objective of the microscope (see Fig. 5B). Details of this research are provided in Kripfgans et al, 2004.

For each picture taken an individual droplet was positioned on the central line of the screen of the video system. The first image was taken before the sound wave reached the tube. Subsequent frames were either placed back-to-back in order to monitor the process of ADV in finer detail or were separated by several hundred nanoseconds to monitor the droplet during the insonification, before ADV started. Each droplet was exposed to a series of acoustic tone bursts of increasing acoustic power until the droplet vaporized. For each power level a set of seven full frames and one streak image were acquired and saved.

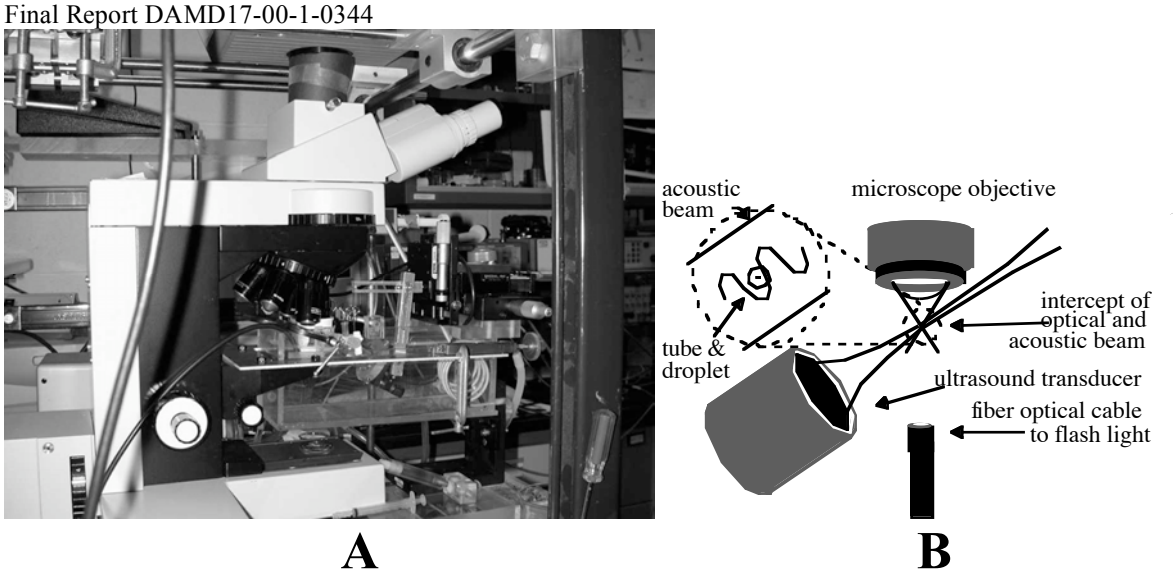

Figure 5 – (A) Photograph of the experimental arrangement. A water tank is mounted under a microscope to image single droplets as they are being vaporized using a single ultrasound tone burst. To capture sub microsecond video frames, a high speed video system is attached to the microscope (not shown here). (B) Diagram of arrangement. The 3.5 MHz transducer has an aperture of 25.4 mm and a lateral focal beam diameter of 0.96 mm. The polyethylene flow tube has a 200 um inner diameter and 50 um wall thickness. For comparison, a 3.5 MHz two cycle tone burst is shown in the inset. (Not to scale)

In Figure 6, the droplet being investigated is seen as the circular object in the center of each of the first seven images in the two sequences (A and B). The eighth frame in each of the two sequences of Fig. 6 contains the streak image. This image allows monitor of the droplet motion. In the first case (Fig. 6A), the acoustic pressure is insufficient to cause vaporization. The droplet remains approximately the same size during the ultrasound exposure with only a slight variation in its position as will be discussed below. However, increasing the output to 6.5 MPa peak-to-peak resulted in the rapid formation of a bubble (Fig. 6B). By the second frame in the sequence, there is a substantial increase in size of the object. The initiation of the vaporization event is not immediate at this pressure as can be seen in the streak image but rather the droplet oscillates for several acoustic cycles (in this case approximately 8 cycles) before the vaporization begins.

In order to quantify the motion of the droplets, the streak images were analyzed by tracing position of the apparent boundaries of the droplets. This would correspond to the position of the droplet and its thickness assuming the streak line is through the center of the droplet. The term thickness is used here as opposed to diameter since nonspherical modes are the likely result of the virtually incompressible nature of the liquid. Figure 7 is one of these images showing that the droplet moves with predominantly a dipole-like oscillation (translating back and forth) as it is exposed to the ultrasound pulse. There are asymmetric oscillations near the beginning and end of the droplet motion and one can see the onset of oscillation at the bottom trace, before onset occurs in the top trace. However, once the transient response of the droplet dissipates, the two traces move substantially up and down in phase suggesting translatory oscillation is the predominant motion of the droplet in the presence of the ultrasound field.

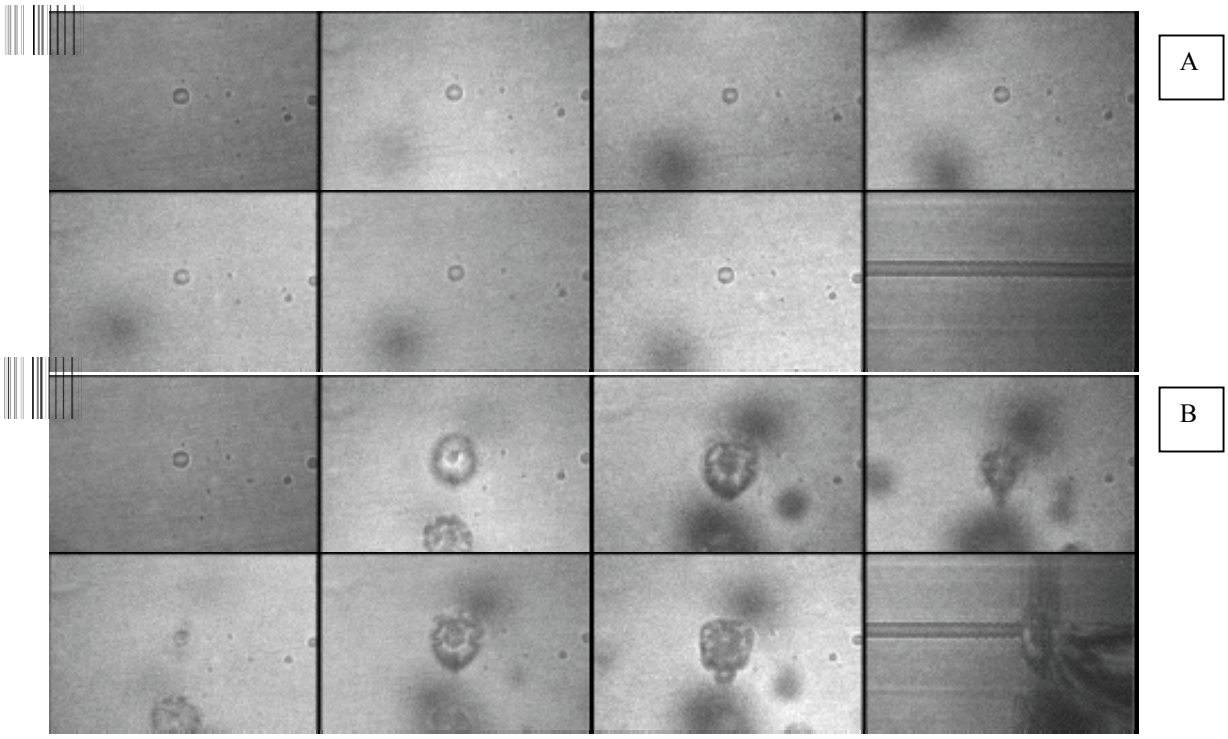

Figure 6 Acoustic vaporization of an 18 um diameter droplet. Two sequences are shown. (A) Images 1 to 7 are full frame pictures of the droplet in the flow tube. The 8th frame is a streak image. The acoustic pressure in the first sequence is not sufficient to vaporize the droplet. In the center of the streak image, one can see a translatory motion of the droplet for the duration of the 10 cycle, 3 MHz tone burst. (B) Increasing the acoustic pressure to 6.5 MPa peak-peak (which is P-=2.6 MPa) leads to the vaporization of the droplet after 8 cycles. From Kripfgans et al., 2004.

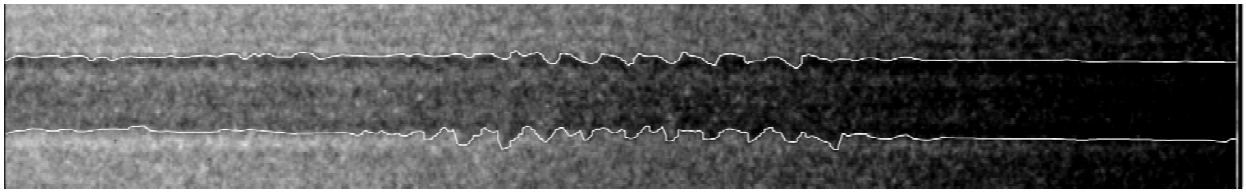

Figure 7 – Expanded view of the eighth frame in Fig. 6A. Hand-traced streak line of a 16 um diameter droplet. One can see the onset of oscillation at the bottom trace, before onset occurs in the top trace. From Kripfgans et al., 2004.

The displacement of the droplet (overall dipole motion) and thickness (normalized to the initial droplet diameter) were determined and spectral analysis showed that the amplitude of the displacement oscillation was 40 dB above the noise for this system and 13 dB above the image resolution. In general, it has been observed that the thickness oscillation also shows a spectral response at the frequency of the ultrasound field.

Droplets of various diameters were analyzed for the magnitude of dipole oscillation at the threshold

of vaporization (Figure 8A). The peak-to-peak amplitude was found to be 2.7±0.4 um and 2.5±0.4 um at 3 and 4 MHz, respectively. These displacements were not adjusted for any possible out of plane oscillation of the droplets due to the 45-degree angle between ultrasound transducer and microscope objective. This would indicate that the requisite displacement for vaporization is relatively independent of droplet size. In Figure 8B, the average displacement amplitude at a given frequency was used to compute the average velocity (circles) at which the droplet was assumed to be moving relative to the host fluid. Due to the image quantization of 0.46 um per pixel plus image noise an error of approximately 20% must be expected. Additionally the corresponding Reynolds number was computed (squares). At these flow velocities one can anticipate flow separations that could result in perturbations to the superheated droplets, resulting in their vaporization. This could be the mechanism for ADV and its quantification should lead to a better understanding of the droplet vaporization and its control *in vivo*. The pressure threshold for ADV was also evaluated as a function of droplet diameter (Fig. 8C). In general smaller droplets required higher pressures for vaporization. This is consistent with earlier measurements in which the size distribution was controlled by filtering the droplets (Kripfgans et al., 2002). One also notes that the pressure threshold for ADV is lower for 3 MHz than for 4MHz. In our previous studies (Kripfgans et al., 2002) where measurements were made in a free field, we have shown that there is an inverse frequency dependence in the pressure threshold for ADV as seen in Fig. 8D. Therefore, Fig. 8C would appear to contradict the previous frequency dependence measurements. However, modeling of the ultrasonic field in the case of the high speed camera experiments showed that the presence of the optical objective resulted in an interference pattern at the location of the droplet that actually cause the pressure to be less than expected at 4 MHz compared to that at 3 MHz. In other words, this was not a free field condition. Therefore, the apparently higher amplitude for ADV at 4 MHz is an artifact of this interference effect.

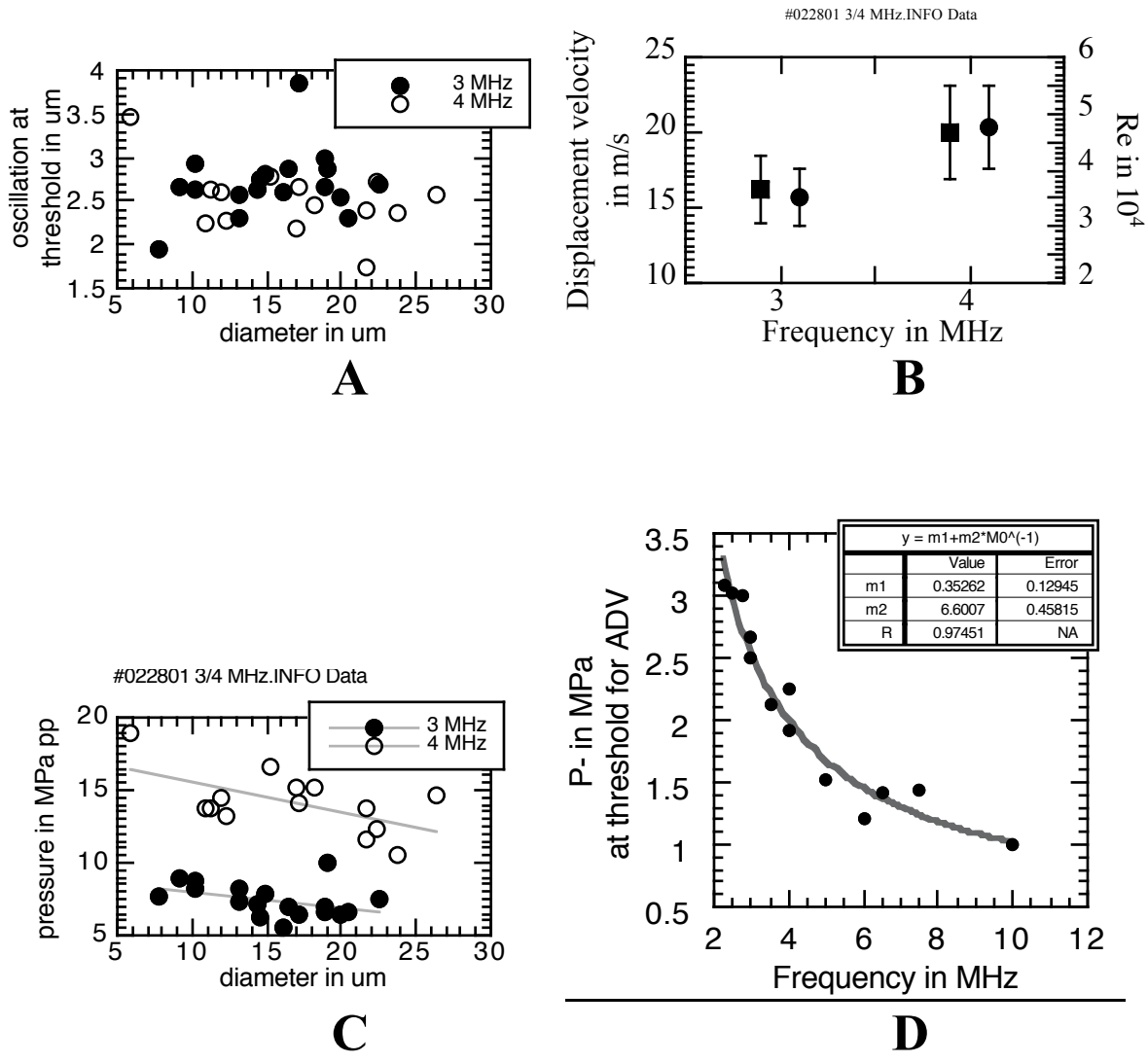

Figure 8 - Evaluation of requisite droplet oscillation for droplet vaporization for various droplet sizes (A) and requisite velocity and corresponding Reynolds number at the vaporization threshold for the two ultrasonic frequencies used (B). The error bars are based on the single standard deviation of the displacement amplitude. (C) Threshold for ADV as a function of droplet size for acoustic frequencies of 3 and 4 MHz. (D) Results of frequency dependent measures under free field conditions show an inverse frequency indicating the effects of the presence of the microscope objective in the optical observation experiments.

Another observation from the high speed optical experiments was that the evolution of the vaporization inside the droplet. The onset of vaporization was monitored as either spot-like, and subsequently expanding centers of nucleation inside the droplet, or as homogeneous throughout the droplet's imaged cross-section. The latter kind is possibly due to the limited temporal resolution of the full frame 2D images of the imaging system. Spot-like centers of nucleation (see Fig. 9) were observed solely along the axis parallel to the direction of oscillation and centered on the droplet along the direction of dipole-type motion of the droplet. This axis is essentially the same as the

direction of the propagating acoustic wave. Typically a second nucleation site was observed. Its location was diametrically opposed to the first site, which conforms to the change in direction of motion, i.e. with the oscillatory movement of the droplet as seen in the streak image in Fig. 7. The streak image of Fig. 9 shows that the gas nuclei complete the phase transition within the droplet on a time scale of 3 us. Complete vaporization was observed to occur in the range of several hundred nanoseconds to this longer 3 us example shown here for clarity. The bubble would then continue to grow since the gas from the surrounding medium would dissolve into the bubble before the perfluorocarbon gas could diffuse out.

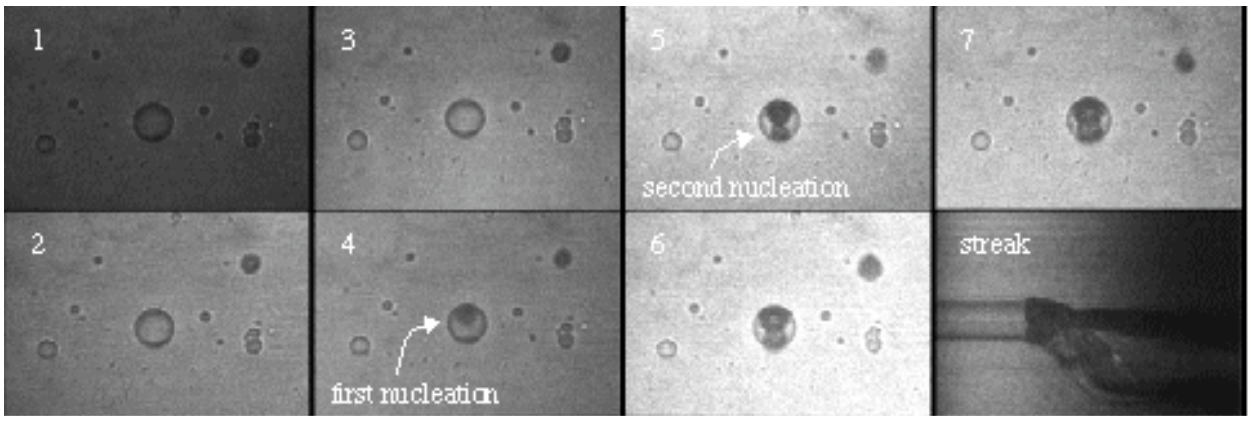

Figure 9 – Sequence of high-speed micrographs show the vaporization process in detail. The first nucleation point of the droplet's vaporization, and frame 5 shows another nucleation site. The frames were placed back to back with 100 ns duration. For this vaporization a 10 MHz and 30 cycles tone burst at 9 MPa.

To summarize these experiments, we now have a much better understanding of the vaporization process involved in converting the superheated perfluorocarbon droplets to gas bubbles. While using very different experimental observation methods, the results were consistent with only notable exceptions explained by modeling the non-free field exposure conditions caused by the presence of the optical microscopy system. These experimental results, along with those previously reported, complete Objectives 1 and 2 of the proposed work.

In Vivo Experiments

B-mode Embolo therapy

The acoustic vaporization of intra-arterial injected droplet emulsion was first successfully demonstrated using the Toshiba scanner in B-mode and reported in Kripfgans et al. 2000 and 2002. Droplets were injected intra-arterial and subsequent insonification of a region in the white and gray matter yielded a dense and spatially stationary gas bubble formation in the VOI (Figure 10). It should be noted that a small, relatively uniform increase in echogenicity of the monitored region was observed while injecting the droplet emulsion, which is assumed to be the non-zero backscatter of the emulsion. The figure shows ADV in occipital region (at the back of the brain, posterior to parietal lobe). The droplets were vaporized using B-mode at 6 MHz. (a) The region before ADV, (b) some time after ADV. A 0.3 ml droplet solution was injected over 2 minutes.

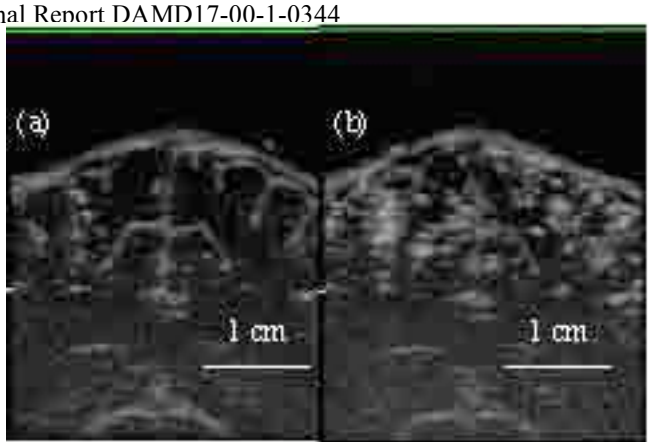

Figure 10 - *In vivo* observation of ADV in canine brain. (a) normal ultrasound appearance in brain following craneotomy. (b) bright echoes appearing after higher amplitude ultrasound applied. From Kripfgans et al. 2002.

In addition, we demonstrated that M-mode could be used to control the location of ADV that might enable selective localization of ADV. M-mode was used to limit ADV to one line in the scan plane or to a region that was scanned by sweeping the M-mode line across that region This is also reported in detail in the 2001Progress Report and published in Kripfgans et al, 2002.

Acoustic imaging at low MI apparently did not evaporate injected droplets since even the intra-arterial injection of a ten-fold increase in concentration showed very little gas bubble formation in the presence of B-mode imaging at an MI of 0.2. This is consistent with the *in vitro* results where a pressure threshold for ADV was observed.

Difference between I.V. and I.A.

Intra-arterial as well as intra-venous injections successfully deposited droplets in the circulatory system. However, the yield from I.A. injections is qualitatively much greater than the yield from I.V. injections. This is the case even for a ten-fold increase in the administered dose in order to compensate for the upper 10% in the droplet's size distribution, which is greater than 6 mm in diameter and therefore likely to be filtered by the lung. Intra-venous remains a challenge and limited our ability to ultimately demonstrate the capability of ADV in a cancer model.

Apparatus for *In Vivo* Lepus Experimentation

In efforts to translate the results obtained previously into a more appropriate *in vivo* model, an experimental system for application of ultrasound in rabbits has been developed. This system is similar to that used in the ADV studies in canine brain above with a water tank is placed over the abdomen (hair removed by shaving and depilation) of the rabbit. The tank had a thin plastic lining that is coupled to the abdomen using ultrasonic coupling gel. The ADV process was guided and monitored by ultrasonic imaging where the intensity of the ultrasound is below that necessary for ADV. The imaging allows selection of the target tissue, which is then exposed to a higher intensity ultrasound field supplied by a second transducer for inducing ADV. This transducer is one of those used in the previous experiments in which droplets are vaporized in tubing or free field. The image plane of the ultrasound array is along the direction of propagation of the ADV transducer and centered on the focal zone to allow monitoring of the bubble production.

Using the same injection procedure as above, initial demonstration experiments were performed in rabbit spleen. In Figure 11, the spleen is shown at two time points during the vaporization of the IV injected droplets. The vertical white steaks in the image are the result of acoustic and/or electrical interference from the ADV transducer. The targeted regions are outlined with a box and the increased echogenicity indicates the presence of bubbles produced by ADV. Between images A and B, the ADV transducer has moved further to the left and thus an enlarged region of increased echogenicity is seen in B. Seen in real-time, the motion of the ADV transducer produces a "painting" effect in which the echogenicity of the tissue suddenly changes as the focus of the ADV transducer passes through the tissue. Such effects are seen with transcutaneous application of ultrasound, which indicates that our efforts to identify ultrasound fields with the potential to perform the ADV therapy have met with success in accomplishing **Objective 3**. It remained to be seen if sufficient bubble production is possible to produce a reduction in blood flow.

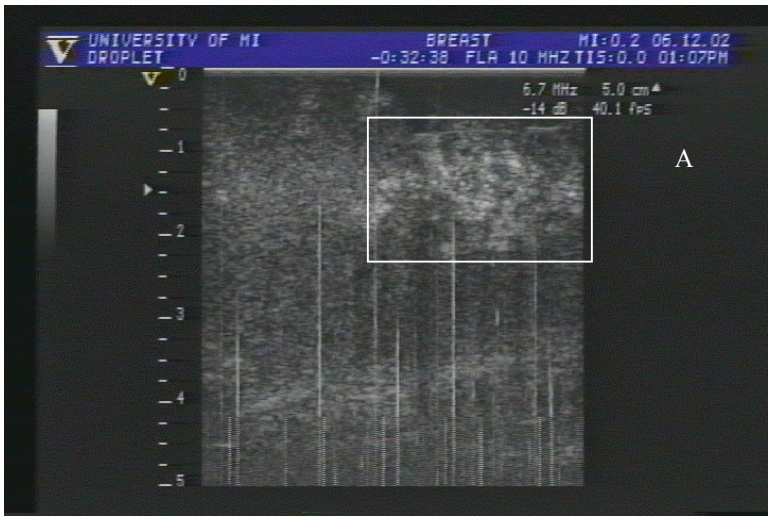

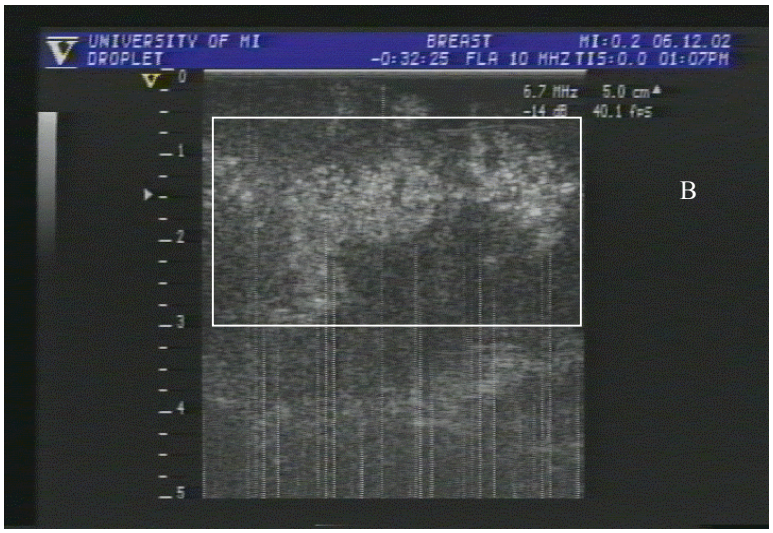

Figure 11 – Images of the rabbit spleen during ultrasound exposure following IV injection of perfluorocarbon droplets. The white box encloses a region of increase echogenicity that appears initially (A) at the location of ultrasound exposure and then expands (B) as the ultrasound beam sweeps to the left.

Effects on Kidney Perfusion

In the experiments investigating Objective 4 are detailed in our publication Kripfgans et al., 2005, rabbits were coupled to the exposure apparatus described section above. This apparatus was applied to externalized kidneys in order to more accurately quantify the ultrasound exposure required for ADV. Ultrasound images of the kidney before and after the ADV treatment appear in Figure 12. The first image is that of the kidney before droplet injection. Note that in this image there is no tissue overlying the kidney since the kidney has been externalized. In the second image, there is a considerable increase in echogenicity indicating the vaporization of droplets into bubbles. However, the level of bubble production is insufficient produce substantial shadowing in the kidney.

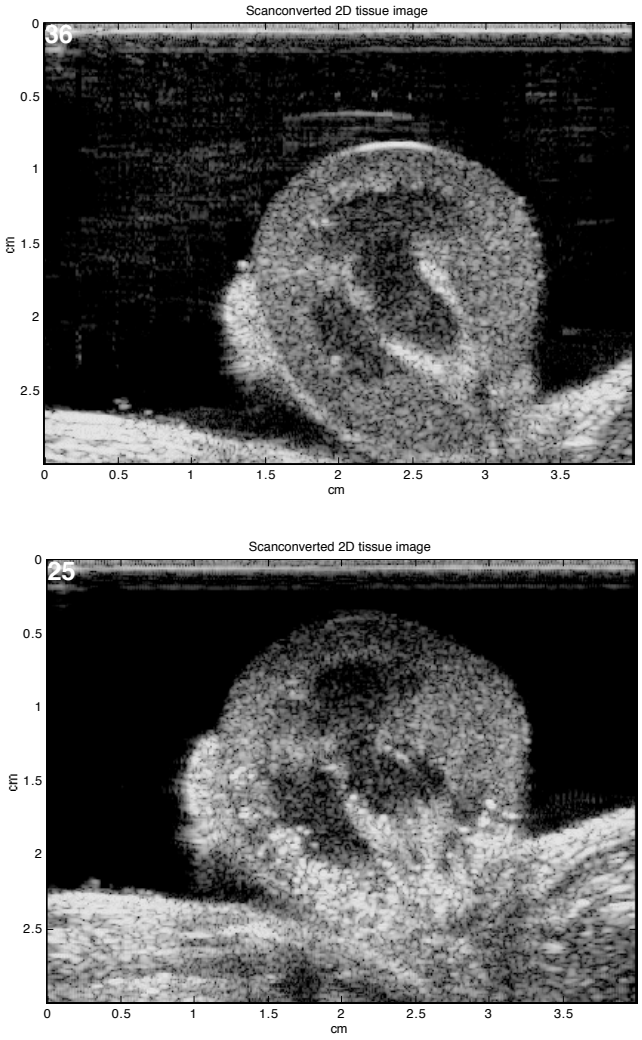

Figure 12 – Images of the externalized rabbit kidney A) before treatment by ADV and B) after. Note the increased echogenicity in lower portion of the kidney.

A series of fluorescence microsphere injections measured tissue perfusion. At specified time point in the ultrasound procedures (before and after occlusion treatment), microspheres of a single color, 15 μm in diameter, suspended in isotonic saline containing 10% Dextran and 0.5% polysorbate (Tween 80) was infused over 10-12 seconds into the left ventricle via a catheter passed through the femoral artery. Reference blood was withdrawn from the left femoral artery at a constant rate (2 ml/min.) beginning 5-10 seconds before the injection of microspheres. The withdrawal of reference blood continued for 1.5 min. After the animal was euthanized, the kidney was sampled for tissue (~1ml volume samples from cortical and medullar portions of the organ) and these, along with the reference blood samples, were sent to a lab for counting to determine the local tissue perfusion.

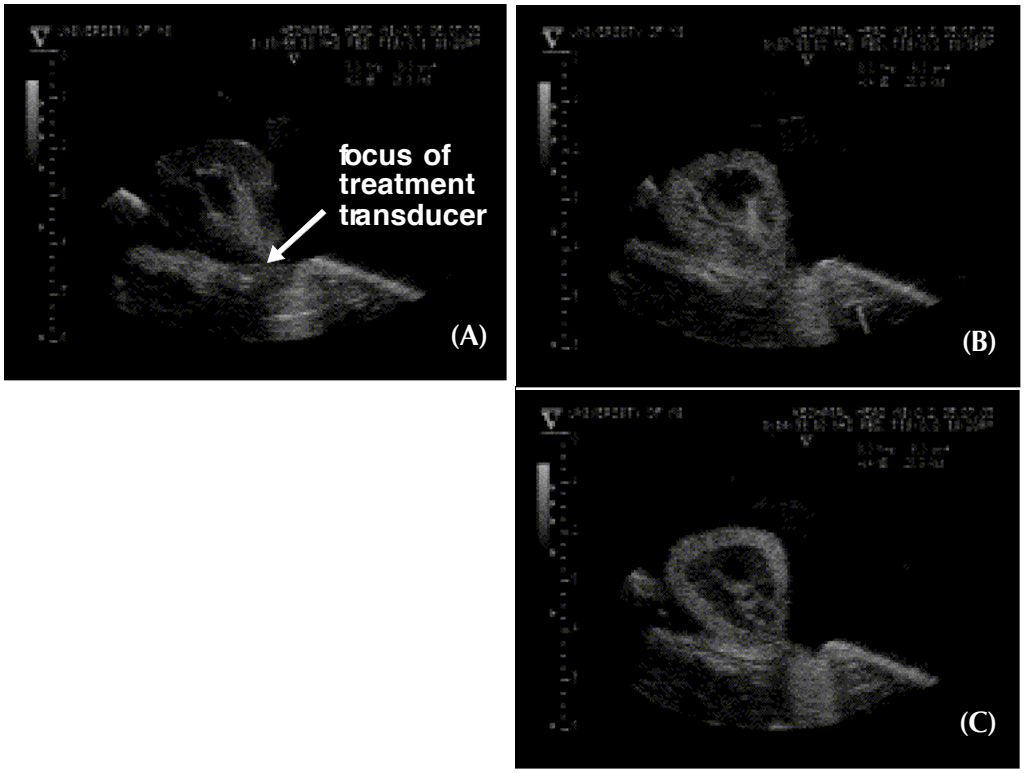

Figure 13 - B-mode image of kidney cross-section before (A), during (B), and after (C) ADV. In (B) one can see how the gas bubbles move downstream via the arterial system and lodge in the cortex (C).

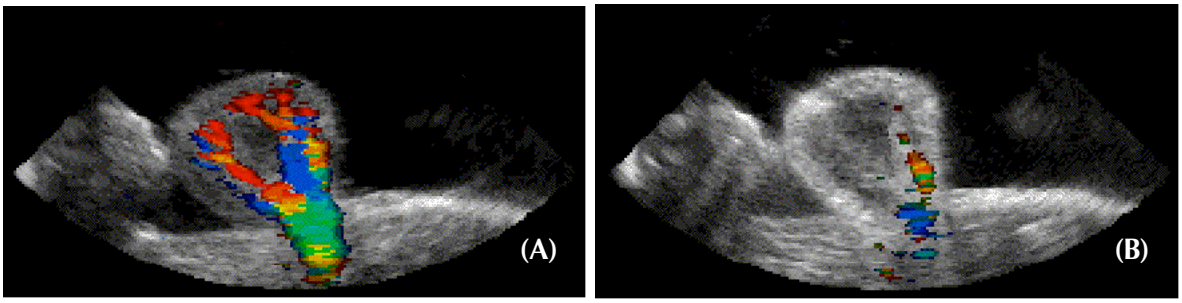

Figure 14 - Color flow mode of the kidney before and after ADV. One can see the renal artery as it enters the organ and branches through the medullary tissue to the capillaries of the cortex.

Following this initial experience with the method, a series of fourteen New Zealand white female rabbits were use to determine the level of occlusion possible. Figure 13 shows feedback of ADV as recorded by the imaging array. Figure 13A is a baseline image before the onset of ADV. The ADV transducer is on, but no emulsion is being injected. Radial streak lines visible on the top are due to interference with the acoustic field from the ADV transducer. The white arrow is pointing to the

renal artery. In Figure 13B, one can see a "horizontal" vascular branch on the lower half of the interior of the kidney as well as a "vertical" vessel on the right side. These vessels are filled with hyperechoic gas bubbles. In Figure 13C the vascular bed (the cortex) is filled with gas bubbles. Other feedback has been acquired by means of color flow mode (CFM) and Spectral Doppler (PW).

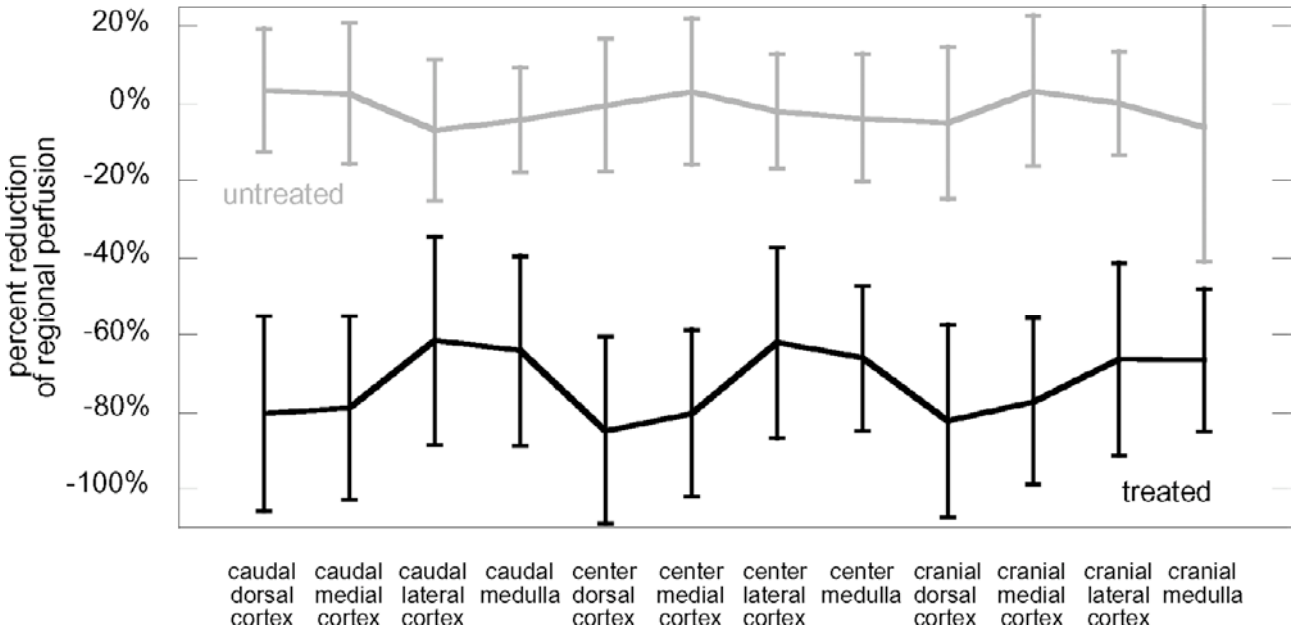

Figure 15 - Change in regional blood flow (RBF) after occlusion via ADV. Shown are results for treated and untreated kidney after ADV. The two curves show percent change in perfusion by tissue type/location. The top, gray graph is measured in the untreated kidney; the lower, solid black graph represents the treated kidney. Both graphs show error bars of single standard deviation of the mean based on statistical evaluation of seven animals.

Quantitative blood flow measurements based on colored microsphere analysis were used to measure reduction in tissue perfusion. Kidney tissue samples were divided into cortex and medulla as well as into three spatial sections (cranial, center, and caudal). Figure 15 shows the results from seven animals reported in Kripfgans et al., 2005. The order of the tissue types is by spatial location in the kidney. These results demonstrate a substantial occlusion effect in the treated kidney. In all cases the infusion of droplets was arterial.

The time courses of the perfusion of the cortex and medulla of treated and untreated kidneys are shown in Figure 16. At 0, 30, 60, and 90 minutes after ADV, the right (untreated) kidney cortex perfusion exhibits a maximum drop of −17%. But, the left (treated) kidney cortex perfusion drops right after ADV to −80% relative to its pre-ADV flow and recovers to −46% within 90 minutes. Similar trends can be seen for medullary tissue. After ADV, the left kidney medulla perfusion drops to −69% and recovers to −14% after 90 minutes. The right kidney medulla perfusion varies between −18% and +1.7%. The ratio of cortex to medulla blood flow has been computed for the left and right kidney. After ADV, the right kidney shows a ratio of 8.2 ± 0.10, but the left kidney's ratio is 7.6 ± .0.79 compared to a value of 9 as determined in other studies. The details associated with all of this work appear in our publications, specifically Kripfgans et al, 2005.

In summary, renal occlusion to an average of 91% flow suppression in the renal cortex has been observed after Acoustic Droplet Vaporization in the renal artery. At the same time the blood flow in the cortex of the contra-lateral/untreated kidney was reduced by 9%. After 90 minutes the capillary flow in both kidneys recovered to 46% and 3% below baseline for treated and untreated kidney respectively.

For individual kidneys it has been seen, that after ADV, blood flow in the contra-lateral kidney may increase or decrease. Left and right kidneys are not independent systems. Autoregulation controls blood flow and urine production and we assume that the unilateral occlusion also caused a certain degree of flow regulation. Two possibilities are (a) increase in blood flow in the untreated kidney to compensate for loss of blood flow in the treated kidney and (b) decrease in blood flow in the untreated kidney to balance the urinary output relative to the treated kidney.

Even though our most successful work was on the kidney in a lepus model, we considered chronic rats (rattus) using a cancer model. Our droplet emulsion had been progressively engineered to be compatible with the selected animal model. In this case strain specific albumin was used and emulsion was made under sterile conditions both to allow chronic animal usage.

A cancer model, MAT LyLu (rat prostate carcinoma) in athymic nude rats, was initially investigated. This is a rapidly growing tumor as evidenced by this photograph and had a reproducible growth rate in our laboratory as shown in Figure 17. However, the complication that arose for this final stage of our work was the IV administration of the droplets. We were unable to obtain sufficient droplet concentration with IV administration to reproducibly produce ADV as detected by our imaging. In the absence of this evidence and at the conclusion of this funding we had not completed this objective. However, this work is continuing and more recent results have shown the first indications of ADV using a rat model that provided reliable imaging feedback for vascular targeting. It is our intention to continue this research given the continuation of funding.

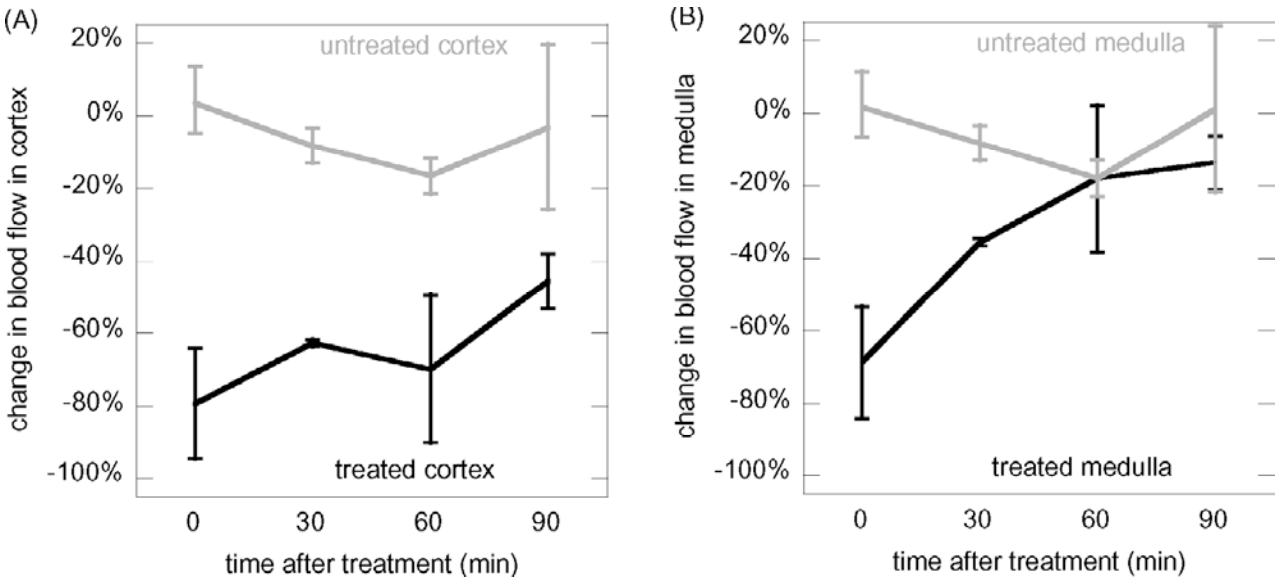

Figure 16 Change in tissue perfusion to the kidneys after ADV. (A) Perfusion in the cortex of treated (black graph) and untreated (gray graph) kidney. (B) Perfusion in treated (black graph) and untreated (gray graph) medulla. The graphs show error bars of single standard deviation of the mean based on statistical evaluation in four animals

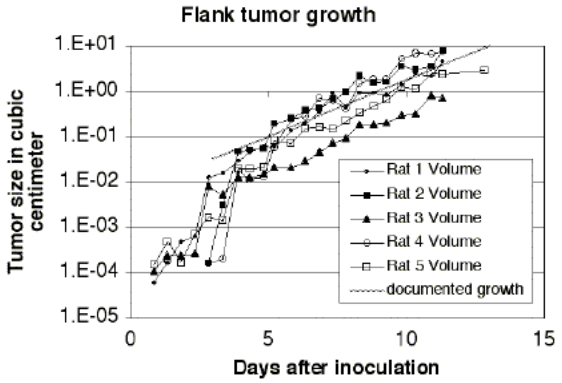

Figure 17 Growth curve of rat prostate tumor growing on the flank of the animal. For additional information see the 2003 progress report.

Key Research Accomplishments

Key results of the research include the following.

- Perfluorocarbon droplets can be formed using albumin from various species, which will allow for chronic studies in animal models with tumors. (Related **Objectives 1 and 2**). This includes the rat that is being planned for use in the continuation of cancer studies. (Related to **Objective 6**)
- Control of the bubble size distribution has been demonstrated by filtration of droplets. Subsequent tests in rabbits reveal that filtered droplets are well tolerated for IV administration, where rabbits are known to be particularly sensitive to perfluorocarbon emulsions. (Related to **Objective 2**)
- Exposure system fully developed and tested for *in vivo* use in a rabbit model and now in rats (Related to **Objectives 3-6**)
- Extensive measurements of modification of blood flow in rabbit kidney indicate a reduction in perfusion as measure with fluorescent microspheres. Flow reductions are now as high as 99% (Related to **Objective 4**)
- Initial experiments in tumors were not successful apparently due to a lack of droplets following IV administration. This work is continuing under subsequent funding with some indications of ADV being achieved in this model. (Related to **Objectives 5 and 6)**

Reportable Outcomes

The following is a list of relevant publications resulting from research conducted during the course of this project. Some publication dates lie outside the project period but were supported in part by this grant funding. Copies of the journal articles and proceeding are included in the appendix for this final report.

Peer Reviewed Journal Articles

Kripfgans OD, Fowlkes JB, Miller DL, Eldevik OP, Carson PL: "Generation and vaporization of Micrometer-Sized Droplets for therapeutic and diagnostic applications: Preliminary results," Ultrasound Med. Biol., 26 (7), 1177-1189, 2000.

Kripfgans OD, Fowlkes JB, Woydt M, Psychoudakis D, Carson PL, “In vivo droplet vaporization for occlusion therapy and phase aberration correction,” IEEE Trans. Ultras. Ferroel. Frequency Control, 49/6, 726-738, 2002.

Kripfgans OD, Fabiilli ML, Carson PL, and Fowlkes JB “On the acoustic vaporization of micrometer-sized Droplets.” J. Acoust. Soc. Am. 116(1), 272-281, 2004.

Kripfgans O.D., Orifici C.M., Carson P.L., and Fowlkes JB, “Acoustic Droplet Vaporization for Temporal and Spatial Control of Tissue Occlusion: A Kidney Study,” IEEE Trans. Ultras. Ferroel. Frequency Control, 52, 1101-1110, 2005.

Invited Presentations

Fowlkes JB : Why Bubbles for Ultrasound Contrast?, Invited lecture for the 45th annual convention of the American Institute of Ultrasound in Medicine, March 11-14, 2001, J Ultrasound Med, 20, S-4, 2001.

Fowlkes JB : Uses of microbubbles in high intensity ultrasound for diagnosis and therapy, International Workshop on Therapeutic Ultrasound Applications, Ultrasonic Industry Association, May 7, 2001, Atlantic City, New Jersey, 2001.

Fowlkes JB, Kripfgans OD, Carson PL, Microbubbles for Ultrasound Diagnosis and Therapy, 2004 IEEE International Symposium on Biomedical Imaging: From Nano to Macro, April 15-18, Arlington, VA, 2004.

Proceedings

Kripfgans OD, Fowlkes JB, Woydt M, Eldevik OP, Carson PL, In Vivo Droplet Vaporization using Diagnostic Ultrasound - A Potential Method for Occlusion Therapy, 2000 IEEE International Ultrasonics Symposium Proceedings, SC Schneider, M Levy and BR McAvoy, eds., Institute for Electrical and Electronics Engineers, Piscataway, 1449-1452, 2000.

Kripfgans OD, Fowlkes JB, Carson PL, High Speed Imaging of Acoustic Vaporization of Single Droplets, 2001 IEEE International Ultrasonics Symposium Proceedings, SC Schneider, M Levy and BR McAvoy, eds., Institute for Electrical and Electronics Engineers, Piscataway, 1323-1326, 2001.

Kripfgans OD, Carson PL, Fowlkes JB, “On the mechanism of acoustic droplet vaporization,” In 2002 IEEE International Ultrasonics Symposium Proceedings, SC Schneider, M Levy and BR McAvoy, eds., Institute for Electrical and Electronics Engineers, Piscataway, 517-520, 2002.

Kripfgans OD, Orifici CM, Carson PL, and Fowlkes JB, “Kidney blood flow occlusion by acoustic droplet vaporization,” In, 2003 IEEE International Ultrasonics Symposium Proceedings, SC Schneider, M Levy and BR McAvoy, eds., Institute for Electrical and Electronics Engineers, Piscataway, 913-916, 2003.

Fowlkes JB, Kripfgans OD and Carson PL, "Microbubbles for ultrasound diagnosis and therapy," in 2004 2nd IEEE International Symposium on Biomedical Imaging: Macro to Nano, pgs 29-32, 2004.

Abstracts

Kripfgans OD, Fowlkes JB, Woydt M, Eldevik OP, Carson PL "In Vivo Droplet Vaporization using Diagnostic Ultrasound. A Potential Method for Beam Aberration Correction?" Presentation at the 86th Scientific Assembly of the Radiological Society of North America, Chicago, November 26-December 1, 2000

Kripfgans OD, Fowlkes JB, Woydt M, Eldevik OP, Carson PL "On the Acoustic Activation of Micrometer Sized Droplets" Presentation at the World Congress on Medical Physics and Biomedical Engineering, Chicago, July 23-28, 2000

Kripfgans OD, Fowlkes JB, Woydt M, Eldevik OP, Carson PL "In Vivo Droplet Vaporization using Diagnostic Ultrasound. A Potential Method for Occlusion Therapy?" IEEE Ultrasonics Symposium, San Juan, Puerto Rico, October 22-25, 2000

Orifici K, Krücker JF, Kripfgans OD, Fowlkes JB, Carson PL, An ultrasound test object utilizing acoustic droplet vaporization (ADV) to produce distributed point target scatterers, AAPM Annual Meeting, Montreal, July 14-17, 2002, Medical Physics.

Kripfgans OD, Fowlkes JB, Woydt M, Eldevik OP, Carson PL; "Occlusion therapy through in vivo droplet vaporization", Era of Hope Department of Defense Breast Cancer Research Program, Sep 25-28, Orlando, 2002.

Kripfgans OD, Carson PL, Fowlkes JB, "Optical observations of single droplets during acoustic vaporization," 143rd Meeting, Acoust. Soc. Amer., June 4-8, Pittsburgh J. Acoust. Soc. Am., 111 (5) Part 2, 2465, 2002.

Kripfgans OD, Orifici CM, Fabiilli ML, Carson PL, Fowlkes JB "Stretching the Limits of Medical Ultrasound - Expanding the Range of Targeted Diagnosis and Therapy", 2003 Biomedical Imaging Research Opportunities Workshop.

Kripfgans OD, Orifici CM, Carson PL, Fowlkes JB, "Kidney Blood Flow Occlusion by Acoustic Droplet Vaporization," 2003 IEEE International Ultrasonics Symposium, Oct. 5-8, Honolulu, 2003.

Grant funding has been obtained from the National Institutes of Health based on this work and is allowing this work to continue. The application of the ADV methods is still directed toward cancer therapy where it is still our intention to find a solution that is effective either by occlusion alone or in combination with other therapy methods. For example, we are currently developing methods to control blood flow in the vicinity of RF ablations where cooling due to perfusion leaves portions of tissues untreated and thus reduces efficacy.

This funding helped launch the career of Dr. Kripfgans. After completing his PhD, supported in part by this grant, Dr. Kripfgan has joined our faculty and has now received NIH funding of his own to work on ADV as a method for improving ultrasound therapy for cancer. He is expected to continue this work as a new investigator in the field as a direct result of this grant support.

As a result of the direct optical observations of ADV and the importance of these on understanding the vaporization process, Dr. Kripfgans applied for and received a shared instrumentation grant for the purchase of a high speed camera. This camera will be used to further this work and provide insights into ADV to allow better triggering mechanisms for more effective *in vivo* treatments.

Katherine Orifici and Mario Fabilli received their Masters of Science in Biomedical Engineering while supported on this grant. After working at Pfizer Pharmaceutical Company, Mr. Fabilli will be returning to the University of Michigan in the fall of 2007 to work on his PhD in our laboratory working on the ADV technology. Andrea Lo will be completing her PhD in 2007 working on a project that was a continuation of the work she began with support of this grant. In total, four students were supported in part by this grant.

Conclusions

This research developed methodology for the production of perfluorocarbon droplets and their controlled vaporization using ultrasound. Acoustic Droplet Vaporization (ADV) was observed in experimental systems that allowed measurement of dependences on a number of acoustic parameters including pressure, frequency and pulse repetition period. Direct observations of ADV by high-speed photography showed that the process might be initiated by motion of the droplet in the acoustic field, which may explain the inverse frequency dependence of the acoustic pressure threshold for ADV. This result is significant as it affects the methodology that might be used for *in vivo* applications. Droplets could be produced using albumin from a variety of species. This may provide methods for additional future testing of ADV in several animal model as may be necessary to achieve sufficient evidence for clinical application. Initial tests in the occlusion of rabbit kidney showed a substantial reduction in blood flow resulting from occlusion by ADV generated bubbles. The flow reduction was up to 90% of normal flow and statistically significant. These results were obtained using arterial injections of droplets and complications with IV injections prevented demonstrations planned in chronic animal studied in cancer. However, the groundwork was laid for such work and the research is continuing as a result of the initial support provided by this grant.

Personnel

The following is a list of personnel supported in part during the course of this work.

Fowlkes, J. Brian
Kripfgans, Oliver
Rubin, Jonathan
Lo, Andrea

References

Kripfgans OD, Fowlkes JB, Miller DL, Eldevik OP, Carson PL: "Generation and vaporization of Micrometer-Sized Droplets for therapeutic and diagnostic applications: Preliminary results," Ultrasound Med. Biol., 26 (7), 1177-1189, 2000.

Kripfgans OD, Fowlkes JB, Woydt M, Psychoudakis D, Carson PL, "In vivo droplet vaporization for occlusion therapy and phase aberration correction," IEEE Trans. Ultras. Ferroel. Frequency Control, 49/6, 726-738, 2002.

Kripfgans OD, Fabiilli ML, Carson PL, and Fowlkes JB "On the acoustic vaporization of micrometer-sized Droplets." J. Acoust. Soc. Am. 116(1), 272-281, 2004.

Kripfgans O.D., Orifici C.M., Carson P.L., and Fowlkes JB, "Acoustic Droplet Vaporization for Temporal and Spatial Control of Tissue Occlusion: A Kidney Study," IEEE Trans. Ultras. Ferroel. Frequency Control, 52, 1101-1110, 2005.

Appendices

Peer-reviewed journal articles and proceedings articles resulting from this research are included in the order in which these are listed in the reported outcomes.

Ultrasound in Med. & Biol., Vol. 26, No. 7, pp. 1177–1189, 2000

0301-5629/00/$–see front matter

PII: S0301-5629(00)00262-3

● *Original Contribution*

ACOUSTIC DROPLET VAPORIZATION FOR THERAPEUTIC AND DIAGNOSTIC APPLICATIONS

OLIVER D. KRIPFGANS, J. BRIAN FOWLKES, DOUGLAS L. MILLER, O. PETTER ELDEVIK and PAUL L. CARSON

University of Michigan Health Systems, Department of Radiology, Ann Arbor, MI, USA

(*Received* 12 *July* 1999; *in final form* 17 *May* 2000)

Abstract—A phase shift droplet emulsion is introduced as an aid to unusual ultrasound (US) applications. The transpulmonary droplet emulsion (90% < 6 μm diameter) is made by mixing saline, bovine albumin and dodecafluoropentane. It has been observed that an acoustic pressure threshold exists, above which the droplets vaporize into bubbles approximately 25 times the original diameter. For frequencies between 1.5 and 8 MHz, the threshold decreases from 4.5 to 0.75 MPa peak rarefactional pressure. This paper presents preliminary results for droplet preparation and their evaporation as a function of applied acoustic pressure and frequency, as well as simulations of the lifetime of these gas bubbles based on gas diffusion. *In vivo* experiments were simulated by the evaporation of droplets in blood flowing under attenuating material. We propose that this agent might be useful for tissue occlusion in cancer treatment, as well as for phase aberration corrections in acoustic imaging.

Key Words: **Contrast agent, Phase shift agent, Cancer treatment, Phase aberration, Medical imaging.**

INTRODUCTION AND LITERATURE

Boehm et al. (1997) showed that it is possible to "starve" cancer cells to death by restricting their blood supply. Angiostatin and endostatin suppress the development of supply arteries that tumors attract chemically and need for their own growth. Occlusion therapy has also been used to control blood flow, including direct injection of material into arteries, which either blocks blood flow at the injection site or immediately downstream. A high density of large solid emboli (40–50 μm) are clearly occlusive and produce permanent damage to tissue (Laccourreye et al 1993). Many different materials have been introduced by intravascular catheters and percutaneously, to occlude flow. These materials have been either absorbable, including blood clot, cellulose and gelatin sponge (Gelfoam), or nonabsorbable including particulates, fluids, coils, balloons and streamers. Hepatocellular carcinoma, occurring in 2–30 per 100,000 males each year, has been treated successfully with embolotherapy where localized drug delivery was included in the procedure (Nakagawa and Castaneda-Zuniga 1997; Di Segni et al. 1997). Renal carcinoma is another condition amenable to embolotherapy. It is the most common cancer in the urinary tract and accounts for ~ 3% of malignancies overall. Several reports have indicated successful treatments by embolization including 78% tumor necrosis (Sandoval et al. 1983). One of the more important factors in the success of such therapies is the ability to direct and confine the treatment of a targeted region. The techniques described here offer a potentially convenient method to target multiple vessels or a capillary bed for occlusion following a simple IV administration of the perfluorocarbon droplets (specifically dodecafluoropentane, DDFP). When acoustic droplet vaporization (ADV) is desired in feeder vessels, target vessels could be identified by a method (currently under development in our laboratory) known as contrast interruption (Fowlkes et al. 1998), where the flow of conventional ultrasound (US) contrast agent can be halted in specific arteries by the targeted application of low amplitude US.

Laplace pressure compresses bubbles made from droplets and increases the diffusion of the internal gas (mainly gaseous DDFP) into the host liquid. However, due to the low solubility and diffusibility of perfluorocarbon gases in water (Table 1), bubbles filled with them

Address correspondence to: J. Brian Fowlkes, Department of Radiology, University of Michigan - Medical Center, Ann Arbor, MI 48104-0553, USA. E-Mail: fowlkes@umich.edu

Table 1. Constants used in simulation of bubble growth and dissolution.

Gas	Diffusion coefficient $D \cdot 10^5$ cm^2 s^{-1}	Water solubility $C_\infty \cdot 10^{-7}$ mole mL^{-1}	% gas content in saline
N_2	2.00	5.84	76.1
CO_2	1.91	267.5	0.697
O_2	2.42	11.04	22.3
Ar	2.5	12.09	0.934
C_5F_{12}	0.6236*	0.0401†	0

Diffusion and solubility constants were taken from Lide (2000), except those for C_5F_{12} (see footnote).

* Computed using molar volume of 177.8 mL mole^{-1} (Simons and Dunlap 1950); † taken from Kabalnov et al (1998, 1998b).

have considerably longer lifetimes in water (and blood) compared to air bubbles of the same size. Therefore, large numbers of relatively large perfluorocarbon gas bubbles should provide extended occlusion, potentially sufficient to infarct tissue (Lipton 1999). Contrast agents containing small perfluorocarbon gas bubbles are already in use (*i.e.*, Optison™, Mallinckrodt, Hazelwood, MO; Definity™, DuPont, Pharmaceuticals, Wilmington, DE; EchoGen™, SONUS Pharmaceuticals Inc., Bothell, WA), and these gases have significantly extended the lifetime of these agents (Yasu et al 1997, 1999).

The second potential application for ADV concerns improvements in the generation of both diagnostic and therapeutic US fields. US is well established as a diagnostic imaging modality. However, it suffers from image distortion (loss of contrast and resolution) when tissue is visualized through paths containing spatially varying speed of sound (Freiburger et al. 1992). Changes in the speed of sound cause errors on transmission (focusing) as well as on reception (reconstruction). Phase- and other beam-aberration corrections have been investigated by various groups (Karaman et al. 1993; Ng et al. 1997; Walker and Trahey 1996). Possible solutions include imaging of known and naturally existing structures (*e.g.*, speckle, Ng et al. 1997) and point targets in or near the volume of interest (VOI) (Walker and Trahey 1996; O'Donnell and Flax 1988). The backscatter of those structures is used to adjust the beam forming for that specific site, according to some model of the target structure and the propagation medium. We propose the possible use of vaporized droplets as point targets for phase-aberration corrections. Similar to the proposed approach for the therapeutic application, droplets would be injected IV and acoustically vaporized upstream of the VOI. In low number density, the resulting bubbles would act as point beacons. The reason for the low concentration is to provide single scatterers to avoid multiple scattering[1] and limit the potential for bioeffects. This application and that of occlusive therapy might not be mutually exclusive. In this case, corrected real-time US imaging should be possible, along with better focusing of ultrasonic fields for therapeutic applications. It is also important that a minimal, but effective, gas bubble diameter be used to avoid infarction, especially when imaging the brain. A minimum gas volume reliable to produce apparently long-term effects, lasting at least 180 min, has been observed in the rabbit brain for carotid bolus injections of 25 μL of air (Helps et al. 1990). For the point target application, we would expect that an injection of 10,000 droplets to the target organ to be sufficient, resulting in a 0.5 μL gas volume (assuming an ADV rate of 100%). The volume is calculated from the normalized droplet size distribution and the maximum size to which the corresponding bubbles would grow.

In addition, the off-resonance scattering based on Medwin (1977) from a 36-μm diameter bubble would provide an estimated 10 dB of scattered signal above brain tissue to act as a point beacon. There is a trade-off in selecting the bubble sizes used. On the one hand, large bubble sizes are necessary to give good backscatter relative to the tissue background and also to last long enough to be imageable. On the other hand, bubbles need to dissolve fast enough to prevent permanent damage to the target tissue, especially in the case of the brain, where there is significant interest in correcting the aberration by the skull. The size of bubbles resulting from the vaporization of perfluorocarbon droplets, including the diffusion of gas from the surrounding liquid, will be examined in this work.

We hypothesize that droplets made by a perfluorocarbon-albumin solution can be stabilized against spontaneous evaporation at body temperature. Furthermore, the resulting agent is also stable to ultrasonic scanning, using a low mechanical index (MI), up to an acoustic pressure threshold above which the agent can be vaporized deliberately.

MATERIALS AND METHODS

Production of droplets

A process for generating droplets was developed, based on mixing saline containing bovine serum albumin and dodecafluoropentane (DDFP, C_5F_{12}, CAS #678-26-2). DDFP has a natural boiling point of 29°C at atmospheric pressure (Simons and Dunlap 1950), which suggests a spontaneous transition into gas bubbles at body temperature. The DDFP droplets were expected to be

[1]Multiple scattering makes the correction impossible, since the relative position of the scatterers is unknown. The relative positions highly affect the phase of the incoming signal.

superheated at body temperature and to vaporize when perturbed by an ultrasonic field. Our goal was to produce 36 μm diameter gas bubbles from droplets, based on considerations described above concerning aberration correction for imaging in the brain. A first approximation of the amount of expansion that might occur upon vaporization of a DDFP droplet can be obtained using the ideal gas law $pV = NRT$ (Halliday et al. 1997), where p is atmospheric pressure [N m^{-2}], V is volume to be calculated [m^3], N is the amount of droplet material [mole], R is the gas constant 8.31 [J mole^{-1} K^{-1}], and T is the ambient temperature [K], with the result being a volume expansion factor of approximately 125 or a radial expansion of approximately 5. Consequently, droplets with a diameter of 6–7 μm and less were planned, a size that happens to correspond to the likely maximum for capillary passage (Best and Taylor 1998).

Previous studies have indicated the formation of micrometer-sized droplets of hydrocarbons when solutions with albumin and saline have been sonicated (Suslick and Grinstaff 1990). The approach presented here is similar, but uses an amalgamator, a high-speed vial shaker (MSD Wig-L-Bug, Crescent Dental Mfg. Co. Elgin, IL). Such devices have been used to form perfluorocarbon gas bubbles for US contrast agents (Unger 1995; Unger et al. 1996). A series of formulations was tested containing between 1 and 16 mg bovine serum albumin per mL saline. Volumes of a saline-albumin solution (900 μL) and DDPF (100 μL) were injected into an approximately 3-mL auto sampler glass vial. The vial was sealed with a rubber stopper and an aluminium crimp top and then shaken for 30 s using the high-speed vial shaker.

Determination of droplet size

The droplets produced for the different formulations were evaluated using optical microscopy. Samples from each vial were diluted with saline by 1:10 or 1:100, based on the concentration of droplets for the specific formulation, and a portion of this solution was placed on a hemocytometer slide and examined under an optical microscope (Leica Microsystems Inc., Deerfield, IL) at a 400× magnification. Optical images were recorded digitally with a CCD camera (Spot, Diagnostic Instruments Inc., Sterling Heights, MI) with an approximate camera resolution of 4 pixels per μm, based on calibration measurements using a stage micrometer (P/N 41416-123, VWR Scientific Products, West Chester, PA). This is 4 to 6 times better than the optical resolution. Droplet sizes were measured within a specified portion of the optical field defined on the hemocytometer grid. Semiautomatic edge and shape detection identified the droplet boundary to determine the perimeter and then to calculate the corresponding droplet diameter. The number density (*i.e.*, the concentration) was estimated from the volume of fluid from which the droplets were counted by noting the area of the hemocytometer counted and knowing the height of the fluid column in the hemocytometer (100 μm). All individual diameter measures were used to compute individual droplet volumes. Based on the optically-scanned volume (V_{total}), a dilution of 1 to X, and the total volume of droplets counted (V_{droplet}), the droplet volume fraction was then:

$$v = X \cdot \frac{V_{\text{droplet}}}{V_{\text{total}}}. \quad (1)$$

Optical observations during droplet heating

Samples of droplets were observed optically during heating by adding 10 μL of a given droplet solution to 10 mL saline in a Petri dish-type container. The dish was then placed in a holder within a water bath (Exacal model, Neslab Instruments Inc., Portsmouth, NH). The holder was positioned below an optical microscope with 320× magnification (Nikon SMZ-U, Melville, NY). The droplets lay at the bottom of the dish due to the elevated density of DDFP (1.66 g ml^{-1}) compared to saline. The bath temperature was then raised gradually (4°C min^{-1}) to a maximum temperature of 60°C, while maintaining continuous observation and digital recording through the CCD camera of the microscope for later review.

Vaporization of droplets in vitro

To study the vaporization of droplets in acoustic fields, a water tank with dimensions 18 × 30 × 23 cm was used that contained two flow tube connections mounted on each of the long sides, 9 cm from the far wall and 7.5 cm from the bottom (Fig. 1). Dialysis tubing[2] (Spectrum Laboratories Inc., Laguna Hills, CA, Spectra/Por membranes, MWCO 12,000–14,000 Daltons) was used as the flow tube. The tank was filled with deionized water and degassed using a multiple pinhole degassing system (Kaiser et al. 1996). An external water bath[3] (Exacal model, Neslab Instruments Inc., Portsmouth, NH) was used to heat the tank water as well as the circulated fluids to 37°C. The bath's external circulation was connected to a heat exchanger in the water tank to maintain its temperature. The surface of the water in the tank was covered with air-filled plastic balls (P-06821-22, Cole-Parmer Inc., Vernon Hills, IL) to minimize regassing and also to reduce heat loss.

An Erlenmeyer flask (1000 mL) with a saline solu-

[2]The acoustic attenuation of dialysis tubing was measured following the setup and measurement guidelines in Madsen et al (1986), as less than 1 dB for the range of 1.5 to 8 MHz.

[3]The word "bath" is used for the external heating system and the word "tank" for the setup that holds the flow tube.

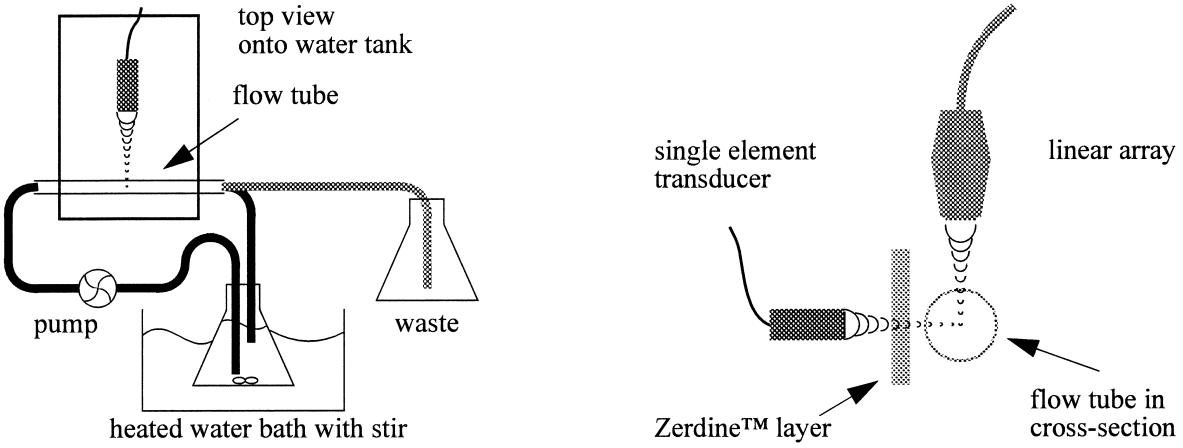

Fig. 1. The setup consists of a water tank (top, on the left) that hosts a flow tube (dialysis tubing) shown in longitudinal and cross-sectional view on the left and right, respectively (not to scale). The single-element transducer is completely submerged. The flow past the outlet on the tank can be directed to a waste container (for one-way flow) or back to the Erlenmeyer flask (for recirculation). All fluids are heated to 37°C.

tion containing droplets was submerged in the water bath and stirred using a magnetic stirrer. The solution of droplets was prepared by adding 100 μL of droplet solution from a shaken vial to 1000 mL of saline. A peristaltic pump (MasterFlex type, Cole-Parmer, Chicago, IL) was used to pump the droplet solution from the flask through the flow tube. Volumetric flow rates from 0.5 up to 2.5 mL s^{-1} could be achieved. For a flow tube of 6-mm diameter, the resulting average velocity was up to 9 cm s^{-1}, assuming a laminar flow condition ($Re = \rho \cdot d \cdot U/\mu = 600$, where ρ and μ are density and viscosity of the host liquid, respectively, d is the diameter of flow tube, and U is the flow speed) (Kundu 1990). The outlet of the flow tube was connected to a waste container, which was placed at a height of 15 cm above the flow tube. The purpose of this arrangement was to create a slight positive pressure in the flow tube to maintain its inflation.

A linear ultrasonic array (nominally 10 MHz) connected to a diagnostic scanner (Diasonics VST series, Milpitas, CA) was placed above the flow tube, facing downward and aligned with the flow tube (Fig. 1). A single-element transducer (V320, Panametrics Inc., Waltham, MA) with a 14-mm aperture, focused at 76.2 mm) was used to vaporize droplets.[4] It was mounted at a 90° angle to the imaging plane of the linear array. Both this ADV transducer and the imaging array were focused on the center of the tube. The ADV transducer was controlled by a function generator (model HP-3314, Hewlett-Packard, Palo Alto, CA) and a power amplifier (model 240L or A300, ENI, Rochester, NY). Tone bursts of typically 3 μs duration with pulse-repetition frequencies from 0.5 to 4.5 kHz were used. The duty cycle was kept below 1%. The ADV transducer was calibrated for its transmitted acoustic pressure using a membrane hydrophone (Reference Shock Wave Hydrophone™, Sonic Industries, Hatboro, PA). The calibration procedure included the acquisition of axial and cross-sectional beam profiles and, for each frequency used, a range of acoustic pressures was measured at the focus.

Observation of gas bubbles

Gas bubbles were monitored as they formed from droplets using ADV. An optical setup, as given in the Materials and Methods section "Optical observations during droplet heating" was used to record images of gas bubbles as they rose in a static fluid (Fig. 8). Based on a video pixel size of approximately 24 μm and a frame rate of 5.6 Hz, rise-time was measured as the distance by which a given bubble moved over the period of N frames. Assuming terminal velocity, the resulting rise speed was used to compute the gas bubble's size (Epstein and Plesset 1950).

Vaporization of droplets in simulated in vivo environments

Two key features were added to the experimental flow setup to simulate *in vivo*conditions. Heparinized canine whole blood (6 mL heparin per 250 liter blood) was introduced as circulating fluid and a 2 cm thick layer of attenuating material, Zerdine™ (CIRS Inc., Norfolk, VA), was placed in the beam of the ADV transducer, proximal to the flow tube (Fig. 1). A solution of 75 mL

[4]Here also referred to as ADV transducer.

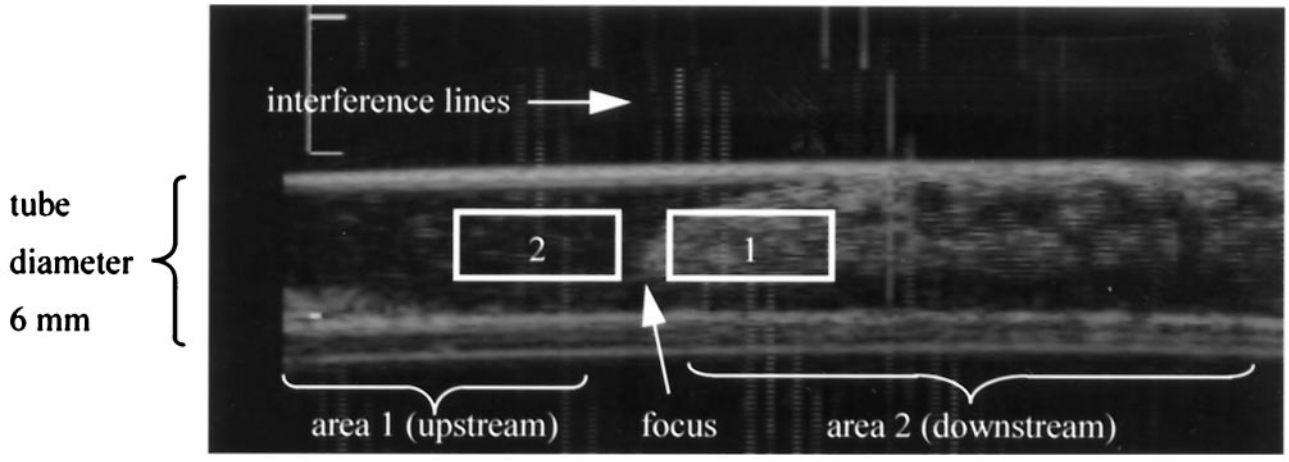

Fig. 2. Ultrasound images taken during ADV, where two areas are selected for the quantification of the echogenicity of the circulated fluid. The mean echo amplitude (MEA) upstream from the focus (area 2) is subtracted from the MEA downstream from the focus (area 1). The resulting value is used as a measure for vaporization because it corrects for echoes from pre-existing scatterers prior to the focus. Acoustical interference is seen as vertical lines in the image. The subtraction method compensates for that artefact. The resulting value is called the relative echo amplitude.

heparinized blood and 50 μL of droplet solution was placed in a 120-mL flask for circulation. The four times higher droplet concentration was used to compensate for the increase in background signal from blood (Fig. 10). Furthermore, the solution was recirculated because the limited amount of blood did not allow a single pass for the constraints of volumetric flow rate and the data acquisition conditions used (see below).

Data acquisition and analysis

Figure 2 shows the dialysis tube in longitudinal view, as imaged by the linear array. The horizontal bright lines are the reflections from the tube's upper and lower walls. The flow direction is from left to right at an average velocity of 9 cm s^{-1}. The droplets were vaporized while passing through the focal zone of the single element transducer located between areas 1 and 2. The increase in echogenicity was due to the change in the impedance difference between the droplet ($\sim$ 0.3 MRayl) and the vaporized droplet ($\ll$ 0.3 MRayl) compared with that of blood. In area 1, there was a measurable increase in echogenicity, relative to area 2, depending on the amount and size of gas bubbles produced. Interference between the ADV transducer and imaging array appeared as vertical lines (dashed) in the image. Therefore, in the absence of vaporization, there were two sources of signals, a finite echogenicity of the host fluid (due to preexisting gas bubbles and/or acoustically visible droplets) prior to the focus of the ADV transducer, and acoustic interference between ADV transducer and imaging array.

Images, such as the one shown in Fig. 2, were acquired by digitizing the video output of the US machine. Subsequent image analysis, including decompression of the grey scale to linearized echo amplitude, was performed using a Matlab™ script (MathWorks Inc., Natick, MA). The images were acquired at a rate of 2 Hz to allow refill of the evaluation areas 1 and 2 with new droplets/gas bubbles.

$$\mathrm{MEA}(n) = \frac{1}{NM} \sum_{j=1}^{M} \sum_{i=1}^{N} A(i, j)$$

$$\mathrm{REA} = \mathrm{MEA}\,(1) - \mathrm{MEA}\,(2). \qquad (2)$$

where $A\,(i, j)$ is the signal at pixel (i, j) ϵ area number n.

The mean echo amplitude (MEA), see eqn (2), of area 2 was evaluated and then subtracted from the MEA of area 1. On average, the resulting value, called relative echo amplitude (REA), was zero for the case where no droplets vaporize. A finite valued REA should occur when droplets evaporate and the echogenicity increases. The time gain control (TGC) was identical for areas at the same imaging depth (*i.e.*, identical for areas 1 and 2). A total of 20 images were taken over 10 s for each sound pressure setting, and the resulting REAs averaged and plotted along with the standard deviation as a function of peak negative pressure.

Thresholds for vaporization from REA as a function of applied pressure were determined by least square fitting to the following two line segments.

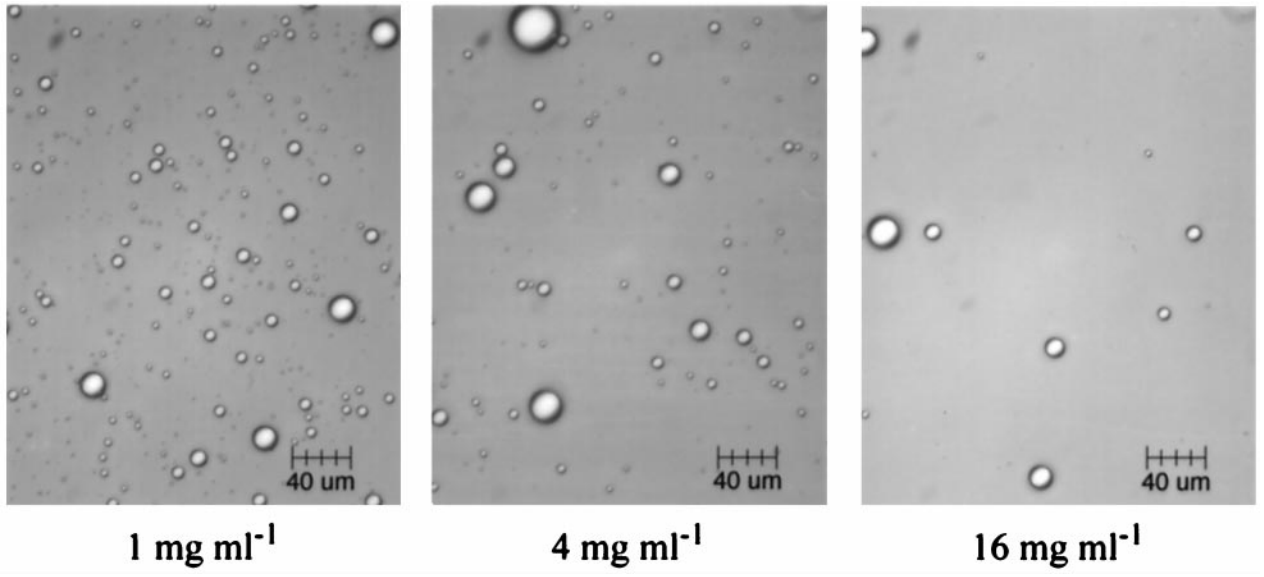

Fig. 3. The three microscope pictures show droplet formation for 1, 4, and 16 mg albumin per mL saline. The concentration of DDFP was the same in all three cases (0.1 mL mL^{-1}). A lower concentration of albumin results in smaller droplets, as well as in a larger number density. The pictures have been taken for the same dilution, as well as with the same magnification. Note that, qualitatively, the average droplet size changes with albumin concentration. The picture on the left shows many small droplets and a few larger droplets. The picture in the middle has fewer small droplets, and the picture on the right has no apparent small droplets. The size of the largest droplets, however, does not change significantly. Note that, for a constant amount of fractional droplet volume ($\sim R^3$), the cross-sectional area ($\sim R^2$) of droplets increases with decreasing mean droplet size. Therefore, one sees more "white" in the image with smaller mean droplet size.

$$\mathrm{REA}(p) = (a_1(p - p_{\mathrm{threshold}}) + b) \cdot w(p, 0, p_{\mathrm{threshold}}) + \ldots \\ (a_2(p - p_{\mathrm{threshold}}) + b) \cdot w(p, p_{\mathrm{threshold}}, p_{\mathrm{max}}) \quad (3)$$

$$w(p, p_1, p_2) = \begin{cases} 1 & p \in [p_1, p_2] \\ 0 & \text{otherwise} \end{cases}$$

The structure of the fitting function was fairly simple. A line with slope a, intercept b and shifted origin was multiplied by a window function that limited the extension of the line to all the data points before/after the pressure threshold to be found.

RESULTS AND DISCUSSION

Generation of droplets

When saline and DDFP were shaken without albumin, the resulting mixture initially contained droplets, but the droplets coalesced substantially within a few seconds; the mixture appeared to return rapidly to its original state of two separate bulk liquids. In contrast, mechanically-shaken mixtures containing albumin formed droplets that, at least in part, remained as an emulsion for several weeks, based on continued observation of ADV using samples stored under refrigeration at 4°C. Figure 3 shows droplets made for three different concentrations of albumin (16, 4, and 1 mg mL^{-1} saline). Using the optical methods above, the size distribution for droplets formed with 1 mg albumin per mL saline is

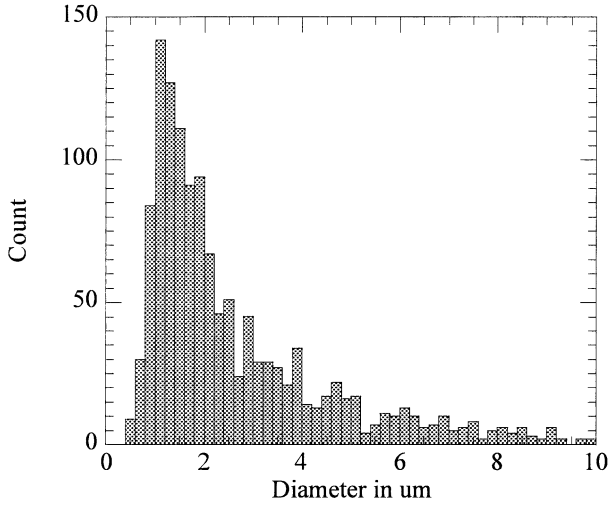

Fig. 4. Size distribution for DDFP droplets made with 1 mg albumin per mL. The mean size is 1.5 μm radius. The total number of droplets was 1332 for an approximately 3×10^{-5} mL sample volume, corresponding to a concentration of 4.82×10^7 droplets per mL.

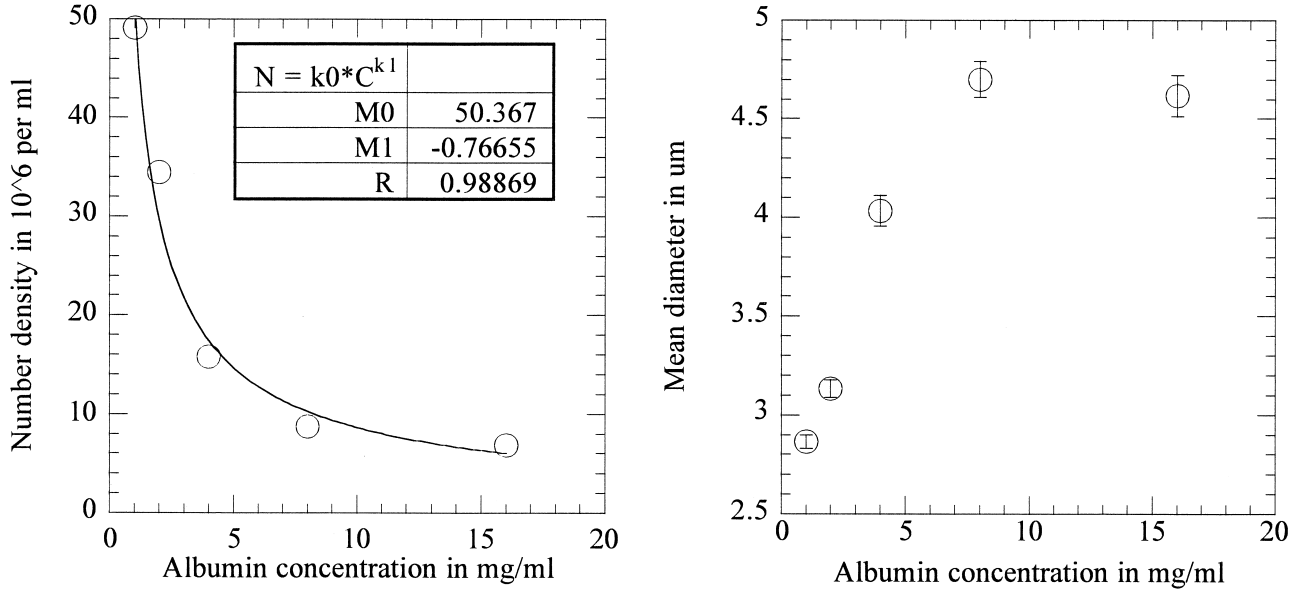

Fig. 5. The number density (left side) and the mean radius (right side) of droplets are plotted as a function of the albumin concentration. The number density decreases, and the mean radius increases, with increasing albumin concentration. The average volume of DDFP incorporated into droplets remained essentially constant.

given in Fig. 4. Note that this emulsion should be substantially transpulmonary based on its size (*i.e.*, it should pass the capillary bed of the lungs) because 90% of the droplets are smaller than 6 μm in diameter. Figure 5 shows that the number density decreases with increasing albumin concentration. Based on the general trend in the data, the points were fit by least squares methods to a power law, $N = k_0 C^{k_1}$, where N is the number density, C is the concentration of albumin and k_0 and k_1 are constants. The coefficients were found to be $k_0 = 50.4$ and $k_1 = -0.767$ ($R^2 = 0.978$). The mean droplet size increased by $\sim$ 62% from 2.9 μm mean diameter to 4.7 μm over the range of albumin concentrations used. The decrease in number density and the increase in size are mutually dependent, because the percentage of DDFP incorporated into droplets remained nearly constant at approximately 30%. Note that, if the total volume fraction of droplets remains the same, the total surface area formed by droplets increases when the average droplet size decreases. In that case, the amount of albumin used to stabilize the surface of the droplets is greater. But, the experiment shows that, when a lower concentration of albumin is used, smaller droplets form. This might seem paradoxical, but could be explained if the albumin used is at a saturation level for droplet stabilization and changes in interfacial surface tension and viscosity of the liquid influenced the size distribution. Suttiprasit et al. (1992) showed that the surface tension of bovine serum albumin solutions increases with increasing serum concentration, and Ni et al. (1998) measured a 35% increase in droplet size for methylmethacrylate suspensions when the interfacial tension was doubled. Our results are consistent with these trends.

Droplet vaporization and frequency dependence

Under optical observation, droplets in static solution did not vaporize when heated to a maximum of 60°C (limit of the heating bath). However, as indicated in Fig. 2, droplets did vaporize in the presence of an ultrasonic field, producing increased echogenicity. So the immediate question was: "Why do they boil in the ultrasonic beam?" A possible mechanism could be inertial acoustic cavitation, whose frequency-dependence for onset has been predicted according to the model of the mechanical index (MI) given by Apfel and Holland (1991):

$$MI = \frac{\text{peak negative pressure in MPa}}{\sqrt{\text{frequency in MHz}}}. \qquad (4)$$

If cavitation was the mechanism for droplet evaporation, then the MI at threshold should be a constant and the peak negative pressure needed would be larger for higher frequencies. Accordingly, the threshold for ADV, in peak negative pressure, was measured as a function of frequency in a series of measurements performed using single-element transducers to transmit short tone bursts at a range of center frequencies, as described in the Methods section.

For each frequency, the relative echo amplitude was

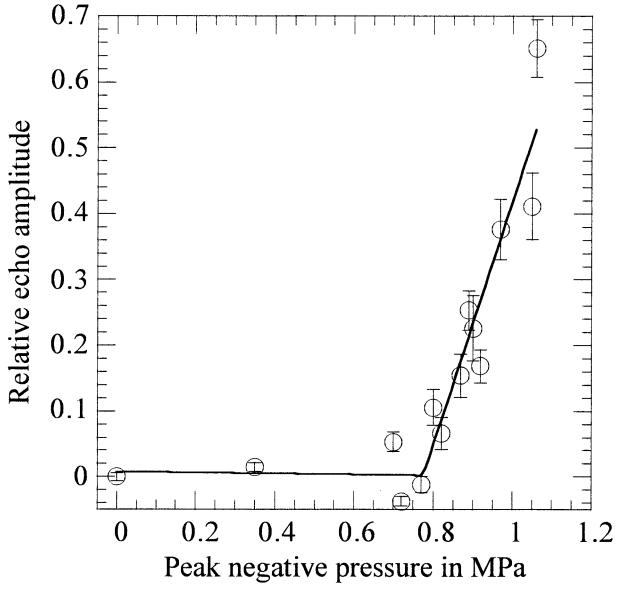

Fig. 6. The plot shows the relative echo amplitude as a function of applied peak negative pressure. The frequency used was 7.6 MHz.

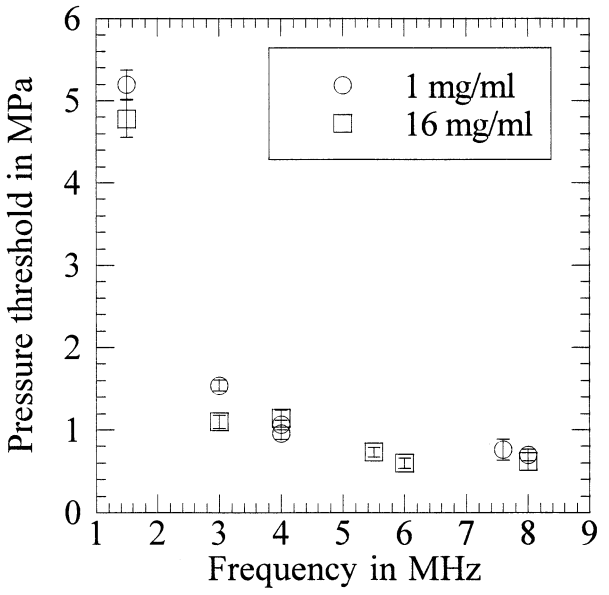

Fig. 7. The frequency-dependence of ADV. For each frequency, REA was fit by means of least square to two line segments; see Fig. 6, for example. The pressure threshold for ADV was found from the pressure amplitude where the two segments intersect.

measured as a function of the peak negative acoustic pressure (see Methods section, as well as Fig. 2). Figure 6 shows results for a focused transducer driven by a 7.6-MHz, 5-cycle tone burst, with a 0.2-ms pulse-repetition period (PRP). Each data point in the chart is an average for 20 measurements of the increased echo amplitude due to ADV. The relative echo amplitude remains at zero with increasing applied acoustic pressure, until the pressure approximately equals 0.7 MPa. At that point, the curve shows a much greater slope. The pressure threshold of 0.7 MPa at 7.6 MHz corresponds to a mechanical index of 0.25, which is well below the maximum available with commercial US systems.

A comment on the functional dependence of the relative echo amplitude as a function of pressure should be given. It has been observed that the relative echo amplitude slightly increased while the applied pressure was below "threshold for ADV." If the subtraction process, eqn (2), is working, why should this happen? In the case of a 1 mg mL^{-1} droplet emulsion, insonified at 8 MHz, the slope below threshold had been up to 14% of the slope after the threshold. We believe that this might be because of the distribution of droplet sizes and the high frequency provides additional scattering from the ADV transducer into the imager.

In a similar manner, the threshold for vaporization was measured at several frequencies ranging from 1.5 to 8.0 MHz. These results are shown in Fig. 7, in which it should be noted that the threshold is not a constant MI value but, rather, even lower at higher frequencies. Even though some of the acoustic pulse parameters, like PRP, duty cycle and beam geometry, were not the same for the different measurements taken, the threshold appears to change strongly and consistently with frequency; if accurate, this dependence is not modeled well by the $f^{-1/2}$ frequency dependence.

Observation of gas bubbles

Gas bubbles made by ADV (7.6-MHz, 5-cycle tone burst, 0.9-MPa peak negative pressure, 0.2-ms PRP) were observed optically as described in the Methods section. The droplets used were from the 1 mg mL^{-1} albumin formulation diluted into saline (1:10,000). Figure 8 shows the overlay of 15 optical images from the microscope, when focused inside the tube where droplets were acoustically vaporized.

Several bubble traces are visible, such as the traces of bubble 1 and bubble 2. Their diameters were measured to be $\sim$ 108 μm and $\sim$ 91 μm, respectively based on rise time estimates. Several other bubbles were measured, ranging from of 75 to 150 μm diameter. Based on the droplet size distribution, such large bubbles could not be explained with ordinary droplet-to-gas bubble conversion using a volume expansion factor of 125 based on an ideal gas law calculation. In addition, a simple measurement of the volume expansion of evaporating pure DDFP

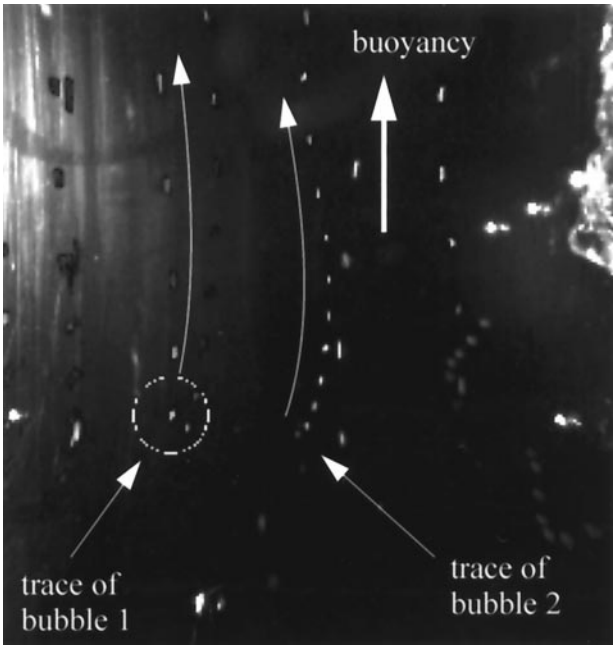

Fig. 8. Gas bubbles formed from evaporated droplets have been monitored under a microscope. The picture shows multiple, superimposed frames of a movie. Based on the microscope's magnification, bubble 1 is approximately 100 μm in diameter. Assuming simple drag force, the frame rate used (180 ms per frame) yields a bubble size of 108 μm; whereas bubble 2 yields 91 μm.

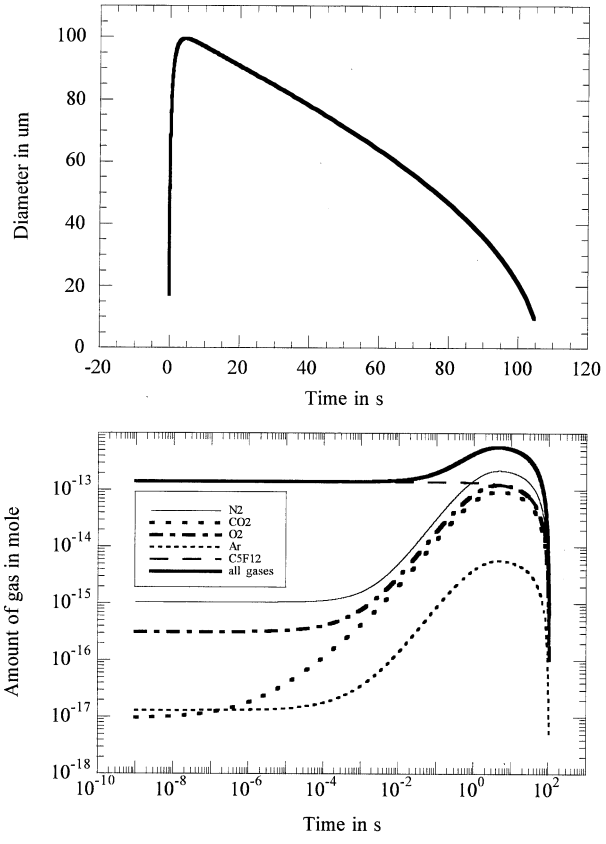

Fig. 9. Top graph shows the diameter of an initially 17-μm diameter DDFP bubble as it expands due to gas diffusion from the host liquid (time interval from 10^{-9} to $\sim$ 5 s), as well as subsequent dissolution of the gas bubble (time interval from $\sim$ 5 s to 100 s), see eqn (6). Bottom graph shows the amount of the individual gases as they diffuse in and out of the bubble.

was found to be approximately 151 at 37°C. Such a volume expansion factor would correspond to an increase in diameter by only a factor of 5.3 (*i.e.*, a droplet as large as 10 μm diameter expanding to only a 53 μm diameter bubble of pure DDFP). A reason for further expansion is intake of dissolved gases from the surrounding fluid. An initial gas bubble contains only DDFP gas. The host liquid is air-saturated, containing dissolved N_2, O_2, CO_2, and Ar. A simulation using the formulation of Neppiras (1980), eqn (5), was extended to multiple gases, eqn (6), to predict the uptake of gas into the bubble:

$$\dot{R} = \frac{C_0 D}{\rho}\left(\frac{C_\infty}{C_0} - 1 - \frac{2\sigma}{p_0 R}\right)\left(\frac{1}{R} + \frac{1}{\sqrt{\pi D t}}\right), \quad (5)$$

where R_0 is the current gas bubble radius, C_0 and C_∞ are saturation concentration and concentration at infinity in the surrounding host liquid, respectively, D is the gas's constant of diffusion, ρ is the density of the gas inside the gas bubble, σ is the surface tension between gas and liquid, p_0 is the ambient static pressure, and t is time. For multiple gases,

$$\dot{n}_j(t) = \frac{4\pi R^2(t)}{M_j} D_j\left(C_{j,\infty} - \mathrm{Min}\left(C_{j,0}, \frac{n_j(t)}{(4/3)\pi R^3(t)}\right) \times \left(1 + \frac{2\sigma_j}{p_0 R(t)}\right)\right)\left(\frac{1}{R(t)} + \frac{1}{\sqrt{\pi D_j t}}\right) \quad (6)$$

$$\dot{R}(t) = \frac{1}{4\pi R^2(t)}\frac{1}{N}\sum_{j=1}^{N}\frac{\dot{n}_j(t) M_j}{\rho_j} = \frac{R(t)}{3}\frac{1}{N}\sum_{j=1}^{N}\frac{\dot{n}_j(t)}{n_j(t)},$$

where n_j is the current concentration of gas j inside the gas bubble, M_j is the molar mass of gas j, and N is the total number of gases. (A similar formulation for contrast agents can be found in Kabalnov et al. 1998a, 1998b.)

Using the experimentally-observed DDFP volume expansion of 151 (diameter expansion of 5.3), a droplet with an initial diameter of approximately 3 μm will form a 17-μm diameter gas bubble of pure DDFP. A 17-μm DDFP bubble expands, due to inflowing gases, to 100

Table 2. Numerical results of the fitting algorithm on ADV data for simulated *in vivo* environments.

Case	Frequency (MHz)	Pressure threshold (MPa for 16 mg mL^{-1})	Pressure threshold (MPa for 1 mg mL^{-1})	Frequency (MHz)	Pressure threshold (MPa for 16 mg mL^{-1})	Pressure threshold (MPa for 1 mg mL^{-1})
Droplets in saline	1.5	4.78 (0.23)	5.20 (0.18)	4.0	1.14 (0.10)	1.00 (0.08)
Droplets in saline plus Zerdine™	1.5	5.49 (0.24)	–	4.0	–	1.71 (0.01)
Droplets in blood	1.5	5.42 (0.18)	6.09 (0.07)	4.0	–	1.12 (0.05)
Droplets in blood plus Zerdine™	1.5	6.21 (0.16)	–	4.0	–	–

Standard deviation values are given in parentheses.

μm diameter (see top graph in Fig. 9). This could explain quite well the occurrence of the 91- and 108-μm diameter gas bubbles seen in Fig. 8. The bottom graph of Fig. 9 shows the contributions of the individual gases. The gas bubble is completely dissolved after approximately 100 s. In the case of using bubble formation to occlude blood vessels, the lifetime could possibly increase for several reasons. The formation of bubble clouds collected in the vessels may reduce the gas diffusion due to the exclusion of surrounding blood, the reduction of diffusion boundaries (gas-blood interface) and an increasing local concentration of DDFP. Bubbles may coalesce into larger bubbles when in sufficient numbers for bubble-bubble contact. There is likely a reduced diffusibility and/or convection of gases in tissue compared to pure water. However, the flow of fluid around the bubbles may increase the dissolution of bubbles due to the disruption of the concentration gradient in the liquid surrounding the bubbles. The calculations presented here are for the case of a static fluid, which may only exist after the blood flow is reduced, or for the case when it can be considered that the fluid is essentially stationary with the respect to the bubble (bubble substantially moves with the fluid).

It should be mentioned again that very sparse blockage will most likely not affect the tissue because collateral flow compensates for a reduction in the primary supply vessels. In the case of nuclear perfusion scans, macroaggregated albumin particles (MAA) are used as tracers. These particles (26-μm diameter) are clearly larger than capillaries. However, side effects from particles transit to the arterial system by bypassing the capillaries of the lung *via* RL shunts (*i.e.*, vessels that bypass the lung by effectively connecting the right ventricle to the left atrium), have not been detected or are, at least, not common (Potchen and Evens 1971; Davis and Taube 1978).

ADV in simulated in vivo environments

Where penetration is an issue, lower frequencies are generally better for medical applications because layers of sound-absorbing tissue have to be overcome; a typical value for the acoustic attenuation in soft tissue is 0.5 dB MHz^{-1} cm^{-1}. However, in the case of using US for the vaporization of droplets, the pressure threshold for ADV is significantly reduced at higher frequencies, as shown in Fig. 7. To use ADV for *in vivo* applications, one would have to penetrate tissue layers between the US transducer and the target (*i.e.*, the tissue or vessel of interest). The attenuation of a 2-cm tissue path with 0.5 dB MHz^{-1} cm^{-1} acoustic attenuation at 1.5 MHz and 4 MHz is 1.5 dB and 4 dB, respectively. However, because the threshold of ADV at 1.5 MHz is more than 4 times higher than at 4.0 MHz, higher frequencies may, nevertheless, be preferred. Experiments to simulate the *in vivo* situation by overlaying 2 cm of Zerdine™ were performed at 1.5 MHz and 4 MHz.[5] As one would expect, a greater acoustic output was necessary for ADV when Zerdine™ was in place. For droplet emulsions containing 16 mg albumin per mL saline (type A) and tone burst centered at 1.5 MHz, the threshold for ADV increased from approximately 4.78 to 5.49 MPa (*i.e.*, 15%) (see Table 2). For comparison, assuming a linear dependence on peak negative pressure, the theoretical increase due to a 1.5 dB signal amplitude attenuation is 19%. A control measurement for the same range of sound pressures, but in the absence of droplets, was made. The REA remained zero and is interpreted as indicating the absence of detectable bubbles in the host liquid, although some cavitation could be occurring and not be imageable. For ADV in saline, using a droplet emulsion with 1 mg albumin per mL saline (type B) and tone bursts centered at 1.5 MHz, the pressure threshold for ADV was found to be 5.20 MPa (*i.e.*, 9% greater than the type A emulsion with the greater mean droplet size), where the Laplace pressure acting on the droplets is smaller.

At 4 MHz, the pressure threshold for ADV was measured for several cases. For type B droplet emulsion, the threshold increased from 1 MPa peak negative pressure to 1.71 MPa (*i.e.*, a 71% increase, theoretically

[5]The following experiments that simulate *in vivo* environments were performed with recirculation of blood and, for comparison, also recirculation of saline.

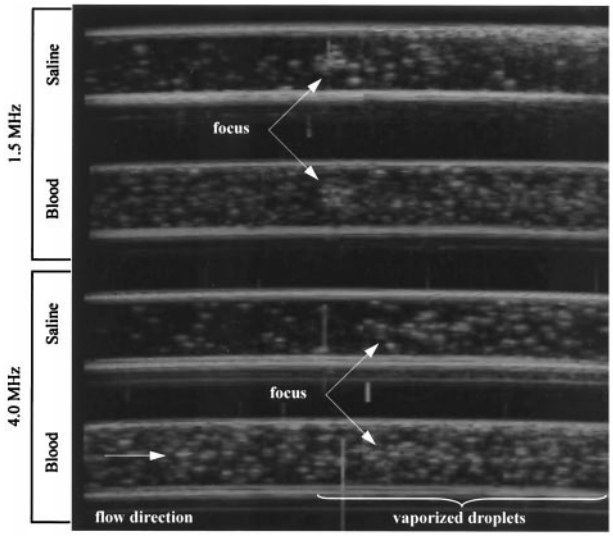

Fig. 10. Grey-scale pictures taken for ADV in saline and blood using tone bursts at 1.5 and 4.0 MHz. One can see the increase in background signal when blood is used as the circulating fluid. However, the vaporization of droplets is still observable, as echogenicity increases above the background signal from blood.

58%), when two layers of Zerdine™ (1 cm each) were mounted in front of the flow tube. This means that we were able to use ADV while penetrating 2 cm "tissue" at 4 MHz. Furthermore, it seems that frequencies of approximately 4 MHz rather than its harmonics at 8 MHz were controlling the vaporization because the increase in threshold was consistent with the overlying attenuation computed for 4 MHz. The threshold for using type A droplet emulsion increased also, but only to 1.12 MPa (*i.e.*, 14%), which is on the order of the standard deviation (see Table 2).

In another series of experiments, the host liquid was changed from saline to heparinized whole blood (50% hematocrit) to achieve a better simulation of the *in vivo* situation. The REA was again measured as a function of sound pressure. Acquired flow tube pictures are shown in Fig. 10. A significant increase of background signal due to the blood was observed. Measurements were taken of REA to determine the threshold of ADV, using tone bursts at 1.5 and 4 MHz. The pressure dependence of REA was evaluated and is given in Fig. 11. The acoustic pressure threshold for ADV at 1.5 and 4 MHz using a 1 mg mL^{-1} droplet emulsion was found to be 6.1 MPa and 1.1 MPa, respectively. At 1.5 MHz, the threshold for a 16 mg mL^{-1} droplet emulsion was measured as 5.4 MPa, 11% less than for the 1 mg mL^{-1} droplet emulsion. Introducing Zerdine™ into the acoustic beam, the pressure threshold increased from 5.4 MPa to 6.2 MPa (*i.e.*, 15%).

SUMMARY

Generating droplets

It has been shown that stabilized droplets can be made from DDFP. The mean size and number density could be changed by altering the droplet's formulation. At the present time, the droplet yield is approximately 30%. The resulting agents, as described here, could

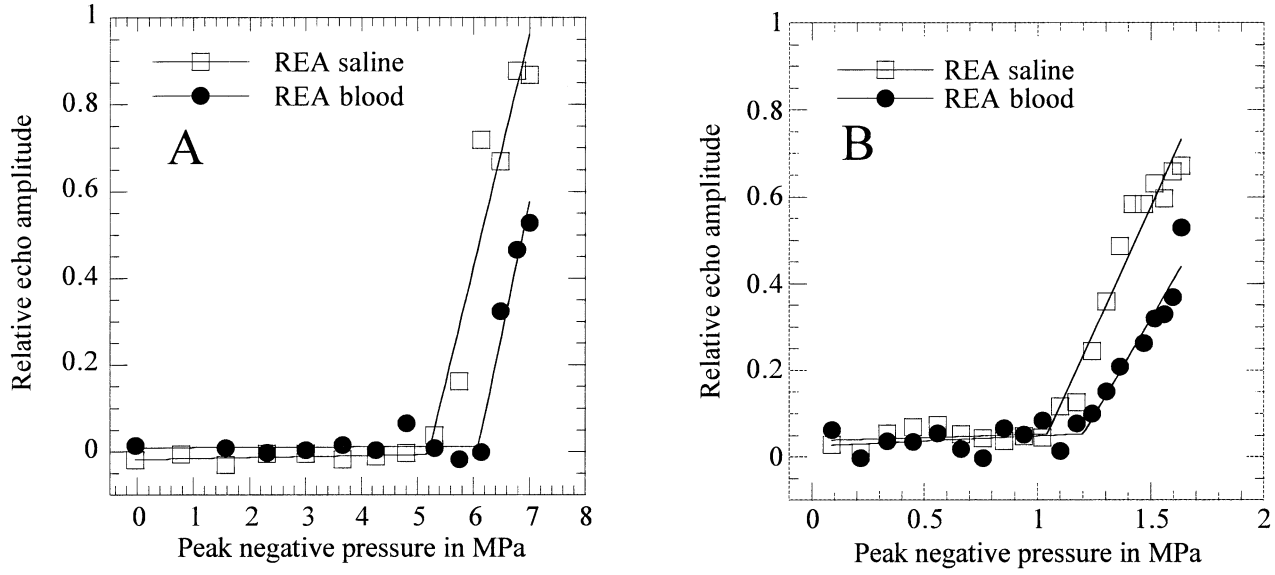

Fig. 11. Acoustic vaporization of droplets in blood using a short tone burst of (A) 1.5 and (B) 4.0 MHz. The relative echo amplitude for ADV was fitted by a least-square piecewise linear function. See Table 2 for thresholds for ADV.

likely be manufactured to be compatible biologically because similar perfluorocarbon liquids are commonly used as blood substitutes (Riess and Krafft 1999) and EchoGen™, an agent of very similar chemical composition, is already in use in clinical trials (Correas and Quay 1996; Quay 1996). Pretreatment and spontaneous evaporation causes EchoGen™ to become an injectable dispersion of microbubbles. Droplets made in our laboratory also show spontaneous conversion, after they are introduced to an environment with a temperature above their boiling point. However, only a small fraction of them boil, leaving stable droplets that are in a superheated state. A pretreatment scheme similar to that of EchoGen™ could eventually be used to limit the possibility of spontaneous vaporization to a nonrisk level at which collateral blood flow can fully compensate for any small-scale temporal occlusion. In addition, human serum albumin (HSA) has also been used to stabilize US contrast agent with perfluorocarbon gas (Optison®, Mallinckrodt Medical, St. Louis, MO). It is expected that droplets of the type described here will also be formed in solutions of HSA, but this has not yet been tested.

Vaporizing droplets

Experiments showed that droplets superheat up to 60°C, well beyond the natural boiling point of pure DDFP of 29°C. Droplets in the superheated state can be vaporized in an acoustic field. Pressure variations in the transmitted acoustic signal showed that an acoustic pressure threshold for ADV exists, and measurements at various frequencies in the range from 1.5 to 8 MHz showed that the threshold apparently decreases with increasing frequency. This leads to a trade-off situation in medical applications, in which overlying tissue attenuation would favor the use of lower frequency US. So far, we have vaporized droplets in simulated *in vivo* environments at 1.5 and 4 MHz. The frequency of choice for real *in vivo* ADV depends on factors such as attenuation by overlying tissues. For the presented case of 0.5 dB MHz^{-1} cm^{-1}, an ADV transducer operating at 4 MHz would be preferable over one at 1.5 MHz, up to a penetration depth of 10 cm.

It has been observed that the acoustic pressure threshold for ADV decreases with increasing frequency, which is opposite to what is known for the frequency-dependence of acoustic cavitation. If acoustic cavitation is not the mechanism by which the droplets boil, the underlying physical mechanism has yet to be determined. There are phenomena in the droplet literature (*e.g.*, deformation of droplets in acoustic fields) that increase with increasing frequency, which might explain the characteristics as seen in our experiments (Tian et al. 1993).

Further investigations are needed to achieve ADV *in vivo* and to study the extent to which blood vessels are occluded from resulting gas bubbles. From a medical point of view, safety issues such as size distribution, number density, and lifetime of the bubbles produced, as well as stability of droplets in the absence of US, are very important.

Furthermore, phenomena warranting study include rate of vaporization and gas bubble size distribution, as well as sensitivity to changes in blood pressure, blood constitution and temperature.

Acknowledgement—This work was supported in part by PHS Grant No. R01 HL54201 from the National Heart, Lung and Blood Institute.

REFERENCES

Apfel RE, Holland CK. Gauging the likelihood of cavitation from short-pulse, low-duty cycle diagnostic ultrasound. Ultrasound Med Biol 1991;17:179–185.

Best CH, Taylor NB. Structure-Function Relations in the Peripheral Circulation. In: West JB, ed. The physiological basis for medical practice 11th ed. London: Williams & Wilkins, 1998:119–123.

Boehm T, Folkman J, Browder T, O'Reilly MS. Antiangiogenic therapy of experimental cancer does not induce acquired drug resistance. Nature 1997;390:404–407.

Correas JM, Quay SD. EchoGen™ Emulsion: A new ultrasound contrast agent based on phase shift colloids. Clin Radiol 1996; 51(Suppl. 1):11–14.

Davis MA, Taube RA. Pulmonary perfusion imaging: Acute toxicity and safety factors as a function of particle size. J Nuclear Med 1978;19:1209–1213.

Di Segni R, Young AT, Zhong Q, Castaneda-Zuniga WR. Embolotherapy: agents, equipment, and techniques. In: Castaneda-Zuniga W, ed. Interventional radiology 3rd ed. Baltimore: Williams and Wilkins, 1997:81–84.

Epstein PS, Plesset MS. On the stability of gas bubbles in liquid-gas solutions. J Chem Phys 1950;11:1505–1509.

Fowlkes JB, Sirkin DW, Ivey JA, et al. Transcutaneous interruption of ultrasound contrast agents for blood flow evaluation. Invest Radiol 1998;33:893–901.

Freiburger PD, Sullivan DC, LeBlanc BH, Smith SW, Trahey GE. Two dimensional ultrasonic beam distortion in the breast: in vivo measurements and effects. Ultras Imag 1992;14:398–414.

Halliday D, Resnick R, Walker J. Fundamentals of physics. New York: John Wiley & Sons, Inc., 1997:485.

Hayduk W, Laudie H. Prediction of diffusion coefficients for nonelectrolytes in dilute aqueous solutions. Am Inst Chem Eng 1974;20: 611–615.

Helps SC, Parsons DW, Reilly PL, Gorman DF. The effect of gas emboli on rabbit cerebral blood flow. Stroke 1990;21:94–99.

Kabalnov A, Bradley J, Flaim S, et al. Dissolution of multicomponent microbubbles in the bloodstream: 2. Experiment. Ultrasound in Med & Biol 1998a;24:751–760.

Kabalnov A, Klein D, Pelura T, Schutt E, Weers J. Dissolution of multicomponent microbubbles in the bloodstream: 1. Theory. Ultrasound Med Biol 1998b;24:739–749.

Kaiser AR, Cain CC, Hwang EY, Fowlkes JB, Jeffers RJ. A cost effective degassing system for use in ultrasonic measurements: The multiple pinhole degassing system. J Acoust Soc Am 1996;99: 3857–3859.

Karaman M, Atalar A, Köymen H, O'Donnell M. A phase aberration correction method for ultrasound imaging. IEEE Trans Ultrason Ferroelec Freq Control 1993;40:275–282.

Kundu PK. Fluid mechanics 1st ed. San Diego: Academic Press, Inc., 1990:638.

Laccourreye O, Laurent A, Polivka M, Wassef M, Domas L, Grasnu D, Merland J. Biodegradable starch microspheres for cerebral arterial embolization. Invest Radiol 1993;28:150–154.

Lide DR. Handbook of chemistry and physics 80th ed. Boca Raton: CRC Press; 2000:8-86–6-190.

Lipton P. Ischemic cell death in brain neurons. Physiol Rev 1999;79: 1431–1568.

Madsen EL, Frank GR, Carson PL, et al. Interlaboratory comparison of ultrasonic attenuation and speed measurements. J Ultrasound Med 1986;5:569–576.

Medwin H. Counting bubble acoustically: A review. Ultrasonics 1977; 15:7–13.

Nakagawa N, Castaneda-Zuniga WR. Transcatheter chemoembolization for hepatocellular carcinoma and other promising transarterial therapies. In: Castaneda-Zuniga WR, ed. Interventional radiology 3rd ed. Baltimore: Williams and Wilkins, 1997:138–163.

Neppiras EA. Acoustic cavitation. Phys Rep 1980;61(3):159–251.

Ng GC, Freiburger PD, Walker WF, Trahey GE. A speckle target adaptive imaging technique in the presence of distributed aberrations. IEEE Trans Ultrason Ferroelec Freq Control 1997;44:140–151.

Ni X, Zhang Y, Mustafa I. An investigation of droplet size and size distribution in methylmethacrylate suspensions in a batch oscillary-baffled reactor. Chem Eng Sci 1998;53:2903–2919.

O'Donnell M, Flax SW. Phase aberration correction using signals from point reflectors and diffuse scatterers: Measurement. IEEE Trans Ultrason Ferroelec Freq Control 1988;35:768–774.

Potchen EJ, Evens RG. The physiologic factors affecting regional ventilation and perfusion. Semin Nuclear Med 1971;1:153–160.

Quay SC. Inventor Sonus Pharmaceuticals, Bothell, WA, assignee. Phase shift colloids as ultrasound contrast agents. USA patent 5,558,853. Sep. 24, 1996.

Riess JG, Krafft MP. Fluorocarbons and fluorosurfactants for in vivo oxygen transport (blood substitutes), imaging, and drug delivery. Materials Res Soc Bull 1999;24(5):42–48.

Sandoval PR, Wingartz PHF, Gonzalez HF. Renal embolization: experience in 81 patients. World Urol Update Ser 1983;11:2–7.

Simons JH, Dunlap RD. The properties of n-pentforane and its mixtures with n-pentane. J Chem Phys 1950;18:335.

Suslick KS, Grinstaff MW. Protein micro-encapsulation of nonaqueous liquids. J Am Chem Soc 1990;112:7807–7809.

Suttiprasit P, Krisdhasima V, McGuire J. The surface activity of α-lactalbumin, β-lactoglobulin, and bovine serum albumin I. Surface measurements with single-component and mixed solutions. J Colloid Interface Sci 1992;154:316–326.

Tian YR, Holt RG, Apfel RE. Deformation and location of an acoustically levitated liquid-drop. J Acoust Soc Am 1993;93:3096–3104.

Unger EC. Inventor ImaRx Pharmaceutical Corp. (Tucson, AZ), assignee. Stabilized compositions of fluorinated amphiphiles for methods of therapeutic delivery. USA patent 5,997,898. 1995.

Unger EC, Fritz TA, Matsunaga T, et al. Inventors ImaRx Pharmaceutical Corp. (Tucson, AZ), assignees. Methods of preparing gas-filled liposomes. USA patent 5,935,553. 1996.

Walker WF, Trahey GE. Speckle coherence and implications for adaptive imaging. J Acoust Soc Am 1996;101:1847–1858.

Yasu T, Schmid-Schoenbein GW, Cotter B. Intravital microscopic study of QW7437, a new dodecafluoropentane contrast agent: Potential mechanisms for prolonged myocardial enhancement. Circulation 1997;96:1181.

Yasu T, Schmid-Schoenbein GW, Cotter B. Flow dynamics of QW7437, a new dodecafluoropentane contrast agent, in the microcirculation—Microvascular mechanisms for persistent tissue echo enhancement. J Am Coll Cardiol 1999;34:578–586.

In Vivo Droplet Vaporization for Occlusion Therapy and Phase Aberration Correction

Oliver D. Kripfgans, *Student Member, IEEE*, J. Brian Fowlkes, *Associate Member, IEEE*, Michael Woydt, Odd P. Eldevik, and Paul L. Carson, *Member, IEEE*

***Abstract*—The objective was to determine whether a transpulmonary droplet emulsion (90%, <6 μm diameter) could be used to form large gas bubbles (>30 μm) temporarily *in vivo*. Such bubbles could occlude a targeted capillary bed when used in a large number density. Alternatively, for a very sparse population of droplets, the resulting gas bubbles could serve as point beacons for phase aberration corrections in ultrasonic imaging. Gas bubbles can be made *in vivo* by acoustic droplet vaporization (ADV) of injected, superheated, dodecafluoropentane droplets. Droplets vaporize in an acoustic field whose peak rarefactional pressure exceeds a well-defined threshold [1], [2]. In this new work, it has been found that intraarterial and intravenous injections can be used to introduce the emulsion into the blood stream for subsequent ADV (B- and M-mode on a clinical scanner) *in situ*. Intravenous administration results in a lower gas bubble yield, possibly because of filtering in the lung, dilution in the blood volume, or other circulatory effects. Results show that for occlusion purposes, a reduction in regional blood flow of 34% can be achieved. Individual point beacons with a +24 dB backscatter amplitude relative to white matter were created by intravenous injection and ADV.**

I. Introduction

PERFLUOROCARBONS are in increasing demand as agents in medical imaging. They are used as gas inside of contrast agent (CA) gas bubbles for ultrasonic imaging and as tracers for magnetic resonance imaging. This paper will make use of the effect that superheated micrometer-sized droplets can be vaporized into larger gas bubbles inside the body. In particular, the use of that effect for two applications will be investigated. When vaporized in large quantities up stream of the capillary level of tissue, these gas bubbles are likely to become trapped where the arteries narrow in diameter to arterioles and capillaries. For cancer tissue, this effect of blood flow blockage is called occlusion or embolotherapy. The second application is ultrasonic image enhancement. The vaporization of very few droplets into gas bubbles could create reference objects whose theoretical backscatter can be compared with the actual, *in situ*, backscatter, and discrepancies between the two can be used to correct for image distortions. These and other uses such as localized drug delivery are covered in a patent by Apfel [2].

Manuscript received August 15, 2001; accepted December 17, 2001. This work was supported in part by PHS Grant No. R01 HL54201 from the National Heart, Lung and Blood Institute and the US Army Medical and Materiel Command under grant no. DAMD17-00-1-0344.

O. D. Kripfgans, J. B. Fowlkes, O. P. Eldevik, and P. L. Carson are with University of Michigan Health Systems, Department of Radiology, Ann Arbor, MI 48109-0553 (e-mail: fowlkes@umich.edu).

M. Woydt is with University of Würzburg, Neurosurgery, Joseph-Schneider-Straße 11, 97080 Würzburg, Germany.

A. Perfluorocarbons

Perfluorocarbon, one of the six greenhouse gases, is used in industry for acoustic coupling, for leak detection, and as a sealant [3]. It is also used in medicine and biology as an oxygen carrier, for liquid ventilation [4], as a blood substitute, and for dissolution of thrombotic arterial occlusions [5]. Emulsions such as Oxygent^{TM} (Alliance Pharmaceutical Corp., San Diego, CA) are used for immediate blood substitutes. Oxygent^{TM} is a perflubron-based emulsion of tiny particles (about 0.2 μm in diameter vs. about 7.0 μm for red blood cells). The small size of the particles may enable them to travel around blockages in vessels or into very distant capillaries [6], [7]. Microbubbles such as Echovist® (Schering Aktien Gesellschaft, Berlin, Germany) and Albunex® (Mallinckrodt, Inc., St. Louis, MO) have been used as ultrasound CA for 20 years, and the first observation of the contrast-enhancing effect of micro gas bubbles dates back to Gramiak and Sham's paper from 1968. Quay [8] and Correas and Quay [9] reported a phase shift ultrasound contrast media comprising perfluoropentane and perfluorohexane gas. Their emulsion (EchoGen^{TM} [SONUS Pharmaceuticals, Inc., Bothell, WA]) is administered intravenously and is converted into gas bubbles (2 to 5 μm in diameter). The conversion is due to the body temperature, which is above its boiling point, and pre-injection decompression in the syringe. Emulsions of lipid-encapsulated liquid perfluorocarbons, with similar size to the blood substitutes, have been studied by Lanza *et al.* [10]. The agent was found to be suitable for ultrasonic image enhancement of targeted pathology and a magnetic resonance imaging CA [11].

B. Embolotherapy

Embolotherapy utilizes materials that can be categorized as absorbable (blood clot, cellulose, and gelatin sponge) and non-absorbable (particulates, fluids, coils, balloons, and streamers). Particulates can be as large as 50 μm in diameter. Currently, occlusive therapy is used for cancer treatment, including renal and hepatocellular carcinoma. According to Sandoval *et al.* [12], kidney tumors

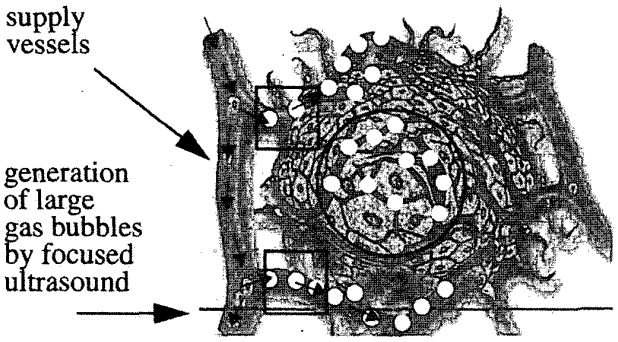

Fig. 1. Schematic for embolotherapy applied to a tumor. Focused ultrasound can be used to generate large gas bubbles (>30 μm in diameter) from an injected droplet emulsion potentially to locally occlude malignant tissue. Droplets could be vaporized in the supply arteries (indicated by the squares) or in the capillary bed (indicated by the circle) of the tumor. (Adapted with permission from [13]).

were successfully embolized and displayed tumor necrosis after the first embolization in 78% of the cases studied.

Intravenous injection of a transpulmonary, inherently inert, droplet suspension with localized vaporization would require no arterial catheterization for *in situ* placement of potentially embolic materials. Localization of the treatment would be achieved by using a focused, non-ionizing radiation source, such as a sound field produced by a existing diagnostic ultrasound scanner or a specialized unit. For tumors with well-defined arterial supply vessels, those vessels could be insonified by ultrasound (squares in Fig. 1) to create large gas bubbles that would block the blood flow at the capillary end or small arteriolar level. For tumors with less defined or accessible supply vessels, the capillary bed itself could be treated with ultrasound and subsequent bubble formation (circles in Fig. 1).

It is obvious that the intended and even more unanticipated generation of large gas bubbles in the human body results in possible embolization of vessels other than the region of interest. Therefore, the bioeffects of this treatment are a major consideration.

Arterial air emboli are not uncommon in clinical procedures. They can be found in 15 to 50% of all patients after closed-chamber procedures and in virtually all patients after open-chamber heart surgery [14]. Padayachee *et al.* [15] investigated the use of inline filters to remove arterial micro gas bubbles, and Dexter *et al.* [16] studied absorption rates of microscopic arterial air emboli during cardiac surgery. For damage to the blood-brain barrier (BBB) in cat brain from physical pressure differences, Fritz *et al.* [17] divided ischemia into three groups: complete ischemia, microembolisms, and air embolism. The first two in this group constitute extreme situations. In the first case, there is apparently no damage to the BBB for total interruption of the blood flow to the brain, even when other barrier breakers supervene. The second situation is the blockage of a small number of capillaries with 15-μm spheres, which is directly followed by BBB damage. Air embolism (<30 min; 370 μL·kg^{-1}), the third part in the group, is not likely to lead to barrier lesions in the observations by Fritz *et al.* However, the same paper reports that BBB damage has been observed in the past after embolization with air.

The effects of the amount of air introduced to the body have been studied by Helps *et al.* [18]. Four hundred microliters of air were infused into the left internal carotid artery of a rabbit, which caused suppression of the cortical somatosensory (evoked) response and a progressive decline in ipsilateral cerebral blood flow. This process required the presence of leukocytes. An injection of 5 μL of air (corresponding to a single 2.5-mm diameter bubble) into rat brain showed no consistent change in blood pressure in a study by Johansson [19]. Davis and Taube [20] reported safety factors as a function of particle size in a study on pulmonary perfusion imaging. They suggest following FDA (Food and Drug Administration) guidelines, which recommend an intravenous injection of <250,000 particles per patient, with virtually all particles in the range from 10 to 50 μm. This recommendation prevents overload of all but highly compromised pulmonary vasculature and has limited or no effect in cases of small cardiac septal defects (see for example FDA approval of the use of Technetium-99m-MAA (macroaggregated albumin) for imaging of vascular beds [21]). It has been found that micro emboli resulting from cardiac surgery were essentially suppressed by the use of a 25-μm filter, which showed a 100% cut-off at 50 μm. For cases in which filters were not used, Dexter *et al.* reports (maximum) dissolution rates of large single gas bubbles of the order of 1.6 μm·s^{-1}. This value was found in numerical simulations of the gas bubble diameter as a function of time.

More kinetical studies on air embolisms in the brain and possible therapies have been published by Annane *et al.* [22]. After the injection of 0.5 mL of air into ~12-kg canines, the effects of mechanical ventilation with normobaric oxygen therapy were evaluated. The results showed a three times higher rate of air removal from cerebral arteries than with breathing room air at a low respiratory rate. Cochran [23] and Menasché [24] as well as Spiess [25] reported a reduction of neurologic injury after cardiopulmonary bypass through the injection of a perfluorocarbon emulsion.

Although the introduction of air into the circulatory system bears risks for the patient, it is a well-studied area because it is a common effect in medical practice, such as in heart surgery. For cancer treatment, it seems to be a favorable agent for occlusion therapy when applied in reasonable concentrations and targeted in space as well as in time.

C. Phase Aberration Corrections

Ultrasonic image formation and reconstruction from structures at some depth in the human body can be difficult. This is the case when the volume of interest (VOI) is overlaid by layers with varying thicknesses of nonidentical acoustic wave velocity. Sound waves emitted by an imaging array do not focus in the VOI because the individual

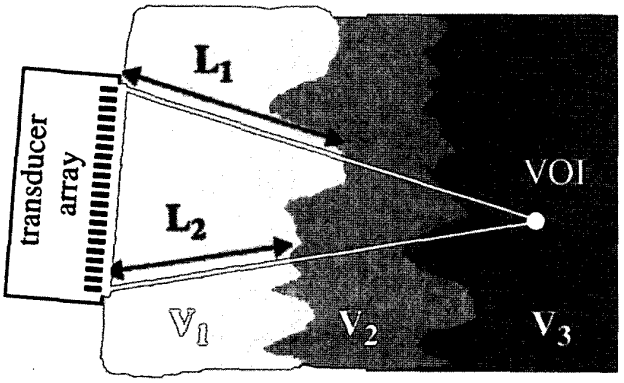

Fig. 2. Example of phase aberration with a linear array. Two effects cause a blurry image. Emitted sound waves do not focus at the VOI, as the transmit phases of individual elements are miscalculated, because the assumption of uniform speed of sound through tissues of differing sound speeds and thicknesses (shown here for propagation paths L_1 and L_2). The same computational error occurs when received sound waves are coherently added. The signals from the various array elements are lined up according to their time of travel, and the corresponding image is reconstructed.

path length, i.e., time of travel multiplied by the speed of sound, is over- or underestimated (Fig. 2).

Extensive research has been published on phase aberration correction methods. Non-invasive approaches include corrections for aberrating layers near the array and for near field speckle statistics. The latter often postulate a statistical spectral distribution of the tissue background (also known as speckle scattering). For example, deviations from that distribution can be used to correct for phase aberrations. Recent investigations include complex algorithms based on near field signal redundancy and shifted multi transmit subapertures [26]–[30].

The following section discusses methods that could be used with a beacon because that is one of our proposed medical applications for ADV. O'Donnell and Flax [32] demonstrated an iterative method that can be used with diffuse scatterers in the near field, correcting for phase errors up to 7 pi rad in an autofocus fashion. However, the authors suggest using a beacon, if available, to estimate the phase error. Image quality factors and their ability to correct phase aberrations were introduced by Zhao and Trahey [33]. For small regions of interest (ROI), point targets with a priori knowledge can be used to employ the mean brightness of the echo amplitude as a measure of image quality. The placement of several beacons and an extension of the algorithm for multiple beacons might make this technique work on larger ROIs as well.

In a paper by Freiburger *et al.* [31], phase aberration corrections are divided into three categories: zero-order corrections, which essentially compensate for a general speed of sound other than 1540 $m \cdot s^{-1}$ or any other assumed value; first-order corrections that adjust the time delays of each element of an array to compensate for aberration effects in the near field, not in the far field, where simple time delays cannot correct for phase aberration image distortion; and second-order methods, which are employed for environments with distributed aberrators for either near or far field. This last category includes time-reversal mirror (TRM), missing signal compensation, back propagation, and translating apertures. This grouping might be superficial relative to newer methods and algorithms. However, it illustrates the underlying physical artifacts of phase aberration in medical imaging. The remainder of the paper by Freiburger demonstrates a parallel processing technique for speckle brightness based on real time image correction. The authors showed that their algorithms perform well in removing phase aberrations when operating on point targets such as 0.23-mm nylon filaments, which were imaged in cross-section at 3.9 MHz. The concept of TRM has been studied for the last 10 years [34]. A three-paper publication by Fink [35] reports basic principles and experimental results of TRM. This research shows that point targets can be used for phase aberration correction in ultrasonic imaging, for example when focusing ultrasound on kidney stones in lithotripsy applications. Their focusing process can be iterated to work on several point beacons.

Other methods compute the angular spectrum, i.e., the beam shape, to identify and correct phase aberrations. Liu *et al.* [36] reported a compensation method working on waveforms emitted by point-like sources.

The vaporization of droplets into gas bubbles on a low number density scale suggests their use as beacons for phase aberration correction. Gas bubbles with diameters less than 50 to 250 μm ($ka < 0.5$) essentially scatter sound omnidirectionally, i.e., like a point scatterer, for frequencies between 5 and 1 MHz, respectively (more refined criteria are given in [37]). A separation of three standard deviations between the pulse echo signal and noise would thus correspond to 10 dB. This is due to speckle statistics, in which the standard deviation of the signal is of the same order as the signal itself.

This paper will test whether large gas bubbles, made by the acoustic vaporization of albumin-stabilized dodecafluoropentane droplets, are feasible to serve both as point beacons, with a large enough backscatter amplitude for phase aberration correction, and for aid in the local occlusion of tissue by providing a gas body that lasts long enough to cause ischemia.

II. Materials and Methods

A. In Vitro Experiments

The existence of an acoustic pressure threshold for ADV and its functional dependence on the frequency of the transmitted pulse has been shown previously [1], based on the droplets also used here.

A matched set of transducers was used to repeat these experiments on the threshold for ADV to verify the previous results under more controlled circumstances. Ultrasound images taken during ADV in flow tube experiments

were used to analyze the rate of vaporization as a function of applied acoustic pressure and frequency. The flow was imaged along the axis of the flow tube using a 10-MHz, linear array scan head of a clinical ultrasound scanner (Diasonics VST series, Milpitas, CA). Four transducers (A381S, A321S, A305S, and A308S; Panametrics Inc., Waltham, MA) with center frequencies ranging from 2.25 to 7.5 MHz, 2.54-cm (1-inch) apertures, and 3.81-cm (1.5-inch) foci were used to test for ADV over a frequency range from 2 to 10 MHz. A more detailed description of the setup can be found in [1]. An optical microscope, with an attached CCD camera (Nikon SMZ-U, Melville, NY) and a Kodak strobe light system [12-Hz PRF (pulse repetition frequency)] were used to image individual gas bubbles made from droplets by acoustic vaporization. The bubble size distribution was measured by image analysis [1].

B. In Vivo Experiments

In an acute study, 12 adult canines (mongrel, 20 to 30 kg) were used to verify ADV *in vivo*. The animals were premedicated with 0.8 mg·kg^{-1} ace-promacine maleat (Acepromacine®, Vedco, St. Joseph, MI) subcutaneously 15 min prior to induction. After placing an intravenous line, thiopental sodium (Pentothal®, Abbott Lab., Chicago, IL) was given intravenously at 20 mg·kg^{-1} for induction of anesthesia. The intubated canine was placed in supine position and connected to a forced ventilator (Ohio 7000, Ohio Medical Products, Madison, WI). The ventilation was maintained at a level that was adjusted to acquired appropriate blood gas levels. Anesthesia was started with 2% isoflurane (Isoflurane USP®, Abbott Lab., Chicago, IL) in 2 L of room air and 350 mL oxygen for 5 min, reducing to 1% isoflurane 30 min prior to the ADV experiment.

An arterial pressure monitoring device (Mennen Medical 742, Mennen Medical Inc., Clarence, NY) was placed in the left femoral artery. The same system monitored the electrocardiogram (ECG). In four canines, the right femoral artery was dissected to insert a 1.67-mm (5 Fr) angiographic catheter (Cook Com., Bloomington, IN), which was pushed up to either the right renal artery or in the left ventricle under fluoroscopy guidance. Oxygen saturation and esophageal temperature were recorded continuously with a pulse oxymeter (Nonin 8600 V, Nonin Medical Inc., Minneapolis, MN) at the tongue and a thermocouple probe (Omega DP 41, Omega Engineering Group, Stamford, CT).

All animal procedures were reported to and approved by the office of the University Committee on Use and Care of Animals of the University of Michigan.

C. Abdominal Tissue

The kidneys were chosen to investigate the possible vaporization of droplets in highly vascular tissue. An abdominal incision was made to externalize both kidneys (midline laparotomy). Droplet emulsion could be injected intraarterially into the right renal artery through the previously mentioned catheter. The acoustic field for ADV was applied in either the renal artery or in the cortex and with the anticipated detection of gas bubbles in the capillary bed of the kidney. ADV was also examined in the left kidney, where droplets should be found only after recirculation, i.e., transition through the capillaries of the kidneys and the lungs. A Toshiba Power Vision 6000 clinical ultrasound scanner was used to image the kidneys before and after the administration of droplets [9 MHz; mechanical index (MI) of 0.6]. A linear array was used to focus to a depth of 30 mm. This path included an approximately 10-mm fluid path through saline, used for coupling purposes.

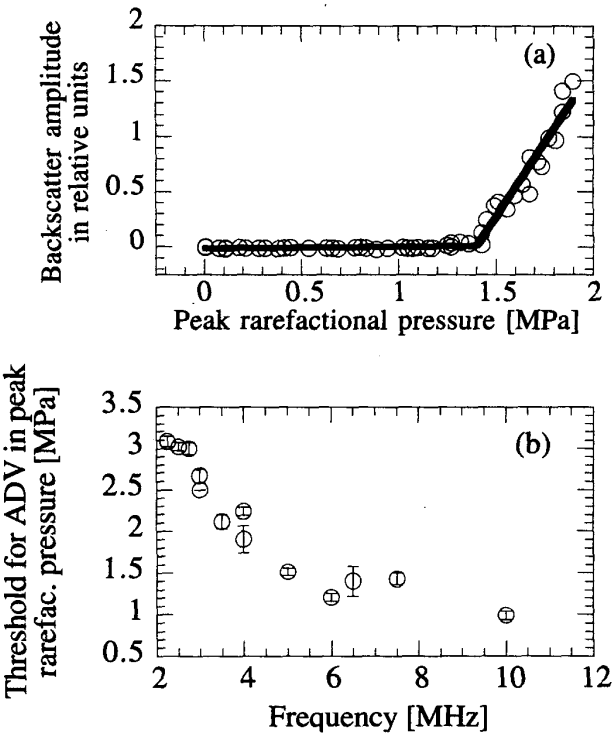

Fig. 3. a) At 7.5 MHz, the threshold for acoustic vaporization of droplets is approximately 1.5 MPa peak rarefactional pressure (P-). At lower pressures, droplets rarely, if ever, boil into gas bubbles. Therefore, ultrasonic images of the area to be treated can be taken at pressures below 1.5 MPa P-. The threshold for ADV is a function of frequency; it rises with decreasing frequency (b).

D. Brain Tissue

For observations of the brain, the skull was opened by a standard bilateral craniotomy. The brain was used as a model because brain tissue has modest acoustic attenuation ($\leq$0.5 dB cm^{-1}·MHz^{-1}) [38] and provides good conditions for initial tests on ADV *in vivo*. Intravenous and intraarterial injections were used to administer $\sim 10^7$ and $\sim 10^6$ droplets, respectively. For occlusion therapy, a coronal slice of the brain was treated with M-mode, and the ipsilateral side of the brain served as a reference. The ul-

trasound procedure involved exposing with M-mode for 180 s while manually sweeping the M-mode line. Three contiguous planes of tissue centered on the selected ROI were treated in this fashion with the separation of the three planes chosen equal to the elevational beamwidth (see subsequent calibration) of the transducer array as measured in M-mode. Colored microspheres (NuFLOW fluorescent microspheres, dosage of 10^5 spheres per kg, 15-μm sphere diameter; Interactive Medical Technologies, Ltd., Irvine, CA) were injected in the right ventricle via an arterial catheter to measure the change in regional blood flow. Two different colors were injected, one before and another after the treatment. Following euthanasia, the treated volume as well as reference volumes (approximately 10 mm $\times$ 10 mm and 3 mm thick) were dissected. The two samples were processed by a commercial laboratory to dissolve the tissue and count the trapped microspheres. Flow cytometry yields the concentration of the spheres in tissue samples along with that contained in reference blood samples to estimate the regional perfusion. The reduction in perfusion was computed by taking the ratio of the regional blood flow after ADV to that measured before ADV.

As in the kidney study, a Toshiba Power Vision 6000 clinical ultrasound scanner was used. This time the scanner was operated at 6 MHz for treatment purposes and at 9 MHz for imaging. The penetration depth into the tissue was 10 mm based on the range at which effects of ADV were seen, and, for focusing purposes, a 10-mm stand-off pad (AquaFlex, Ultrasound Gel Pad; Parker Laboratories, Fairfield, NJ) was used to set the focus to 20 mm. The acoustic output of the scanner was measured in water for M-mode at maximum acoustic output and 6-MHz center frequency using a planar hydrophone (Reference Shock Wave Hydrophone^{TM}, Sonic Industries, Hatboro, PA). A 3-D volume scan of the center M-mode line indicated an elevational and lateral beamwidth of 1.43 $\times$ 1.14 mm [full-width at half-maximum (FWHM)] which was found at a depth of 20 mm. The acoustic pressure at this depth was approximately 3-MPa peak rarefactional pressure.

Additionally, a Diasonics MasterSeries clinical scanner was used to image the brain after the formation of point beacons. For this scanner, a radio frequency (rf) line output was available, which provided raw data prior to the time gain control (TGC). The study on the formation of point beacons and their scattering strength was compared with ultrasound CA (MP1950, Mallinckrodt Medical, St. Louis, MO) administered intravenously at 0.1 μL$\cdot$kg$^{-1}\cdot$min^{-1}. For any generated point beacon, the rf line was envelope-detected, and the corresponding amplitude ($a_{\text{gas bubble}}$) was compared with the tissue signal (a_{tissue}), which was present before the droplet reached that location and before the droplet was vaporized.

The resulting value is normalized for differences in the gain setting on the ultrasound scanner and averaged across multiple point targets.

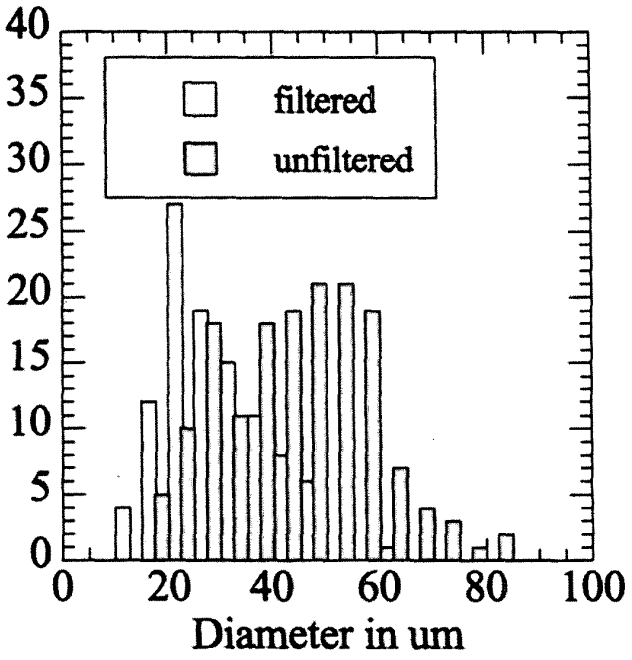

Fig. 4. Size distribution of gas bubbles formed by acoustic vaporization of droplets. A focused, 10-MHz single element transducer was used, sending a 1-MPa P-, 33-cycle tone burst at a PRF of 200 Hz. The experiment was performed for filtered and unfiltered DDFP emulsions. A 5-μm syringe filter disc was used to limit the size distribution of the emulsion to approximately the size of capillaries.

III. Results

A. In Vitro Verification of ADV

ADV has been successfully repeated and continues to exhibit a sharp threshold [Fig. 3(a)]. For a transmit frequency of 7.5 MHz, the pressure threshold for ADV is approximately 1.5 MPa peak rarefactional pressure (P-). Fig. 3(b) shows how the pressure threshold for ADV decreases with increasing frequency from $\sim$3 MPa P- at 2 MHz to less than 1 MPa P- at 10 MHz. Despite the frequency-dependent attenuation in tissue, this trend suggests the use of higher rather than lower frequencies for ADV *in vivo*. At a strict 0.5 dB MHz^{-1} cm^{-1}, there remains some advantage for higher frequencies for ADV up to 2.7 cm depth. A curve fit of the pressure threshold for ADV as given in Fig. 3(b) of the form $a\cdot 10^{b\cdot x}$ yields $a = 3.98$, $b = -0.154$, and $R^2 = 0.896$. This corresponds to a 1.34 dB MHz^{-1} decrease in threshold with increasing frequency. *In vitro* experiments showed gas bubble sizes of the order of 30 to 60 μm in diameter (Fig. 4).

B. Embolotherapy—In Vivo B-Mode

As a first step, the acoustic vaporization of an intraarterially-injected droplet emulsion was attempted using the Toshiba scanner in B-Mode at 6 MHz. Approximately 3.3 $\times$ 10^6 droplets were injected intraarterially, and

subsequent insonification of a region in the white and gray matter yielded a dense and spatially stationary gas bubble formation in the VOI [Fig. 5(b)]. It should be noted that a small, relatively uniform increase in echogenicity of the monitored region was observed while injecting the droplet emulsion.

C. Embolotherapy—In Vivo M-Mode

M-mode was used to limit ADV to one line in the scan plane or to a region that was scanned by manually sweeping the M-mode line across that region (Fig. 6). For the case in Fig. 6, the perfusion on the left side of the brain was reduced by up to 34% relative to the untreated area on the right side of the brain. In the four cases studied, an average reduction in regional perfusion of $21.2 \pm 11.2\%$ was found. However, these four cases included one case that actually lead to an increase in blood flow! Discarding that case, the average reduction was $32 \pm 1.3\%$. (See the discussion for possible explanations for the lack of complete occlusion.)

The region was then imaged for ~20 min after the formation of gas bubbles. Analysis of the average pixel intensity in a selected area (Fig. 7) showed decay rates of the relative echogenicity in that area of approximately 0.24 $dB \cdot min^{-1}$.

D. Spontaneous Evaporation

Acoustic imaging at low MI apparently did not vaporize injected droplets because even the intraarterial injection of a 10-fold increase in concentration showed very little gas bubble formation in the presence of B-mode imaging at an MI of 0.2. This is consistent with the *in vitro* results, where a pressure threshold for ADV was observed.

E. Point Beacons—Kidney Cortex

Singular echogenic regions that might be suitable as point targets were first observed in the medulla of the right kidney. Presumably, individual gas bubbles were imaged, as they traveled through the cortex of the kidney. Fig. 8 shows the traces of three gas bubbles. Each trace is approximately 5 mm long.

The echogenicity of gas bubble point targets from droplets was analyzed and compared with the background tissue, which was recorded before the droplet emulsion was injected. A scatter amplitude of 5.19 ± 0.059 times kidney cortex was found, which corresponds to 14.3 dB. Similarly the scatter amplitude of CA was found to be 9.1 dB above the kidney cortex. However, the CA data were collected from a highly filled capillary bed, which might not be suitable as a point target. The imager was then repositioned over the left kidney, which was not administered with droplets other than by recirculation. The creation of gas bubbles was observed as soon as the acoustic output of the imager was increased from an MI of 0.2 to 0.6, corresponding to a level of 3.1 MPa P- at the focus, as measured in a free-field calibration.

F. Point Beacons—Cerebral Cortex

Similar to the observations in the kidneys, a formation of sparse gas bubbles was anticipated after intravenous injection of approximately 200,000 droplets/kg. A 10-MHz linear array operating at 7 MHz was used in B-mode to first image the ROI at low amplitude and then vaporize the injected droplets by increasing the acoustic output beyond threshold. Fig. 9 shows a coronal slice between frontal and parietal lobes of the brain before and after ADV. Radio frequency data from individual B-mode scan lines was analyzed for the scattering strength of the formed gas bubbles as described in Section II. The backscatter amplitude of large gas bubbles made by the vaporization of droplets was found to be a factor of 14.5 ± 0.66 greater than tissue background, which corresponds to 23 dB (Fig. 10).

For comparison, ultrasound CA (MP1950) was infused intravenously at 0.1 $\mu L \cdot kg^{-1} \cdot min^{-1}$. Image analysis (Fig. 11) yields an average scatter amplitude of 2.24 ± 0.42 times tissue background, which corresponds to 7 dB. Fig. 12 shows the rf A-mode line for a CA scatterer.

IV. Discussion

A. In Vitro Verification of ADV

The frequency-dependent threshold for ADV as shown here differs somewhat from the results shown in [1]. It is believed that the generally higher threshold is due to the greater focal gain of the transducers used in the present study, because this is the only substantial difference between the two studies. The focal dimensions (FWHM) ranged from a 3 mm diameter, 19 mm length at 2.25 MHz down to 1 mm diameter, 9 mm length at 7.5 MHz. More physical insight into the mechanism of ADV is necessary, especially why and how focal gain changes the pressure threshold for ADV.

Gas bubbles as observed in *in vitro* experiments (Fig. 4) should be large enough to block capillaries [20].

B. Embolotherapy

As mentioned in Section III, a small and uniform increase in echogenicity in the imaging plane was observed while injecting the droplet emulsion. First, this is due to the small, but non-zero echogenicity of the droplet emulsion itself [11]. Second, a small number of droplets may undergo spontaneous evaporation in the vasculature or at the arterial injection site because of the pressure drop between syringe and artery if injected too fast.

C. In Vivo M-Mode

Focal occlusion using M-mode ultrasound showed a maximum reduction in regional blood flow of only 34%.

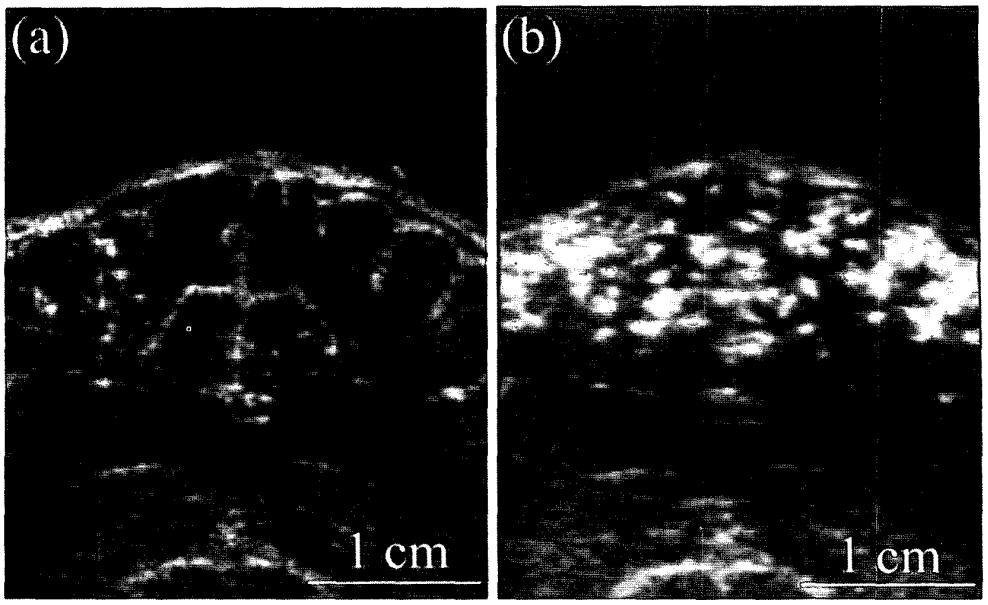

Fig. 5. ADV in occipital region (at the back of the brain, posterior to the parietal lobe). The droplets were vaporized using B-mode at 6 MHz. a) The region before ADV; b) some time after ADV. A 0.3-mL droplet solution was injected intraarterially over 2 min (total = 3.3×10^6 droplets). The image format differs because of the change in frequency between the treatment performed at 6 MHz and imaging at 9 MHz.

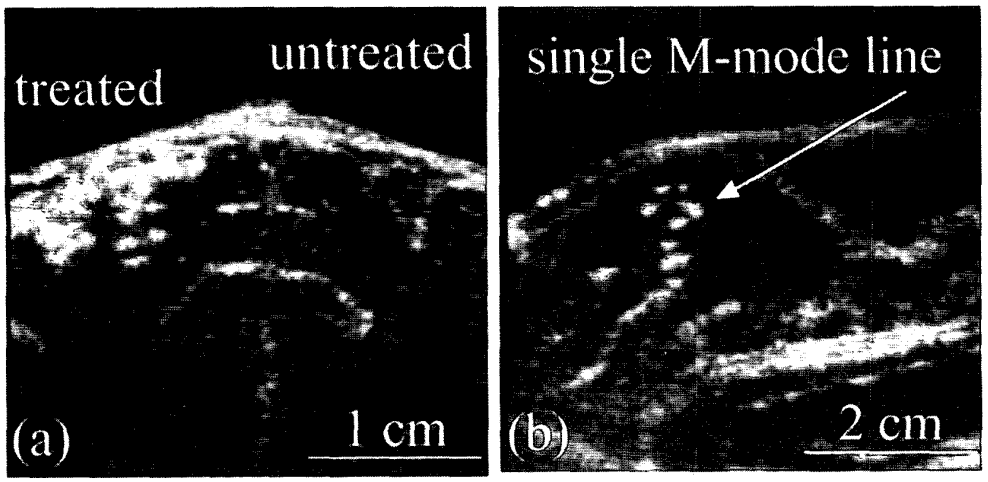

Fig. 6. Tissue occlusion in the occipital lobe. Droplets were vaporized using M-mode at 6 MHz (see arrows) during an intraarterial infusion of a 0.3-mL droplet solution over 2 min (total = 3.3×10^6 droplets). a) Coronal view with a swept M-mode line to cover a plane (treated area) of tissue. For the next 30 min, this region was scanned to monitor the gas bubble lifetime. See Fig. 7 for the integrated echogenicity of a particular region plotted as a function of time. b) Sagittal view of single M-mode line.

We believe that a potential source of error for the microsphere analysis is the location and dissection of treated tissue. If the extracted tissue volume is larger than the actual treated region, the average reduction in perfusion will differ from the true reduction in the treated region. By treating a large and continuous volume of tissue, one could ensure the dissection of only 'occluded' tissue and measure the maximum possible effect. An alternative method for estimating the spatial extent of perfusion reduction is by histologic sectioning. After the injection of colored microspheres or particulate dye suspensions at high concentration, one could find regions of no or suppressed perfusion. The use of dye is probably the better choice. Colored microspheres might be too low in number density on the histologic section slides (in our case it is estimated at 0.1 spheres per slide!).

A possible counteragent for the use of dodecafluoropentane (DDFP) emulsion for occlusion therapy is the property of the perfluorocarbon droplets to carry oxygen [6], [7]. The DDFP emulsion has very small particles (<1 μm

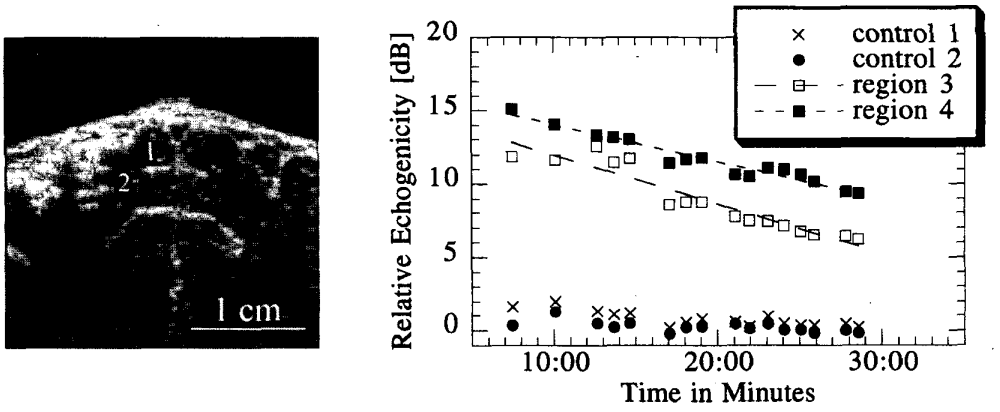

Fig. 7. 'Lifetime' of gas bubbles made by ADV. The treated region is shown in Fig. 6. The echogenicity is plotted as a function of time relative to the intensity of the same region before ADV.

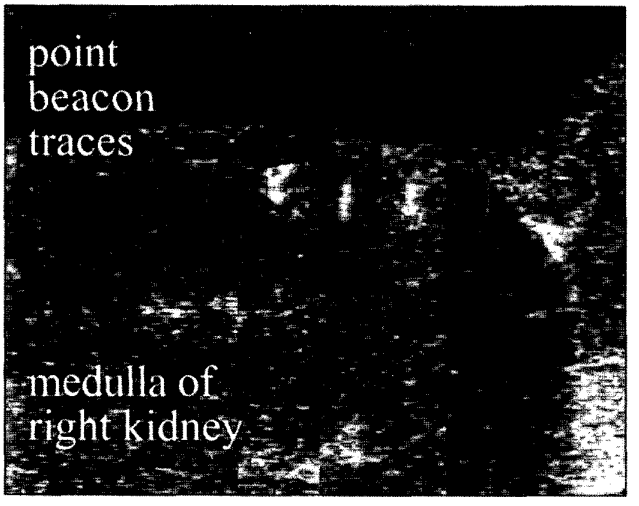

Fig. 8. Traces of three gas bubbles made from injected droplet emulsion as they travel through the cortex of the externalized right kidney. The image shows the superposition of three traces acquired at three different times. These traces are visible as vertical lines inside the ellipse. Single point targets appear as single spots such as in Fig. 9(b). Through the overlay of images at successive times, a trace forms (as shown).

diameter), which might reach even occluded capillaries, where the "occlusion" is relative to the size of red blood cells. This means that a treated region is still perfused as long as these micro particles, in sufficient concentration, are able to deliver oxygen.

The longevity of gas bodies formed by ADV was estimated from the decay of their acoustic backscatter. It is assumed that this decay is due to the dissolution of larger bubbles and subsequent wash-out of bubbles small enough to pass the capillaries. Measurement of the decay in echogenicity for gas bubbles after ADV will require a more elaborated study. A benchtop *in vitro* experiment with optical and acoustical observation of single gas bubbles would give the functional relationship between decay of echogenicity and decrease in size. The knowledge of

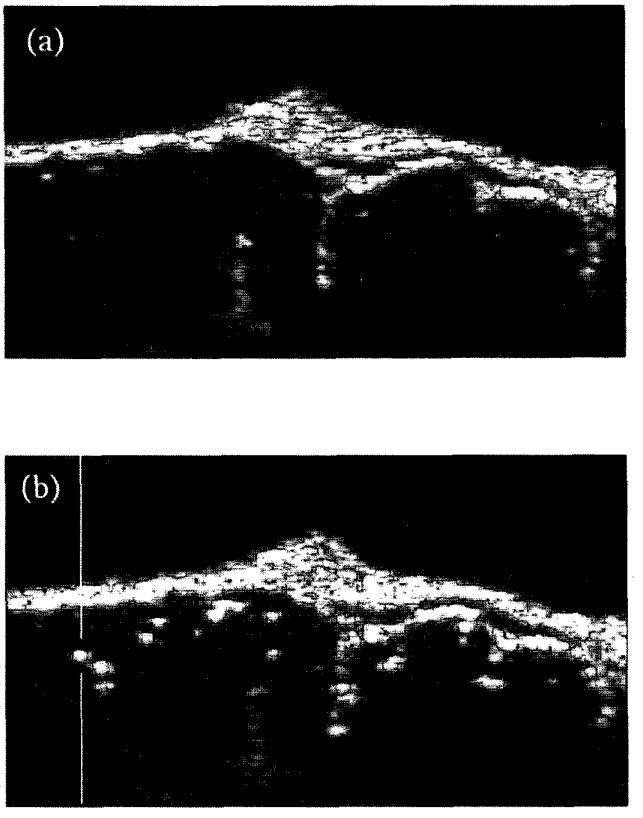

Fig. 9. a) Canine brain, prior to ADV; coronal slice between frontal and parietal lobe. b) ADV with clinical scanner, linear array at 7 MHz center frequency, B-mode. The dashed line indicates a sample rf trace, which was analyzed for the scattering strength of the beacon and is shown in Fig. 10. It should be pointed out that the number of beacons per unit volume could easily be reduced by spatially selective ADV using M-mode and, of course, by dilution of the administered agent.

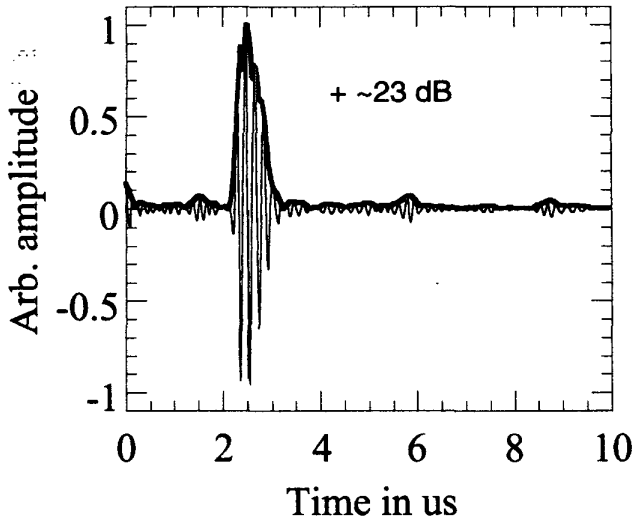

Fig. 10. rf line through a large gas bubble point beacon.

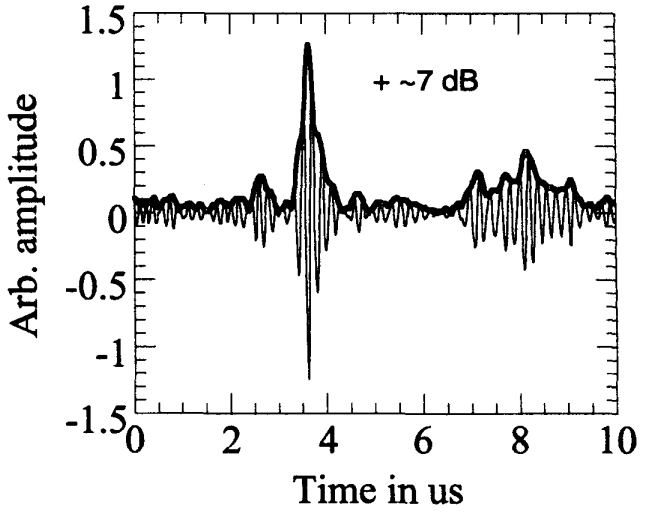

Fig. 12. rf line through CA point beacon.

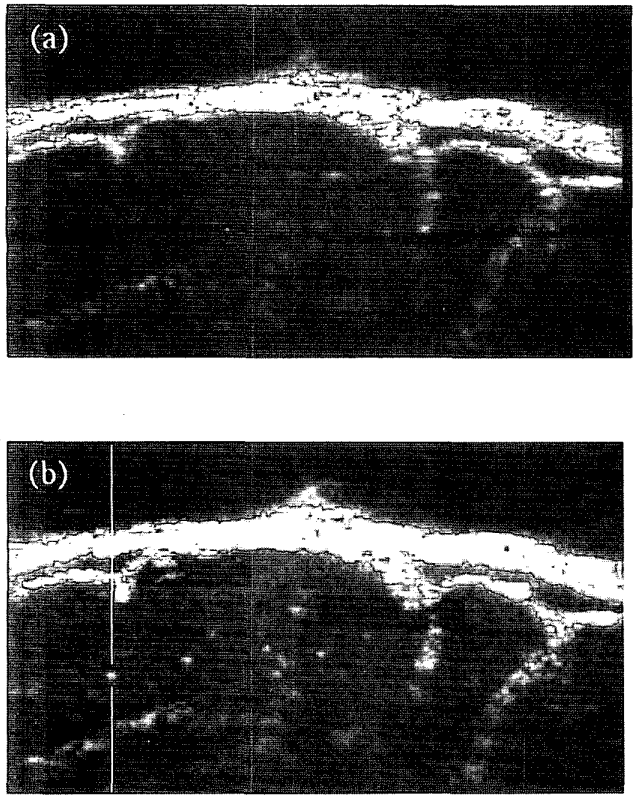

Fig. 11. a) Canine brain, prior to CA injection; coronal slice between frontal and parietal lobe. b) Formation of several point beacons can be seen after CA administration. As in Fig. 9, the dashed line is as a sample rf trace shown in Fig. 12.

that relationship would help to predict how long occlusion by ADV might be effective. However, the qualitative yield from the presented experiments is that the gas body is large enough not to be carried away in the blood stream.

It is essential to know how much reduction in regional blood flow (and duration) is necessary to compromise the tumor to be treated. We use values given for brain cells as landmark values. A vast amount of literature and a very nice review is given by Lipton [39]. He describes how focal ischemia develops in contrast to global ischemia. The former one produces a contiguous mass of damaged brain tissue termed an infarct, whereas global ischemia, interestingly enough, leads to isolated regions with neuronal cell death. Furthermore, different durations of focal ischemia lead to graded involvement of different regions [40]. Ten to 20 min of occlusion duration "simply" causes scattered dead neurons in the core of the lesion [40], [41]; 1 h leads already to an infarct in the core [40], [42]; and, finally, a fully developed infarct of the target volume can be observed after 2 to 3 h of occlusion [41], [42]. Moreover, after this period of time, the size of the infarct will be the same as it is in permanent ischemia [40], [43], although it develops more slowly [43]. Another important time factor is that as little as 30 min of focal ischemia also lead to an infarct in the core region, but this first appears after 3 d and takes 2–3 wk to mature to its full size [44]. Thus, it is concluded that the observed duration of gas bodies is sufficient enough to form the basis for focal ischemia. This local anemia would lead to an infarct of the core region of a tumor and possibly expand to its penumbra if applied in a large enough vicinity of the assumed tumor delineation.

D. Difference Between Intravenous and Intraarterial

Intra-arterial as well as intravenous injections successfully deposited droplets in the circulatory system. However, the yield from intraarterial injections is quantitatively much greater than the yield from intravenous in-

jections. This is the case even for a 10-fold increase in the administered dose. The low yield rate is problematic for occlusion treatment, but not for phase aberration corrections, where only a low number density of targets is required anyway.

Ultrasound at diagnostic levels and albumin-stabilized DDFP droplets injected intravenously and intraarterially were employed to create gas bubbles selectively. If substantial occlusion can be achieved to block primary and collateral flow, and if the resulting ischemia is maintained for an extended period of time, this would result in ischemic necrosis. This makes ADV a possible procedure for occlusion therapy.

E. Point Beacons

Acoustic targets for phase aberration correction were created in canine kidney and brain tissue. ADV in both regions showed promising backscatter amplitudes for image correction with signals of 14.3 and 23 dB above background tissue for kidney and brain tissue, respectively. Intravenous injections were found to be adequate for droplet delivery to the site of interest and subsequent point beacon creation.

The further interaction between gas bubble and ultrasound (1 to 10 MHz) will be simple compared with that of imaging CA in the same frequency range. Contrast agents, and much more pronounced free gas bubbles of the same size, show effects such as rectified diffusion or cavitation, because these bubbles undergo great radial oscillations. Large gas bubbles, such as those shown in this paper, are not at resonance. The used frequency is much higher than resonance, and the bubbles' response is therefore linear, which is important for simple and performable algorithms for phase aberration correction using the "beacon of truth."

Studies on the effect of air bubbles in brain (Section I) suggest the conclusion that collateral flow and restricted air bubble volumes will allow sufficient blood supply to the VOI. Submicron droplets may supplement the oxygenation of the tissues. It is yet to be determined the threshold of perfluorocarbon bubble diameter at which local ischemia may do damage, i.e., damage that is significant relative to the need for these techniques in various diagnostic and therapeutic imaging procedures. A maximum diameter of 50 μm may prove of low enough risk for important high yield diagnostic procedures.

V. Summary

Ultrasound at diagnostic levels and albumin-stabilized DDFP droplets injected intravenously and intraarterially were employed to create gas bubbles selectively to potentially cause ischemia or to generate point beacons for phase aberration correction.

Twelve canines were used in this preliminary *in vivo* study. Ten of 12 animals showed successful vaporization of droplets *in situ*. The first case, which was not fully successfully offered, limited acoustic access because of bleeding of the dura. This formed a layer between the brain and the transducer, which was acoustically difficult to penetrate. The other case is believed to have failed because of the improper storage of the droplet emulsion prior to the injections.

Overall, ADV worked reasonably well *in vivo*. Six out of nine intravenous injections led to successful formation of gas bubbles, and intraarterial injections were followed in all cases by acoustic vaporization *in situ*. Typically, injected volumes were 0.3 mL (16 million droplets/mL) for intravenous administration and 0.03 mL for intraarterial. Based on the animal weight, ~200,000 droplets/kg were injected (intravenous dose). Only 2.8% of the droplets are in the range from 10 to 50 μm, which is the range covered by the FDA recommendation for particulates (Section I). Optison® (Mallinckrodt Inc., Molecular Biosystems Inc., San Diego, CA), an ultrasound CA approved by the FDA, has microsphere bubble sizes with 7% larger than 10 μm. For comparison, if these perfluorocarbon bubbles are considered as particulates, in recommended Optison® doses of $4.6{\cdot}10^6$ microspheres/kg, in an average human of 70 kg, this FDA limit was exceeded by 56%. The number of bubble beacons from vaporized droplets is relatively negligible. If one bubble is desired in every milliliter of a large organ, such as a 1600-mL liver [45], and an equal number of bubbles are generated in the veins by not limiting the focus to an artery, there would still be a factor of 150 safety margins relative to the FDA recommendation.

Two applications for ADV *in vivo* were tested. For therapeutic purposes, a large number density of larger than capillary size gas bubbles was created, and a subsequent decrease of up to 34% in regional perfusion was observed. Gas bubbles were observed as being stationary for at least 30 min with a decrease of acoustic backscatter of ~ 0.24 dB$\cdot$min^{-1}. Future studies will have to determine whether the reduction in blood flow and time duration can be made sufficient for occlusion therapy, e.g., cancer treatment. If not, repeated treatments and larger ROI may have to be used to compensate for dissolution of the induced gas bodies as well as for obstruction of co-lateral flow, which impairs the localized occlusion.

Point beacons for phase aberration purposes were also formed *in vivo*. Spatially and temporally controlled acoustic targets were created in the kidney as well as in the cortex of the brain. Scattering amplitudes of 23 dB above canine brain tissue and 14 dB above kidney tissue were seen. Furthermore, this would predict a scattering amplitude of 13 dB above liver tissue.

A model for targeting the supply arteries of a specific tissue for subsequent bubble production in the vessel may be necessary. One method, called contrast interruption, is currently under development in our laboratory [46]. This method could potentially be used to identify the supply vessels for a tumor, arterio-venous malformation, or other target.

ACKNOWLEDGMENT

Special thanks to Dr. Kim Ives for her support with the animals.

REFERENCES

[1] O. D. Kripfgans, J. B. Fowlkes, D. L. Miller, O. P. Eldevik, and P. L. Carson, "Acoustic droplet vaporization for therapeutic and diagnostic applications," *Ultrasound Med. Biol.*, vol. 26, no. 9, pp. 1177–1189, 2000.

[2] R. E. Apfel, "Activatable Infusable Dispersions Containing Drops of a Superheated Liquid for Methods of Therapy and Diagnosis," U.S. Patent 5,840,276, Apfel Enterprises, Inc., 1998.

[3] K. Nagdi, *Rubber as an Engineering Material: Guideline for Users.* Munich, Germany: Hanser, 1993.

[4] E. A. Kazerooni, T. Pranikoff, P. N. Cascade, and R. B. Hirschl, "Partial liquid ventilation with perflubron during extracorporeal life support in adults: Radiographic appearance," *Radiology*, vol. 198, no. 1, pp. 137–142, 1996.

[5] T. Nishioka, H. Luo, M. C. Fishbein, B. Cercek, J. S. Forrester, C. J. Kim, H. Berglund, and R. J. Siegel, "Dissolution of thrombotic arterial occlusion by high intensity, low frequency ultrasound and dodecafluoropentane emulsion: An *in vitro* and in vivo study," *J. Amer. Coll. Cardiol.*, vol. 30, no. 2, pp. 561–568, 1997.

[6] J. G. Riess and M. P. Krafft, "Fluorocarbons and fluoro surfactants for in vivo oxygen transport (blood substitutes), imaging, and drug delivery," *Mater. Res. Bull.*, vol. 24, pp. 42–48, 1999.

[7] D. E. Sakas and K. W. Whittaker, "Perfluorocarbons: Recent developments and implications for neurosurgery," *J. Neurosurgery*, vol. 85, no. 2, pp. 248–254, 1996.

[8] S. C. Quay, "Phase shift colloids as ultrasound contrast agents," U.S. Patent 5,558,853, 1996.

[9] J. M. Correas and S. D. Quay, "EchoGenTM emulsion: A new ultrasound contrast agent based on phase shift colloids," *Clin. Radiol.*, vol. 51, Suppl. 1, pp. 11–14, 1996.

[10] G. M. Lanza, C. H. Lorenz, S. E. Fischer, M. J. Scott, W. P. Cacheris, R. J. Kaufmann, P. J. Gaffney, and S. A. Wickline, "Enhanced detection of thrombi with a novel fibrin-targeted magnetic resonance imaging agent," *Acad. Radiol.*, vol. 5, Suppl. 1, pp. 173–176, April 1998.

[11] G. M. Lanza, K. D. Wallace, W. P. Cacheris, D. R. Abendschein, D. H. Christy, A. M. Sharkey, M. J. Scott, J. G. Miller, P. J. Gaffney, and S. A. Wickline, "A novel site-targeted ultrasonic contrast agent with broad biomedical application," *Circulation*, vol. 94, pp. 3334–3340, 1996.

[12] P. R. Sandoval, P. H. F. Wingartz, and H. F. Gonzalez, "Renal embolization: Experience in 81 patients," *World Urol. Update Ser.*, vol. 11, no. 3, pp. 2–7, 1983.

[13] J. Blech, "Krebs aushungern," *Die Zeit*, Hamburg, 1999, p. 45, Mar. 25, 1999.

[14] J. Tingleff, F. S. Joyce, and G. Pettersson, "Intraoperative echocardiographic study of air embolism during cardiac operations," *Ann. Thorac. Surg.*, vol. 60, pp. 673–677, 1995.

[15] T. S. Padayachee, S. Parsons, R. Theobold, R. G. Gosling, and P. B. Deverall, "The effect of arterial filtration on reduction of gaseous microemboli in the middle cerebral artery during cardiopulmonary bypass," *Ann. Thorac. Surg.*, vol. 45, no. 6, pp. 647–649, 1988.

[16] F. Dexter, B. J. Hindman, and J. S. Marshall, "Estimate of the maximum absorption rate of microscopic arterial air emboli after entry into the arterial circulation during cardiac surgery," *Perfusion*, vol. 11, pp. 445–450, 1996.

[17] H. Fritz and K.A. Hossmann, "Arterial air embolism in the cat brain," *Stroke*, vol. 10, pp. 581–589, 1070.

[18] S. C. Helps and D. F. Gorman, "Air embolism of the brain in rabbits pretreated with mechlorethamine," *Stroke*, vol. 22, no. 3, pp. 351–354, 1991.

[19] B. B. Johansson, "Cerebral air embolism and the blood-brain barrier in the rat," *Acta Neurologica Scand.*, vol. 62, pp. 201–209, 1980.

[20] M. A. Davis and R. A. Taube, "Pulmonary perfusion imaging: Acute toxicity and safety factors as a function of particle size," *J. Nuclear Med.*, vol. 19, no. 11, pp. 1209–1213, 1978.

[21] *PULMOLITE (2001). Technetium Tc99m Albumin Aggregated for Injection.* Bedford, MA: CIS-US Inc.

[22] D. Annane, G. Troche, F. Delisle, P. Devauchelle, D. Hassine, F. Paraire, J. C. Raphael, and P. Gajdos, "Kinetics of elimination and acute consequences of cerebral air embolism," *J. Neuroimag.*, vol. 5, no. 3, pp. 183–189, 1995.

[23] R. P. Cochran, K. S. Kunzelman, C. R. Vocelka, H. Akimoto, R. Thomas, L. O. Soltow, and B. D. Spiess, "Perfluorocarbon emulsion in the cardiopulmonary bypass prime reduces neurologic injury," *Ann. ThoracSurg.*, vol. 63, pp. 1326–1332, 1997.

[24] P. Menasché, E. Pinard, A. M. Desroches, J. Seylaz, P. Laget, R. P. Geyer, and A. Piwnica, "Fluorocarbons: A potential treatment of cerebral air embolism in open-heart surgery," *Ann. Thorac. Surg.*, vol. 40, no. 5, pp. 494–497, 1985.

[25] B. D. Spiess, B. Braverman, A. W. Woronowicz, and A. D. Ivankovich, "Protection from cerebral air emboli with perfluorocarbons in rabbits," *Stroke*, vol. 17, no. 6, pp. 1146–1149, 1986.

[26] G. C. Ng, P. D. Freiburger, W. F. Walker, and G. E. Trahey, "A speckle target adaptive imaging technique in the presence of distributed aberrations," *IEEE Trans. Ultrason., Ferroelect., Freq. Contr.*, vol. 44, no. 1, pp. 140–151, 1997.

[27] W. F. Walker and G. E. Trahey, "Speckle coherence and implications for adaptive imaging," *J. Acoust. Soc. Amer.*, vol. 101, no. 4, pp. 1847–1858, 1997.

[28] Y. Li, "Small element array algorithm for correcting phase aberration using near-field signal redundancy—Part I: Principles," *IEEE Trans. Ultrason., Ferroelect., Freq. Contr.*, vol. 47, no. 1, pp. 29–48, 2000.

[29] Y. Li and B. Robinson, "Small element array algorithm for correcting phase aberration using near-field signal redundancy—Part II: Experimental results," *IEEE Trans. Ultrason., Ferroelect., Freq. Contr.*, vol. 47, no. 1, pp. 49–57, 2000.

[30] R. F. Wagner, S. W. Smith, J. M. Sandrik, and H. Lopez, "Statistics of speckle in ultrasound B-scans," *IEEE Trans. Sonics Ultrason.*, vol. 30, no. 3, pp. 156–163, 1983.

[31] P. D. Freiburger and G. E. Trahey, "Parallel processing techniques for the speckle brightness phase aberration correction algorithm," *IEEE Trans. Ultrason., Ferroelect., Freq. Contr.*, vol. 44, no. 2, pp. 431–444, 1997.

[32] M. O'Donnell and S. W. Flax, "Phase aberration correction using signals from point reflectors and diffuse scatterers: Measurement," *IEEE Trans. Ultrason., Ferroelect., Freq. Contr.*, vol. 35, no. 6, pp. 768–774, 1988.

[33] D. Zhao and G. E. Trahey, "Comparisons of image quality factors for phase aberration correction with diffuse and point targets—Theory and experiments," *IEEE Trans. Ultrason., Ferroelect., Freq. Contr.*, vol. 38, no. 2, pp. 125–132, 1991.

[34] C. Prada, F. Wu, and M. Fink, "The iterative time-reversal mirror—A solution to self-focusing in the pulse echo mode," *J. Acoust. Soc. Amer.*, vol. 90, no. 2, pp. 1119–1129, 1991.

[35] M. Fink, "Time-reversal of ultrasonic fields. 1. Basic principles," *IEEE Trans. Ultrason., Ferroelect., Freq. Contr.*, vol. 39, no. 5, pp. 555–566, 1992.

[36] D.-L. Liu and R. C. Waag, "Correction of ultrasonic wavefront distortion using backpropagation and a reference waveform method for time-shift compensation," *J. Acoust. Soc. Amer.*, vol. 96, no. 2, pp. 649–660, 1994.

[37] D. Psychoudakis, J. B. Fowlkes, J. L. Volakis, O. D. Kripfgans, and P. L. Carson, "Potential of microbubbles for point targets in phase aberration correction," presented at 141st meeting of ASA, Chicago, IL, June 4–8, 2001.

[38] F. A. Duck, *Physical Properties of Tissue.* San Diego, CA: Academic Press, 1990.

[39] P. Lipton, "Ischemic cell death in brain neurons," *Physiol. Rev.*, vol. 79, no. 4, pp. 1431–1568, 1999.

[40] H. Memezawa, M.-L. Smith, and B. K. Siesjo, "Penumbral tissues salvaged by reperfusion following middle cerebral artery occlusion in rats," *Stroke*, vol. 23, no. 4, pp. 552–559, 1992.

[41] Y. Li, M. Chopp, N. Jiang, Z. G. Zhang, and C. Zaloga, "Induction of DNA fragmentation after 10 to 120 minutes of focal cerebral ischemia in rats," *Stroke*, vol. 26, no. 7, pp. 1252–1258, 1995.

[42] J. H. Garcia, S. Wagner, and K.-F. Liu, "Neurological deficit and extent of neuronal necrosis attributable to middle cerebral artery occlusion in rats: Statistical validation," *Stroke*, vol. 26, no. 4, pp. 627–635, 1995.
[43] R.-L. Zhang, M. Chopp, H. Chen, and J. H. Garcia, "Temporal profile of ischemic tissue damage, neutrophil response and vascular plugging following permanent and transient (2H) middle cerebral artery occlusion in the rat," *J. Neurol. Sci.*, vol. 125, pp. 3–10, 1994.
[44] C. Du, R. Hu, C. A. Csernansky, C. Y. Hsu, and D. W. Choi, "Very delayed infarction after mild focal cerebral ischemia: A role for apoptosis," *J. Cereb. Blood Flow Metab.*, vol. 16, no. 2, pp. 195–201, 1996.
[45] W. S. Snyder, M. J. Cook, E. S. Nasset, L. R. Karhausen, G. P. Howells, and I. H. Tipton, *Report of the Task Group on Reference Man*, vol. 23, 1st ed. Oxford: Pergamon Press, 1974.
[46] J. B. Fowlkes, D. W. Sirkin, J. A. Ivey, E. A. Gardner, R. T. Rhee, J. M. Rubin, and P. L. Carson, "Transcutaneous interruption of ultrasound contrast agents for blood flow evaluation," *Invest. Radiol.*, vol. 33, no. 12, pp. 893–901, 1998.

Oliver Daniel Kripfgans (S–00) was born in 1969 in Saarbrücken, Germany. After finishing Gymnasium, he received his Diploma in Physics from the University of Saarbrücken in 1996. During his graduate studies (1989–1996), he was a research assistant in the Department of Ultrasound at the Fraunhofer Institut for Biomedical Engineering, St. Ingbert, Germany. His work included industrial as well as biomedical ultrasound, mostly related to microbubble detection and characterization. Mr. Kripfgans is currently working as a graduate research assistant toward a Ph.D. in applied physics at the University of Michigan, Ann Arbor. His current research interests include the interaction of micro-bubbles and -droplets with ultrasound, therapeutic, and diagnostic ultrasound as well as acoustic material properties and acoustic sensors. Mr. Kripfgans is a member of the Deutsche Physikalische Gesellschaft (DAGA), the Acoustical Society of America, and has been a Student Member of the IEEE since 2000. He received the Norman H. Horwitz Award at the Young Investigators Spring Symposium of the American Association of Physicists in Medicine and Health Physics Society (AAPM, Great Lakes Chapter) and the Best Student Paper Award in Biomedical Ultrasound/Bioresponse to Vibration from the Acoustical Society of America (ASA).

Jeffery Brian Fowlkes (A'94) is an associate professor in the Department of Radiology and an associate professor in the Department of Biomedical Engineering. He is currently directing and conducting research in medical ultrasound, including the use of gas bubbles for diagnostic and therapeutic applications. His work includes studies of ultrasound contrast agents for monitoring tissue perfusion, acoustic droplet vaporization for bubble production in cancer therapy and phase aberration correction, and effects of gas bubbles in the use of high intensity ultrasound. Dr. Fowlkes received his B.S. degree in physics from the University of Central Arkansas in 1983 and his M.S. and Ph.D. degrees from the University of Mississippi in 1986 and 1988, respectively, both in physics.

Contributions to the scientific community by Dr. Fowlkes include educational and research efforts and organizational service. Dr. Fowlkes is presently Principal Investigator on two grants from the National Institutes of Health and one grant from the U.S. Army Medical Research and Materiel Command. Dr. Fowlkes has served the medical ultrasonic community by his participation in the American Institute of Ultrasound in Medicine as a member of its Board of Governors, as the Chair of its Bioeffects Committee, and as a member of its Technical Standards and Annual Convention Committees. He also received the AIUM Presidential Recognition Award for outstanding contributions and service to expanding the future of ultrasound in medicine. As a member of the Acoustical Society of America, Dr. Fowlkes has served on the Physical Acoustics Technical Committee and the Medical Acoustics and Bioresponse to Vibration Technical Committee and on a standards committee working group on cavitation detection and monitoring. As an Associate Member of the IEEE, he has worked with the IEEE I&M Society Technical Committee on Imaging Systems.

Michael Woydt was born in 1962 in Hamburg, Germany. He graduated from Gymnasium with Abitur in 1981 and started medical school in Hamburg, Germany as well as in Portland, OR. Dr. Woydt received his M.D. in 1990 from the 'Medizinische Hochschule' in Hannover, Germany. He was in training for neurology neurosurgery in Frankfurt/Main, Germany; Basel, Switzerland; and Würzburg, Germany from 1990 to 1999 and became a specialist in neurosurgery in 1999. Dr. Woydt is staff member of the Neurosurgical Department in Würzburg since 1999.

Dr. Woydt has served the medical community with intra-operative ultrasound in neurosurgery. He contributed more than 70 talks, 10 publications, and 40 published abstracts. Currently, Dr. Woydt is investigating implementations of new ultrasound techniques for intra-operative applications and functional ultrasound. In 2000, Dr. Woydt received the Tönnis-Stipend of the Germany Society of Neurosurgery and spent his sabbatical at the Department of Radiology at the University of Michigan. Dr. Woydt is the team leader of the interdisciplinary work group ultrasound in neurosciences at the University of Würzburg and a member of the international network of ultrasound in neurosurgery, founded in 1999. Since 1995, Dr. Woydt is a member of the Germany Society of Neurosurgery and since 1998 also a member of the Neurosonology Research Group of the World Federation of Neurology.

Odd Petter Eldevik, M.D., Ph.D., is Clinical Professor of Radiology, Division Director for MR, and a faculty member of the Division of Neuroradiology in the Department of Radiology, University of Michigan Health System in Ann Arbor, Michigan.

Dr. Eldevik received his M.D. from the University of Bergen, Norway in 1966 and Ph.D. in 1983 at the University of Oslo, Norway. After internships, residency in diagnostic radiology in Norway in 1968, he underwent fellowships in Neuroradiology at Ullevål Hospital (1972–1973) and a research fellowship at Medical College of Wisconsin, Milwaukee (1977–1978). He served as radiologist (overlege) at Oslo University Hospital Ullevål, Oslo, Norway, from 1979 to 1990; as Chairman for Department of Neuroradiology from 1983 to 1990; and Chairman of Department of Radiology and Medical Services from 1989 to 1990. From 1990 to 1992, he acted as visiting Associate Professor at the Department of Radiology, University of Michigan, Ann Arbor, and, from 1992 to 2000, as Associate Professor. Then, since 2000, he has acted as Clinical Professor.

Dr. Eldevik has served in many committees and in the offices of national and international professional associations, among them as Chairman for the Norwegian Association for Radiology (1983–1988) and Chairman for the Advisory Committee on Clinical Track Appointments and promotions (University of Michigan Medical School, 1999–2001).

Dr. Eldevik has more than 50 peer-reviewed publications, most in neuroradiological topics, several on safety of contrast media. He has given a similar number of invited presentations at national and international meetings.

Dr. Eldevik's focus of teaching is neuroradiological topics including MR and CT of the brain, head, and neck and spin. Research topics are in functional MR, QA, and outcome studies in neuroradiology.

Paul L. Carson (M'74) received the B.S. degree from Colorado College, Colorado Springs, and the M.S. and Ph.D. degrees from the University of Arizona, Tucson, in 1969 and 1971, respectively, all in physics. From 1971 to 1981, he served in the Department of Radiology at the University of Colorado Medical Center, Denver, and since 1981, he has served as Associate Professor or Professor and as Director of Basic Radiological Sciences in the Department of Radiology, University of Michigan Health System. His responsibilities have been in research, clinical support, and teaching of radiological sciences. The research has been in diagnostic ultrasound (quantitative imaging, functional imaging, equipment performance, safety, and new or improved diagnostic and therapeutic applications) and in magnetic resonance imaging.

Dr. Carson is a fellow, past vice president, and J.H. Holms Basic Science Pioneer Award Recipient of the American Institute of Ultrasound in Medicine and is a fellow and past-president of the American Association of Physicists in Medicine. He is a fellow of the Acoustical Society of America, the American College of Radiology, and the American Institute of Medical and Biomedical Engineering. He is certified in Radiological Physics and in Clinical Engineering.

On the acoustic vaporization of micrometer-sized droplets

Oliver D. Kripfgans[a)]
Applied Physics Program, University of Michigan, Ann Arbor, Michigan 48109-1120

Mario L. Fabiilli, Paul L. Carson, and J. Brian Fowlkes
Department of Radiology, University of Michigan, Ann Arbor, Michigan 48109-0553

(Received 8 November 2002; revised 22 January 2004; accepted 5 April 2004)

This paper examines the vaporization of individual dodecafluoropentane droplets by the application of single ultrasonic tone bursts. High speed video microscopy was used to monitor droplets in a flow tube, while a focused, single element transducer operating at 3, 4, or 10 MHz was aimed at the intersection of the acoustical and optical beams. A highly dilute droplet emulsion was injected, and individual droplets were positioned in the two foci. Phase transitions of droplets were produced by rarefactional pressures as low as 4 MPa at 3 MHz using single, 3.25 μs tone bursts. During acoustic irradiation, droplets showed dipole-type oscillations along the acoustic axis (average amplitude 1.3 μm, independent of droplet diameter which ranged from 5 to 27 μm). The onset of vaporization was monitored as either spot-like, within the droplet, or homogeneous, throughout the droplet's imaged cross section. Spot-like centers of nucleation were observed solely along the axis lying parallel to the direction of oscillation and centered on the droplet. Smaller droplets required more acoustic intensity for vaporization than larger droplets, which is consistent with other experiments on emulsions. © *2004 Acoustical Society of America.* [DOI: 10.1121/1.1755236]

PACS numbers: 43.35.Bf, 43.35.Ty, 43.28.Kt, 43.35.Ei [AJZ] Pages: 272–281

I. INTRODUCTION

It has been observed in the past that micrometer sized droplets of perfluorocarbon liquids in emulsions can be vaporized into gas bubbles by the application of tone bursts in the frequency and power range of diagnostic ultrasound.[1–3] This phenomenon is here referred to as acoustic droplet vaporization (ADV). More recently Giesecke and Hynynen[4] reported the acoustic vaporization of droplet emulsions by the application of low amplitude and high duty cycle bursts. These emulsions can be produced with up to 97% of the particles being smaller than 10 μm in diameter and an average diameter of 3 μm.[5] After filtering, such particles are transpulmonary thereby remaining in the blood stream as they are circulated through the body. Exposure to ultrasound creates larger than 6 μm gas bubbles that become trapped in the vasculature. Depending on the dilution of the emulsion, the effects of ADV *in vivo* can, for example, be used for tissue occlusion or for the creation of point targets.[5]

This paper will show the experimental results of the vaporization of single, albumin-stabilized droplets as they are exposed to single, acoustic tone bursts.

Possible mechanisms for ADV will be hypothesized and discussed using experimental results as well as findings from the literature. These include: (a) hydrodynamic cavitation which could potentially nucleate the superheated droplet; and (b) droplet deformation which could lead to shell rupturing or a nonuniform Laplace pressure on the sphere.

There are several scenarios in which hydrodynamic cavitation might occur. First of all, it is known from ship propellers that the motion of a body in water will cause cavitation on that body.[6] For venturi liners, this damage has been found to be proportional to the flow velocity.[7] Observations have shown that phase changes occur when, for example, a sphere touching a wall is pulled away,[8] or in small water tunnel experiments, using flow past lead specimen[9] at 14–23 $\mathrm{m\,s^{-1}}$. The former case could occur during the collision of two droplets or when a droplet interacts with a wall; whereas the latter one is possible for just a single droplet without contact to any surface.

One of the classic acoustic experiments involving droplets is acoustic levitation.[10–12] Twenty to sixty kilohertz are usually used to levitate drops of millimeter diameter. Shi and Apfel,[13] for example, levitated a 1.18 mm radius water drop in air at 28 kHz and up to 3 kPa sound pressure. This corresponds to a ka value of 0.14. During the experiment they observed shape oscillations with aspect ratios of up to 2. Similar experiments were performed by Su and Feng.[14] They reported translational oscillations of levitated drops as a result of the shape oscillation, and counteraction of gravitational force and radiation pressure. For millimeter-sized water drops (22 kHz driving frequency), shape oscillations of 100–200 Hz were observed and even slower translational oscillations. Observations reported in this paper are based on experiments with similar ka values. Droplets in the 10 μm range will be exposed to ultrasonic waves in the MHz range. Even though levitation experiments are performed under continuous wave conditions, one can expect a droplet–wave interaction which includes droplet translation and deformation.

II. MATERIALS AND METHODS

More than 2000 high speed photography images were analyzed, where the data in this paper represent 32 individual droplets. Each droplet was measured for its diameter, the

a)Electronic mail: oliver.kripfgans@umich.edu

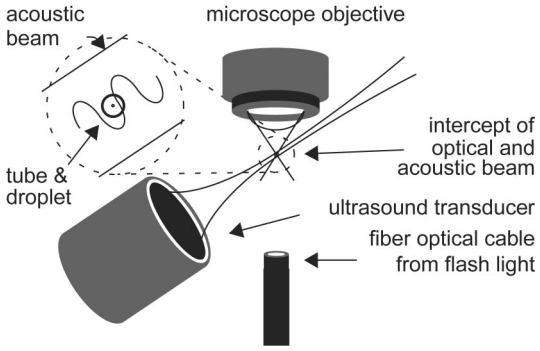

FIG. 1. The ultrasound transducer (3.5 MHz) has an aperture of 25.4 mm and a lateral focal beam diameter of 0.96 mm. The polyethylene flow tube has a 200 μm inner diameter and 50 μm wall thickness. The inset (not to scale) shows the geometric arrangement, including a 3.5 MHz two cycle tone burst.

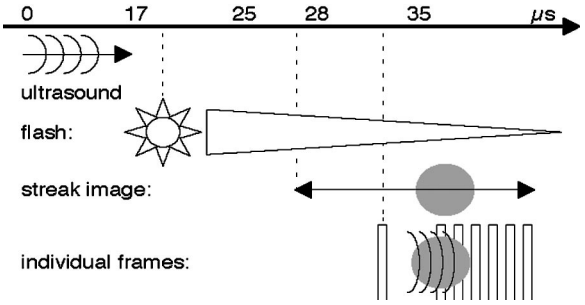

FIG. 2. Timing diagram of the transmitted ultrasound burst, light pulse, acquired streak image, and individual frames. The launch of the acoustic tone burst is time zero. It triggers the flash/strobe light with a 17 μs delay, 3.3 μs before the tone burst arrives at the focus. Eight microseconds later, at 25 μs, the streak image starts recording for 10 μs and at 28 μs the first full frame picture is taken. The remaining six images are taken at various time points to investigate either the translation or the vaporization process.

acoustic pressure necessary to vaporize it, and any optically observable action when exposed to ultrasound.

A. High speed video setup

An Imacon 468 high speed video system (DRS Technologies, DRS Hadland, Inc., Cupertino, CA) was used to optically image the process of ADV. Full-frame pictures of 576×385 pixels were taken with an exposure time of 100–200 ns. In streak mode, the vertical center line of an image was captured at 57.6 MHz (17.4 ns per streak line). Since ADV occurs at a micron scale, an optical microscope (JenaVAL, Carl Zeiss Jena GmbH, Jena, Germany) was connected to the video system. Micrometer-sized droplets were monitored full frame at 0.1 μs temporal and 0.46 μm spatial resolution. The light of a 2.5 kW argon flash lamp was guided into the optical path, facing the 100× objective of the microscope (see Fig. 1). An estimate for the potential of the light as a heat source will be addressed in Sec. VI.

The acoustic exposure occurred in a small tank (26 ×9×10 cm) with degassed water. A polyethylene tube (200 μm i.d., 50 μm wall thickness) was mounted 5 cm from the far end of the tank just below the water surface. Two single-element, 2.54 cm aperture, 3.81 cm focus transducers, with center frequencies of 3.5 and 10 MHz, were used. Transmit bandwidth and focal diameter were 41% and 90% as well as 0.96 and 0.34 mm, respectively. For a given experiment one of the transducers would be mounted on a three-dimensional micro-positioner and aimed at the intersection of the tube and the optical beam (see Fig. 1). The calibrated ultrasound transducer was driven by a rf gated amplifier (model 350, Matec, Northboro, MA) and controlled by a multipurpose function generator (HP3314, Agilent, Palo Alto, CA). Three frequencies were used in the experiments: 3, 4, and 10 MHz. The burst length was selected for a constant time duration, i.e., 10, 13, and 33 cycles, respectively. rf signals were monitored using an oscilloscope (9310L, LeCroy Corp., Chestnut Ridge, NY). The transducers were calibrated for transmitted acoustic pressure using a membrane hydrophone (Reference Shock Wave Hydrophone™, Sonic Industries, Hatboro, PA).

Droplet emulsions were made from 75 vol % saline-albumin solution (5 mg mL^{-1}) and 25 vol % dodecafluoropentane (DDFP, C_5F_{12}, CAS #678-26-2). The mixture was sealed in a 3 mL auto sampler glass vial and shaken for 30 s at 5000 cpm (MSD Wig-L-Bug, Crescent Dental Mfg. Co., Elgin, IL). A highly concentrated droplet emulsion with 9.5 $\times 10^9$ droplets per mL resulted. This emulsion was diluted (1:10 000 in saline) and small volumes of it were injected into the flow tube.

For each picture taken, an individual droplet was positioned on the center line of the screen of the video system. This center line coincided with the acoustic and optical foci. As seen in Fig. 2, at time zero the function generator produces a 3.33 μs tone burst, which was converted into an acoustic wave by the single element transducer and propagated through the water to the flow tube. The argon flash lamp was triggered at 17 μs, when the camera's gain control could be used to adjust its optical sensitivity to the decaying ambient background light. The persistence of the light flash was long enough to record a 10 μs streak image and 7 individually spaced full frame images. The first image was taken before the sound wave reached the tube. Subsequent frames were either placed back-to-back in order to monitor the process of ADV or were separated by several hundred nanoseconds to monitor the droplet during the insonification before ADV started. Each droplet was exposed to a series of acoustic tone bursts of increasing acoustic power. For each power level a set of seven full frames and one streak image was acquired and saved. The acoustic pressure was increased until the droplet vaporized.

MATLAB™ scripts (MathWorks Inc., Natick, MA) were written to read the image files from the camera and analyze them for droplet size and position. The droplet's top and bottom edge was manually selected in the streak image for analysis for dipole and possible shape oscillation. The white line in Fig. 3 shows the top and bottom trace on the boundary

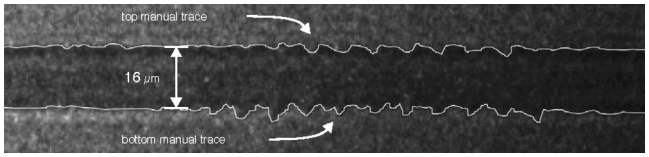

FIG. 3. Traced streak line of a 16-μm-diam droplet. One can see the onset of oscillation at the bottom trace, before onset occurs in the top trace and the eventual dipole motion is established.

of a droplet. The terms dipole and shape oscillation are used for a translational oscillation of the droplet's center of mass and for an oscillation of the droplet's diameter, respectively. Only streak images were used to measure the action of the droplets in the acoustic field (for 3 and 4 MHz). Full-frame images were solely used to monitor the onset and spatial progress of nucleation (for 3, 4, and 10 MHz) as well as any large scale geometric changes of the droplet, if any.

B. Laser vibrometer setup

It is possible that the flow tube which hosts the droplets is moving in the wave field, yielding the impression that the droplet itself moves with respect to its host fluid *in* the tube. Tube stability was not verified in the original high speed video setup. Therefore, a laser vibrometer (OFV 3001S and OVD-04/06, PolyTech PI, Inc., Auburn, MA) was used to measure the possible translation of the flow tube in the acoustic field. Limited by the bandwidth of the vibrometer, a range of 1.1–2.1 MHz was scanned. An acoustic field of maximum pressure of 10 MPa peak-to-peak was used. The raw data were corrected for the filter response of the laser vibrometer, the Doppler angle, and the ultrasound transducer transfer function.

III. THEORETICAL DESCRIPTION

A. Sound field

It was expected that acoustic field inside the flow tube, adjacent microscope objective, is relatively complex (see Fig. 1). Due to the very short focal length of the objective, the tube was in direct contact with the microscope. To calculate the acoustic field, the objective is modeled as a rigid planar wall and the tube is described as an infinite hollow cylinder in the field of a planar wave with boundary conditions on its surface. Modeling the interior of a hollow cylinder is based on the solution of a solid cylinder[15] with an iteration of boundary conditions for a second cylinder on the inside. An incident planar wave is formulated in cylindrical coordinates. Interior fields were modeled with Bessel functions of the first kind, while the scattered fields were described using Hankel functions. The first boundary condition is continuity of pressure on the outer surface of the hollow cylinder. Two equations are derived for each boundary. One equation is the continuity of pressure, at the outer surface, and at the inner surface of the hollow cylinder. The second set of equations on the first boundary is derived for the continuation of normal velocity on the boundary, which is proportional to the gradient of the pressure. This is only valid in linear acoustics, i.e., when the density of the host medium is not a function of the instantaneous pressure. The number of terms in all computations was selected to satisfy a criterion given by Bohren and Huffman,[16] here 20 orders in Bessel functions. The radial step size was typically $2\pi/(100k)$, where k is the wave number. A mirror source was introduced to complete the model for the flow tube being placed next to a rigid wall. The following parameters used were: for water and tube wall: speed of sound 1489 and 2500 $\mathrm{m\,s^{-1}}$, mass density 1000 and 970 $\mathrm{kg\,m^{-3}}$; incident sound pressure amplitude 3.5 MPa, outer and inner tube diameter 208.5 and 152 μm. The simulation is used to estimate the magnitude of interference inside the tube. For the computed spatial pressure distributions the absolute value of the complex valued solution is plotted in order to get the temporal peak pressure.

B. Droplet oscillations

First order models were used to compute the amplitude of oscillation of droplets in an acoustic field. It is assumed that the sole effect of the ''encapsulating'' albumin is prevention of coalescence. Therefore the droplet appears acoustically as a nonrigid sphere. Such a model and its solutions[15] are given in Eq. (1), which describes the total pressure outside a sphere ($r \geqslant a$). The Bessel (j_m) and Hankel (h_m) functions on the right-hand side of Eq. (1) represent the incident and scattered wave, respectively. Legendre polynomials are abbreviated with P_m. The amplitude of the incident wave is A, i is the imaginary unit, and θ is the in plane angle. The droplet radius is denoted by a; mass densities of water and droplet are $\rho = 1000$ and $\rho_e = 1660\,\mathrm{kg\,m^{-3}}$, respectively. Speed of sound of water and inside the droplet are $c = 1489$ and $c_e = 471\,\mathrm{m\,s^{-1}}$, respectively.

$$
\begin{aligned}
p_\omega(r,\theta) &= A\sum_{m=0}^{\infty}(2m+1)i^m P_m(\cos\theta) \\
&\quad \times\cdots\left(j_m(kr) - \tfrac{1}{2}(1+R_m)h_m(kr)\right), \\
R_m &= \frac{h_m'^{*}(ka) + i\beta_m h_m^{*}(ka)}{h_m'(ka) + i\beta_m h_m(ka)}, \\
\beta_m &= i\frac{\rho c}{\rho_e c_e}\frac{j_m'(k_e a)}{j_m(k_e a)},
\end{aligned}
\tag{1}
$$

$$
\begin{aligned}
\mathbf{F} &= \int d\mathbf{F} = \oint_A p_\omega(r,\theta)\,d\mathbf{A} \\
&= \oint_A p_\omega(r,\theta)\begin{bmatrix}\sin\theta\cos\phi\\ \sin\theta\sin\phi\\ \cos\theta\end{bmatrix} a^2\sin\theta\,d\theta\,d\phi, \\
m\ddot{\xi} &= -V\nabla p_i + F_{\mathrm{sc}}, \\
\tfrac{4}{3}\pi a^3\rho\ddot{\xi} &= \left(\frac{3}{2}\frac{\rho_e-\rho}{\rho_e+\tfrac{1}{2}\rho}-1\right)\tfrac{4}{3}\pi a^3\nabla p_i - F_{\mathrm{sc}}.
\end{aligned}
\tag{2}
$$

In this linear approach the droplet's displacement can be computed from the integrated force on the sphere, which is derived from the pressure at the droplet's surface. Newton's second law can be used to estimate the associated motion of the droplet. Furthermore, both the inertia of the moving droplet and that of the displaced water has to be taken into consideration.[17] Equation (2) relates the acceleration of the droplet with the pressure gradient of the incident pressure wave and the force of the scattered field on the droplet's surface. Furthermore, the inertia of the mass of the displaced water is added in the second part of Eq. (2). Here m is the mass of the droplet, ξ is the location of center of mass of the droplet, V is its volume, p_i is the incident acoustic field, and F_{sc} is the force exerted on the droplet by the scattered wave, i.e., the second part of the pressure equation in Eq. (1).

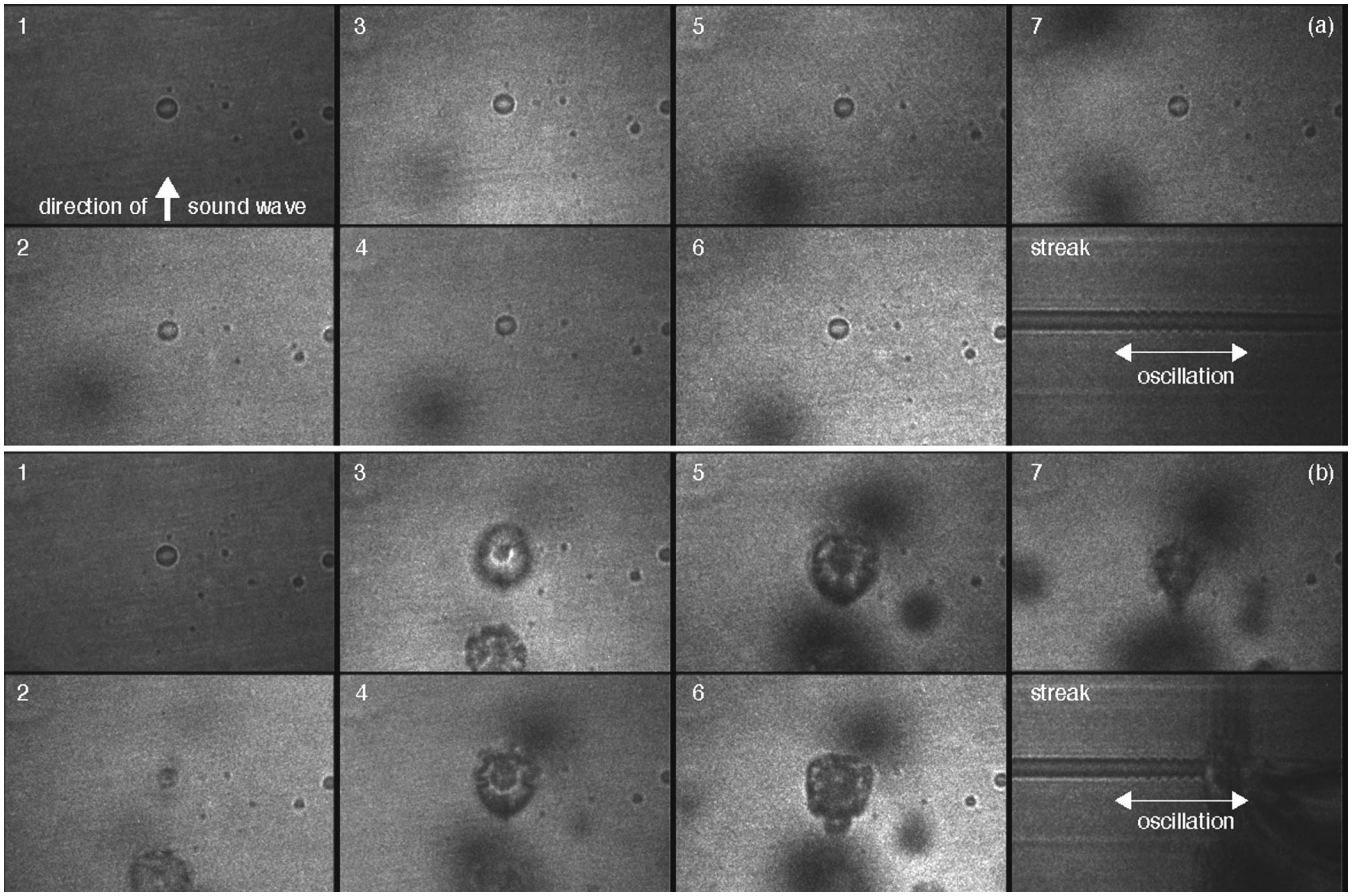

FIG. 4. Acoustic vaporization of an 18-μm-diam droplet. Two sequences are shown. (a) Images 1–7 are full frame pictures of the droplet in the flow tube. The eighth frame is a streak image. The acoustic pressure in the first sequence is not sufficient to vaporize the droplet. In the center of the streak image one can see a translatory motion of the droplet (arrows) for the duration of the 10 cycle, 3 MHz tone burst (magnified image in Fig. 5). (b) Increasing the acoustic pressure to 6.5 MPa peak–peak (which is $P=2.6$ MPa) leads to the vaporization of the droplet after 8 cycles.

Double integration in time, assuming an oscillatory motion at ω, yields the displacement amplitude.

C. Droplet shape oscillation

A theoretical model which allows shape changes[12] was used to evaluate the change in aspect ratio of a droplet in an acoustic field. The acoustic radiation pressure on a droplet as well as the field inside a droplet of fixed shape is computed. Given those, the droplet shape is allowed to change in order to minimize the overall energy of the system. This process is iterated for shape change and subsequently for increasing sound pressures. Equation (3) is an order of magnitude estimate for the coupling of drop shape oscillation and translation.[18] β_l is defined by Eq. (3); U is the droplet's velocity, σ is the interfacial tension, l is the mode of oscillation; a, ρ, and ρ_e were defined earlier. For the cases $\beta_l a/U$: $\gg 1$, $=1$, and $\ll 1$, the drop is isolated, the relative motion between the two phases cannot be neglected, and the droplet does not perform shape oscillations, respectively,

$$\frac{\beta_l a}{U}=\sqrt{\frac{\sigma l(l+1)(l-1)(l+2)}{a^3(\rho l+\rho_e(l+1))}}\frac{a}{U}. \tag{3}$$

IV. EXPERIMENTAL RESULTS

A. Droplet dipole type oscillations

Single, sinusoidal tone bursts of 3 and 4 MHz at P_- up to 4 and 7 MPa, respectively, were sufficient to phase transition individual droplets. High speed video images are shown in Figs. 4–6. The streak image of the droplet in Fig. 4 shows a translational, dipole-type motion with the same frequency and duration as the transmitted 3 MHz acoustic tone burst (see zoomed version in Fig. 5 and manual traced streak in Fig. 3). No motion can be seen in the streak image of Fig. 6, where a droplet is exposed to a 10 MHz sound field.

Measurements were performed on droplets in the size range from 5 to 27 μm diameter. All droplet sizes are larger than the mean size of the emulsion because of the spatial resolution of the microscope used. At the acoustic pressure threshold (i.e., where the droplets vaporize), average displacements of 2.7 ± 0.4 μm and 2.5 ± 0.4 μm at 3 and 4 MHz, respectively, were measured. These displacements were not adjusted for any possible out of plane oscillation of the droplets due to the 45° angle between the ultrasound transducer and microscope objective (see Fig. 1). The measured peak to peak displacement was found to be independent of the droplet's size and the frequency used (see Fig. 7).

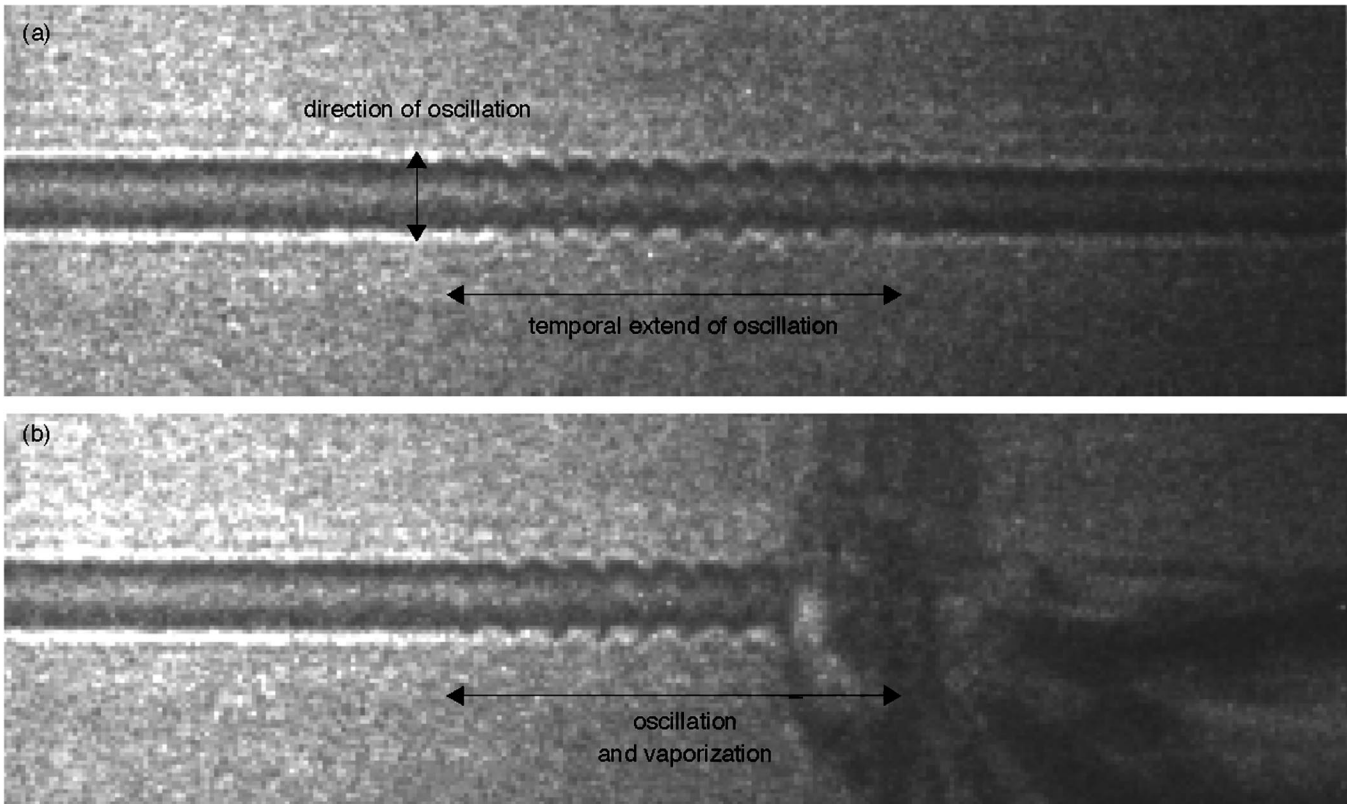

FIG. 5. Zoomed and brightness/contrast enhanced streak images from Fig. 4. Not the dipole (translatory) motion of the droplet.

The average velocity v at which the droplet is oscillating results directly from the oscillation amplitude x and the insonification frequency f as $v=2\times f$. For 3 MHz and 2.7 μm, v is equal to 16.2 ± 2.3 m s^{-1}, the 4 MHz data yields 20 ± 3.1 m s^{-1} for the same displacement. The velocity values are also not corrected for any possible motion out of the image plane. Due to the image quantization of 0.46 μm per pixel, plus image noise, an error of approximately 20% must be expected.

Figure 8(a) shows the dependence of the oscillation amplitude on the sound pressure. For seven droplets the oscillation amplitude has been analyzed as a function of sound pressure. That pressure was normalized to the power needed for vaporization for each droplet since the droplets were of varying size. All seven droplets follow the same relationship between oscillation and power. Moreover, Fig. 8(b) displays that all droplets will follow that path until the amplitude of oscillation reaches a certain value, upon which ADV occurs. Figures 7(a), 8(b), and 11 show the same data points of a three-dimensional data set. For each measured droplet there is a droplet resting diameter (d), the pressure necessary to vaporize it (p), and the amplitude of oscillation (x) when exposed to that pressure. Above-mentioned Figs. 7(a), 8(b), and 11 show the three combinations $x(d)$, $x(p)$, and $p(d)$, respectively.

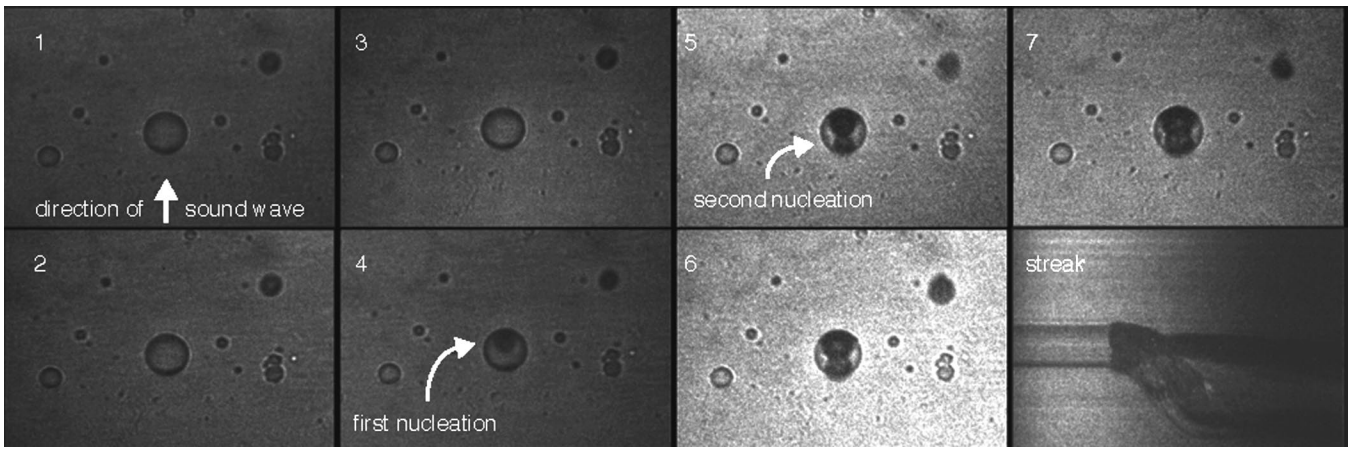

FIG. 6. Frame 4 of the sequence shows the first nucleation point of the droplet's vaporization, and frame 5 shows another nucleation site. The frames were placed back to back with 100 ns duration. A 10 MHz and 33 cycle tone burst at 9 MPa was used, with a 45-μm-diam droplet.

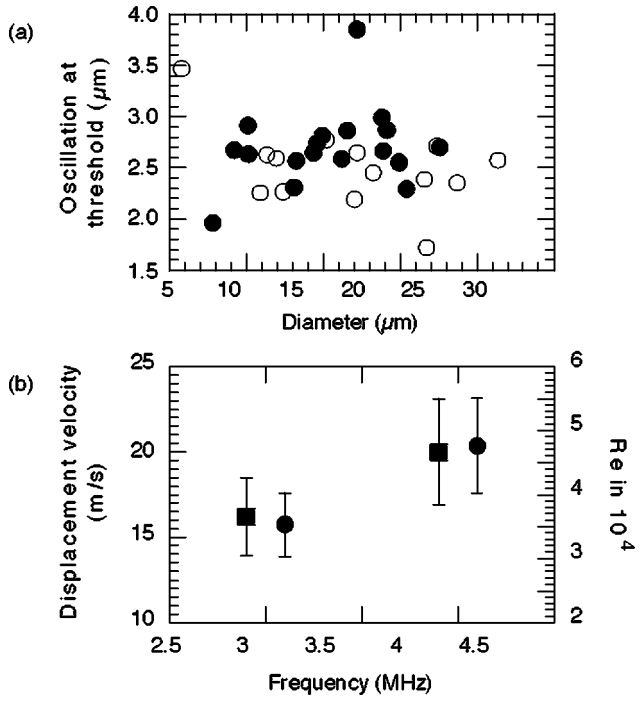

FIG. 7. Droplets of various diameters were analyzed for the magnitude of dipole oscillation at the threshold of vaporization. (a) The peak to peak amplitude was found to be ~2.6 μm, independent of the droplet's size. (b) The average displacement amplitude at a given frequency was used to compute the average velocity (circles) at which the droplet was assumed to be moving relative to the host fluid. Additionally, the corresponding Reynolds number was computed (squares). The error bars are based on the single standard deviation of the displacement amplitude.

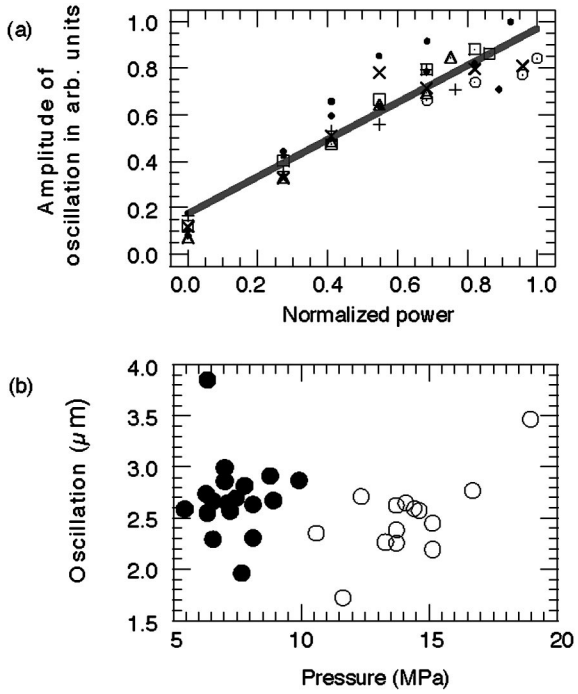

FIG. 8. (a) Amplitude of oscillation of individual droplets as a function of normalized acoustic power. Shown are the results for seven droplets. A linear fit yields $y=0.17+0.80x$ with $R^2=0.87$, i.e., the amplitude of oscillation increases linearly with applied power. (b) Amplitude of oscillation at threshold for ADV as a function of applied pressure. The data points represent distinct droplets of various diameters.

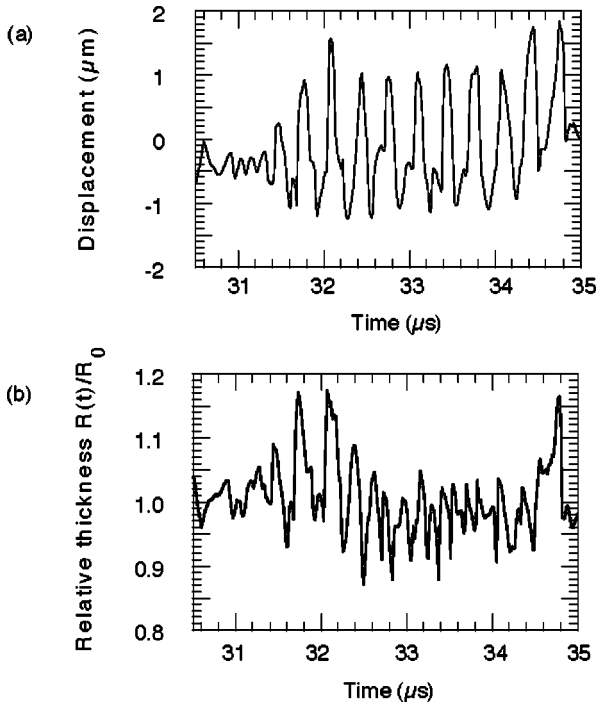

FIG. 9. Dipole (displacement) and thickness oscillation of a 16-μm-diam droplet. The spectral amplitude of the displacement is 40 dB above the noise and 13 dB above the image resolution. The thickness oscillation (i.e., the axial width in the streak image) is 7 dB above the noise and of the same order as the image resolution. However, in general, it has been observed that the initial thickness oscillation does show a spectral response at 3 MHz.

B. Aspect ratio

In terms of a potential variation in the aspect ratio of the droplets, an oscillation of the droplet radius on the order of 0.85–1.15 radii was observed [see Fig. 9(b)]. This magnitude of oscillation is not very large compared to the beforementioned optical resolution of 0.46 μm per image pixel. Streak line traces were transformed into frequency space in order to extract the amount of oscillation at the frequency of the transmitted acoustic wave. Spectral amplitudes were then compared to pixel resolution and noise floor of the spectrum.

Equation (4) was used to evaluate the predicted error in the aspect ratio estimate, which is based on two assumptions: (1) conservation of volume ($V_1=V_2$) and (2) equal deformation in the two dimensions (y and z), which cannot be seen in the streak image,

$$V_1=V_2,\quad \tfrac{4}{3}\pi R_0^3=\tfrac{4}{3}\pi x y^2,\quad \Lambda=\frac{y}{x},$$
$$\delta\Lambda=\sum_{s\in\{R_0,x\}}\left|\frac{\partial}{\partial s}\left(\frac{R_0}{x}\right)^{3/2}\right|\Delta s=\frac{3\Delta R}{R_0}. \tag{4}$$

For Eq. (4), R and x are the initial and "streak" radii, respectively; ΔR and Δx are the experimental errors and they are of the same order. Therefore the error for the aspect ratio (Λ) is 18%, which is of the same order as the magnitude of the thickness vibration.

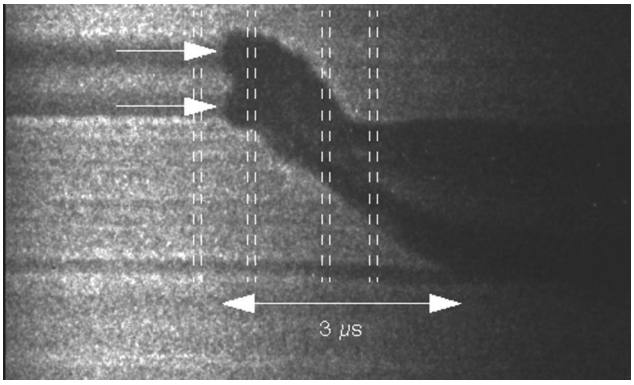

FIG. 10. The streak image shows that the nucleation is starting at the proximal and distal positions on the central axis of the droplet (see arrows). The vertical lines are the beginning and end of exposure of single full frame images. As in Fig. 3, the time axis is from the left to the right.

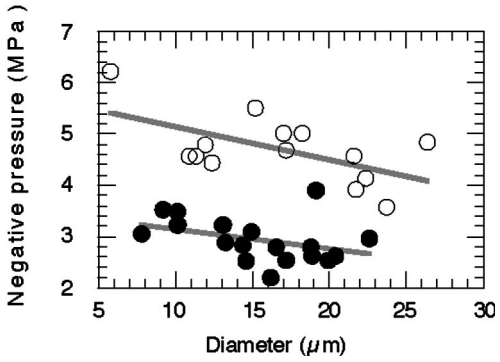

FIG. 11. The pressure threshold for ADV was evaluated as a function of droplet diameter. In general smaller droplets required higher pressures for vaporization. (fit parameters: $P=3.5-0.038\,d$ ($R^2=0.14$) for 3 MHz (closed circles) and $P=5.8-0.065\,d$ ($R^2=0.35$) for 4 MHz (open circles).

C. Nucleation site

The onset of vaporization was monitored as either spot-like and subsequently expanding centers of nucleation inside the droplet, or as homogeneous throughout the droplet's imaged cross section. The latter is possibly due to the limited temporal resolution of the full frame two-dimensional images of the camera system. Spot-like centers of nucleation were observed solely along the axis parallel to the direction of oscillation and centered on the droplet along the direction of dipole-type motion of the droplet. This axis is essentially the same as the direction of the propagating acoustic wave (see Fig. 6). The positions where the nucleation occurs will be referred to as proximal and distal with respect to the incident sound wave, where proximal is toward the incident sound wave and distal is away from it. Typically a second nucleation site was observed. Its location was diametrically opposed to the first site which conforms with the change in direction of motion, i.e., with the oscillatory movement of the droplet as seen in the streak image in Fig. 3. The experiments of Figs. 6 and 10 were performed at an acoustic center frequency of 10 MHz. Each full frame image covers 0.1 μs, which is the same as one cycle of the acoustic wave. If there are motion induced nucleations based on a preferred direction, then those should be occurring in the same full frame image or at least in the following frame. Figures 6 and 10 show that the gas nuclei complete the phase transition within the droplet on a time scale from several hundred nanoseconds to 3 μs. The same dual nucleation site of phase transition was also observed for insonification at center frequencies of 3 and 4 MHz, even though the effect was not well visualized. This was assumed because of the increase in exposure time for each frame from 100 to 200 ns.

D. Acoustic threshold

Observing ADV of droplets with diameters ranging from 7 to 22 μm yielded acoustic peak-to-peak pressure thresholds at 3 MHz of 3.9 to 2.2 MPa, respectively. It has been observed that smaller droplets require more acoustic energy for vaporization than larger droplets (see Fig. 11) This functional dependence of the ADV pressure threshold on droplet size is consistent with earlier experiments where the pressure threshold for vaporization of filtered and unfiltered emulsions was measured [see Fig. 12 and Kripfgans *et al.* (2000) for materials and methods]. Earlier free field experiments on emulsions over a wider frequency range showed a decrease in threshold for ADV with increasing frequency, which is contradictory to the current experiments. However, this contradiction and the higher thresholds for ADV may be caused by the rather complex acoustic field resulting from the presence of the flow tube and its location just beneath the microscope objective. This should not affect the dependence of the pressure needed for ADV on the droplet's size. More on this follows in the numerical results below.

E. Potential motion of the flow tube

Laser interferometry yielded an average tube displacement amplitude of 0.24 μm. This is on the order of the error in the displacement measurement from the streak camera and approximately one order of magnitude smaller than the droplet translatory motion. The tube displacement could be correlated in delay time as well as burst length with the transmitted 20 cycle acoustic tone burst.

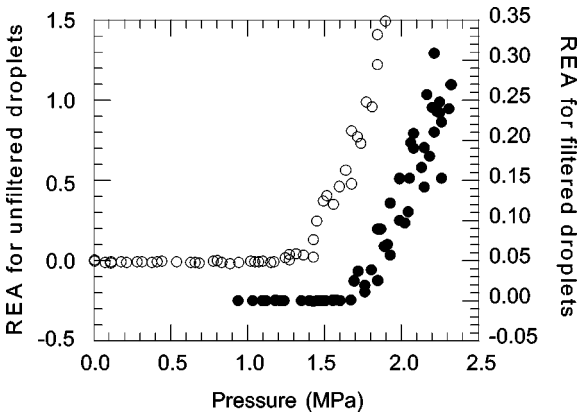

FIG. 12. The pressure threshold for ADV was measured for unfiltered (open circles) and for 8 μm filtered droplets (closed circles). Filtering increased the threshold from 1.4 to 1.7 MPa P.

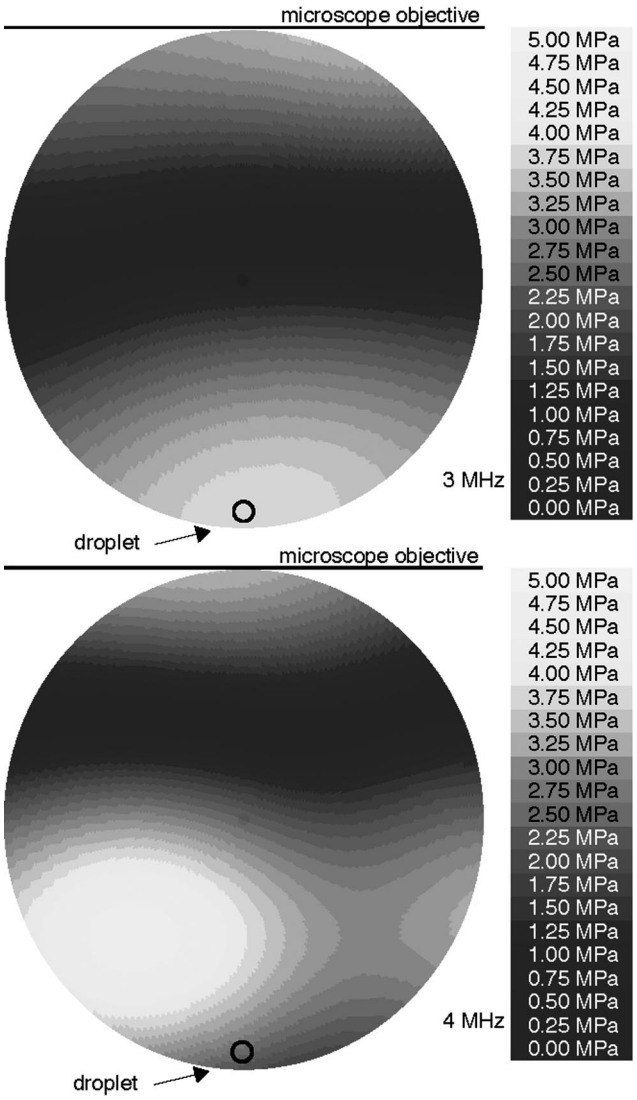

FIG. 13. Envelope of acoustic field inside a 152-μm-i.d. cylinder (50 μm wall thickness). At 3 MHz, the water and solid wavelength are 500 and 833 μm, respectively. Top 3 MHz, bottom 4 MHz. Note that the range of acoustic field at the droplet location (small black circle on top of image) is small (3.3–3.7 MPa) for the case of 4 MHz compared to the 3 MHz case (4.5–4.8 MPa). A nonlinear gamma function has been used for the amplitude to gray scale conversion.

V. NUMERICAL RESULTS

A. Field simulation

Sound fields were computed for 3 and 4 MHz. The goal of the simulation was to derive the pressure amplitude distribution inside the flow tube for various frequencies and to show how unpredictable the acoustic field is due to the interference of tube and microscope objective. The small hollow black circle in Fig. 13 has been added to the bottom of the graphs to illustrate where the droplet would be located. The simulated area is the inside of the flow tube. The acoustic field at the droplet location is smaller (2.5 MPa) for the case of 4 MHz and larger in the 3 MHz case (3.7 MPa). This could explain the apparent discrepancy in frequency dependence for ADV in this experimental arrangement compared to that seen previously.[3,5] Therefore, the actual pressure amplitudes that the droplets experienced were not the free field values obtained by the transducer calibration.

B. Droplet oscillation

A droplet with 8.5 μm radius was simulated to be exposed to a 3 MHz and 6.7 MPa peak-to-peak sound field. Bessel and other functions [see Eq. (1)] were included to order 1. An oscillatory force along the central axis with an amplitude of 0.1 mN results. Subsequently Eqs. (1) and (2) yield a displacement amplitude of 0.128 μm. This is one order of magnitude smaller than the approximately 1.3 μm displacement observed in the experiment.

Earlier measurements on the potential motion of the flow tube were presented indicating that the motion was small compared to that of the droplets. In addition, data already presented can be analyzed in a slightly different way to further argue for the motion of the droplet rather than the tube. Figure 8(a) shows how the observed oscillation increases with acoustic power for any given droplet. Figure 7(a) shows that all droplets oscillate with a maximum amplitude of $\sim$1.3 μm before they are vaporized. Figures 11 and 12 show that smaller droplets require more acoustic energy to vaporize and moreover they also require more energy to oscillate $\sim$1.3 μm [Fig. 7(a)]. However if the droplets oscillated rigidly with the tube, an increase in power should increase the oscillatory motion regardless of the observed droplet and its size. This is not the case as shown in Fig. 8(b) since it is the amplitude of the droplet oscillation, not the amplitude of the acoustic field, that predicts the threshold for ADV. It is therefore concluded that the observed droplets are moving and acoustic scattering as well as hydrodynamic flow lead to a constant amplitude of oscillation which is assumed to be the cause for ADV itself and discussed in the following.

C. Droplet shape oscillation

Shape oscillation amplitudes were computed in addition to translational motion. It has been seen that the diameter of the droplet changes while exposed to the acoustic wave (see Figs. 3 and 9). The experimental deformations were on the order of 15%. The following parameters were used for the simulation: $ka=0.108$, 8.5 μm spherical droplet radius, and a DDFP/saline interfacial tension $33.8\times10^{-3}\,\mathrm{N\,m^{-1}}$ (as measured in our lab). A droplet of that size and acoustic excitation of 1, 2, 5, 10, and 20 MPa (assuming a free field which is likely not the case here) should deform the droplet by 0.56%, 1.1%, 2.8%, 6.0%, and 13.8%, respectively. Slightly higher aspect ratios were observed, even though those values were of the same order as the noise. The thickness oscillation as seen in Fig. 9 is maximum at the beginning and at the end of the acoustic burst. This is where the droplet's center of mass motion, with respect to the surrounding fluid, accelerates and decelerates. A droplet as given before, with a translational velocity of $16.2\,\mathrm{m\,s^{-1}}$ and first-order shape oscillation ($l=2$), yields a coupling of 0.23 (see Sec. III C.). However, while the droplet is in transition from rest to steady state oscillation, the ratio as given in Eq. (3) is closer to unity, *allowing* the droplet to perform shape oscillations (Fig. 14).

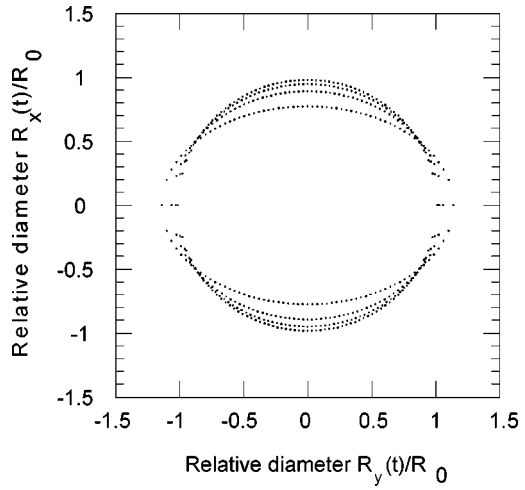

FIG. 14. Simulated droplet deformation using a droplet levitation theory (Ref. 12). The normalized droplet shape is plotted for acoustic pressure amplitudes of 2, 5, 10, and 20 MPa.

VI. DISCUSSION

The apparent oscillations in the streak images (3 and 4 MHz cases) and the derived droplet motion were compared to theoretical models as given in the literature. These models do not account for the complex geometry of the acoustic field or for its highly nonlinear character due to the large sound pressures used. However, these models could provide some understanding of the motion of the droplet in the acoustic field and help build a hypothetical basis for the nucleation. The same holds for the field simulation. However, it is assumed that including focusing and/or nonlinearities will also show that a free field pressure calibration cannot predict the *in situ* pressure. Therefore the result of the pressure threshold for ADV at 3 MHz being smaller than at 4 MHz may not contradict our earlier findings.[3,5] In fact the ratio of the simulated pressure values for 3 to 4 MHz is 1.33. A previously measured frequency dependence of ADV[5] yielded a ratio of 3 to 4 MHz of 1.24, which is close when taking the shortcomings of the model into account.

Dowson and Taylor report nucleation events in the lubrication fluid between a spherical cap sliding in close contact over a plane surface as well as between a sphere separating perpendicularly from a wall.[19] An object separating from a surface is assumed to cause a similar situation as when an object moves through a liquid. Hydrodynamic cavitation and its subsequent shock wave on the object's surface might trigger the vaporization of the DDFP inside the droplet. The location of the cavitation with respect to the relative motion of the fluid is similar to that in our experiments, e.g., the case of the first nucleation as seen in Fig. 6.

The dynamics of flow past a sphere can be easily found in fluid dynamics textbooks.[20] For a Reynolds number of $\mathrm{Re}_{cr} \sim 5 \times 10^5$, a sudden dip in the drag coefficient occurs due to the transition of the boundary layer to turbulence. In super cavitation,[21] cavitation is used to reduce drag. A linear velocity of 50 $\mathrm{m\,s^{-1}}$ is required to induce super cavitation on torpedoes. For ADV the speed for the possible oscillation is 15–20 $\mathrm{m\,s^{-1}}$, and cavitation induced this way would occur first at the direction of motion. Another example of flow induced cavitation has been reported on concrete tunnels. A so-called ''threshold'' velocity of 30 $\mathrm{m\,s^{-1}}$ was necessary to initiate cavitation.[22] A comparison with the above-noted examples should be done with caution, since the exact mechanism for ADV has not been established.

The heating of the droplet due to the radiation from the 2.5 kW light source and possible focusing of the light inside the droplet were estimated. Two cases were evaluated: (1) An evenly distributed light intensity yields a temperature rise of 0.008 °C which lasts for milliseconds, and (2) focusing the light intercepted by the droplet into 2.5% of the droplet's diameter yields a temperature rise to more than 200 °C, which lasts for approximately 50 μs (refer to chapter 15 in Kittel and Kroemer[23] for details on the heat conduction equation). A more precise estimate is beyond this paper because (a) focusing through the curved walls of the droplet (refractive index 1.24, water 1.33), is best described by what is known as a caustic pattern, where the focus is distributed along a epicycloid and (b) the reflection and transmission coefficients vary largely by the angle of the incident light beam.

However, one might argue that the light is not the cause for the vaporization because droplets do not vaporize (a) if the acoustic pressure is too low and (b) focusing of the incident light beam occurs along the axis of the incident light beam, which should appear in the center of the droplet in the images taken, since the axis of the light beam is perpendicular to the image plane (see Fig. 1).

It is assumed that ADV is either (a) the result of the superposition of dipole radiation and the incident field itself leading to acoustic cavitation or (b) hydrodynamic cavitation with a separation of the boundary layer and coupling of the external flow field to the interior of the droplet, causing an internal circulation.

VII. SUMMARY

The vaporization of single droplets has been observed. Experiments revealed translational motion of droplets in the acoustic field with an average 2.6 μm peak to peak displacement (independent of droplet size), at which point vaporization occurred. The theoretical model of a rigid sphere predicts a translation of 0.33 μm peak to peak. Furthermore it has been observed that droplets deform when exposed to ultrasound. A theoretical prediction of up to 15% deformation was confirmed through the experiment. The process of vaporization has been observed with full frame images as well as in streak mode. The nucleation starts at the proximal and distal positions on the central axis of motion. From the droplet displacement amplitude an average droplet speed of 15 to 20 $\mathrm{m\,s^{-1}}$ was computed. The acoustic pressure threshold for ADV was found to be inversely related to the droplet size.

ACKNOWLEDGMENTS

We would like to thank Dr. C. L. Marcelo for use of her microscope. Furthermore we thank Professor K. Grosh and T. Nawar for their great support with their laser vibrometer. Dr. C. P. Lee is acknowledged for letting us use his software

to simulate the action of a droplet in the acoustic field. Supported in part by PHS Grant No. R01HL54201 and U.S. Army Grant No. DAMD17-00-1-0344.

[1] R. E. Apfel, ''The superheated drop detector,'' Nucl. Instrum. Methods Phys. Res. A **162**, 603–608 (1979).
[2] R. E. Apfel, ''Activatable infusable dispersions containing drops of a superheated liquid for methods of therapy and diagnosis,'' US patent 5,840,276 (1998).
[3] O. D. Kripfgans, J. B. Fowlkes, D. L. Miller, O. P. Eldevik, and P. L. Carson, ''Acoustic droplet vaporization for therapeutic and diagnostic applications,'' Ultrasound Med. Biol. **26**, 1177–1189 (2000).
[4] T. Giesecke and K. Hynynen, ''Ultrasound-mediated cavitation thresholds of liquid perfluorocarbon droplets *in vitro*,'' Ultrasound Med. Biol. **29**, 1359–1365 (2003).
[5] O. D. Kripfgans, J. B. Fowlkes, M. Woydt, P. O. Eldevik, and P. L. Carson, ''*In vivo* droplet vaporization for occlusion therapy and phase aberration corrections,'' IEEE Trans. Ultrason. Ferroelectr. Freq. Control **49**, 726–738 (2002).
[6] M. Strasberg, ''Propeller cavitation noise after 35 years of study,'' ASME Symposium on Noise and Fluids Engineering, 1997, pp. 89–99.
[7] D. H. Trevena, ''Cavitation and the generation of tension in liquids,'' J. Phys. D **17**, 2139–2164 (1984).
[8] H. K. Christenson and P. M. Claesson, ''Direct measurements of the force between hydrophobic surfaces in water,'' Adv. Colloid Interface Sci. **91**, 391–436 (2001).
[9] K. K. Shal'nev, I. I. Varga, and D. Sebestyen, ''Investigation of the scale effects of cavitation erosion,'' Philos. Trans. R. Soc. London, Ser. A **260**, 256–266 (1966).
[10] Y. R. Tian, R. G. Holt, and R. E. Apfel, ''Deformation and location of an acoustically levitated liquid-drop,'' J. Acoust. Soc. Am. **93**, 3096–3104 (1993).
[11] Z. C. Feng and Y. H. Su, ''Numerical simulations of the translational and shape oscillations of a liquid drop in an acoustic field,'' Phys. Fluids **9**, 519–529 (1997).
[12] C. P. Lee, A. V. Anilkumar, and T. G. Wang, ''Static shape and instability of an acoustic levitated liquid drop,'' Phys. Fluids A **3**, 2497–2516 (1991).
[13] W. T. Shi and R. E. Apfel, ''Deformation and position of acoustically levitated liquid drop,'' J. Acoust. Soc. Am. **99**, 1977–1984 (1996).
[14] Y.-H. Su and Z. C. Feng, ''Numerical simulation of the dynamics of acoustically levitated drops,'' J. Acoust. Soc. Am. **99**, 2799–2810 (1996).
[15] P. M. Morse and K. U. Ingard, *Theoretical Acoustics* (Princeton University Press, Princeton, NJ, 1986), pp. 418–441.
[16] C. F. Bohren and D. R. Huffman, *Absorption and Scattering of Light by Small Particles* (Wiley, New York, 1983), p. 477.
[17] A. D. Pierce, *Acoustics—An Introduction to its Physical Principles and Applications* (Acoustical Society of America, New York, 1991), pp. 434–435.
[18] O. A. Basaran, T. C. Scott, and C. H. Byers, ''Drop oscillations in liquid-liquid systems,'' AIChE J. **35**, 1263–1270 (1989).
[19] D. Dowson and C. M. Taylor, ''Cavitation in bearings,'' Annu. Rev. Fluid Mech. **11**, 35–66 (1979).
[20] P. K. Kundu, *Fluid Mechanics* (Academic, San Diego, 1990), p. 638.
[21] S. Ashley, ''Warpdrive underwater,'' Sci. Am. **284**, 70–79 (2001).
[22] M. J. Kenn, ''Cavitation and cavitation damage in concrete structures,'' Proceedings of the Sixth International Convention on Erosion by Liquid and Solid Impact., 1983, paper 12, pp. 1–6.
[23] C. Kittel and H. Kroemer, *Thermal Physics*, 2nd ed. (Freeman, San Francisco, 1980).

Acoustic Droplet Vaporization for Temporal and Spatial Control of Tissue Occlusion: A Kidney Study

Oliver D. Kripfgans, *Student Member, IEEE*, Catherine M. Orifici, Paul L. Carson, *Member, IEEE*, Kimberly A. Ives, O. Petter Eldevik, and J. Brian Fowlkes, *Member, IEEE*

***Abstract*—Acoustic droplet vaporization (ADV) has been introduced with the potential application of tumor treatment via occlusion and subsequent necrosis. New Zealand White rabbits were anesthetized, and their left kidney was externalized. An imaging array and single-element transducer were positioned in a tank with direct access to the kidney's vasculature and renal artery. Filtered droplet emulsions (diameter <6 μm) were injected intra-arterially (IA) into the left heart during insonification of the renal artery, and the extent of blood flow reduction by ADV was compared to the untreated right kidney. Flow cytometry (using colored microspheres) of kidney tissue samples and reference blood from the femoral artery allowed the quantitative estimation of regional blood flow. A maximum regional blood flow reduction in the treated region of $>90\%$ and an average organ perfusion reduction of $>70\%$ was achieved using ADV. After treatment of the left kidney, the control kidney on the contralateral side showed a maximum decrease in regional blood flow of 18% relative to the pre-ADV baseline. Image-based hyper-echogenicity from ADV of IA injections was monitored for approximately 90 minutes, and cortex perfusion was reduced by $>60\%$ of its original value for more than 1 hour. This could be enough time for the onset of cell death and possible tumor treatment via ischemic necrosis. Moreover, currently used radiofrequency tissue ablation-based tumor treatment could benefit from ADV due to the decreased heat loss via vascular cooling.**

I. Introduction

Previous in vivo experiments on canines reported that acoustic droplet vaporization (ADV) could be used to reduce the blood flow in brain tissue [1]. Acoustic vaporization of droplets is a technique using the acoustic field of a focused ultrasound transducer to vaporize droplets. These droplets are superheated at body temperature, but remain in the liquid state due to their geometrical shape and possibly due to the added surfactant (serum albumin) that stabilizes them against coalescence. Exposure to an acoustic pressure field transforms droplets from a liquid to gaseous state in which they can be used to occlude blood vessels. In the above mentioned study, ADV produced with a clinical ultrasound scanner was repetitively capable of causing a quantitative blood flow reduction to an average of -34% relative to the baseline. This paper shows to what degree the blood flow in an entire organ can be reduced using a single-element transducer as a therapy transducer. Additionally, in the current study, the renal artery (i.e., the supply vessel of the target tissue site) is insonified, but the previous paper targeted the intended tissue site directly.

Furthermore, this paper will determine to what degree blood flow can be suppressed and for what time frame, which we see as prerequisite information for future methods of cancer treatment either via occlusion therapy, drug delivery, or in support of radiofrequency tissue ablation (RFA). Acoustic targeting can be used to spatially localize ADV-induced blood flow occlusion. Only where the acoustic pressure amplitude exceeds the threshold for ADV will droplets form gas bubbles and occlude downstream vessels. Other tissue sites will not be occluded.

The objective of the following work was to test whether it is possible to reduce the vascular flow in an organ that is strongly perfused. Moreover, investigations included the duration of flow reduction and what systemic effects could be observed.

The lepus (rabbit) model was selected in which the kidney was targeted as the tissue to be treated. Compared to human tumors in the breast or prostate, lepus kidneys are of similar size and possess a greater perfusion [2]–[4]. These two tumor types were chosen due to their superficial location. Of course, it needs to be verified if occlusion with possible localized drug delivery is a suitable treatment type for these malignancies. The supportive use of ADV for RFA in renal carcinoma is an additional reason for choosing kidneys as a target tissue [5].

II. Materials and Methods

A. General Experimental Setup

As mentioned in the introduction, lepus was used as the animal model with the target tissue for occlusion being the kidney. For each rabbit, the left kidney was externalized and a water bath was made from a section of PVC tubing (5-cm tall and 12-cm diameter) was positioned over the externalized kidney and glued to the skin using

Manuscript received May 14, 2004; accepted November 22, 2004. Supported in part by PHS Grant No. R01EB000281-07 and U.S. Army Grant No. DAMD17-00-1-0344.

O. D. Kripfgans, P. L. Carson, O. P. Eldevik, and J. B. Fowlkes are with the University of Michigan, Radiology Department, Ann Arbor, MI (e-mail: greentom@umich.edu).

C. M. Orifici and K. A. Ives are with the University of Michigan, Biomedical Engineering Department, Ann Arbor, MI.

Fig. 1. Left: Standoff water tank to provide acoustic access to the externalized kidney. Right: Single element (f# = 1.5) therapy transducer with focus pointer plus attached imaging array.

medical adhesive (Medical Adhesive, P/N 7730, Hollister, IL). This type of attachment creates a water bath without an interface layer between the transducer and the target tissue (see Fig. 1). Metal cradles attached to the water bath were used to secure the kidney into position, and a specially machined transducer arm held a focused phased array imager and a treatment transducer. The treatment transducer was a single PZT element with a 3.5-MHz center frequency, 25.4-mm aperture, and 37.5-mm focal length (A381S, Panametrics, Waltham, MA). A system of two function generators and an amplifier were used to drive the single-element transducer. One function generator provided the short tone burst signal that was supplied to a gated amplifier and the second function generator provided a gating signal for the power amplifier (55 dB, Model 350, R.F. Gated Amplifier, Matec Instruments, Inc., Northborough, MA) that was driving the treatment transducer, also called the ADV transducer. Typically 500 Vpp with a pulse duration of 13 cycles at 3.5 MHz, i.e., 3.7 μs was applied to the ADV transducer. The pulse repetition interval was kept at 1 ms due to amplifier limitations (1% maximum duty cycle) and to prevent heating of the target tissue. Acoustic pressure amplitudes at this setting were as high as 9.2 MPa peak negative and 20 MPa peak to peak. Pressures were measured using a calibrated membrane hydrophone (Reference Shock Wave Hydrophone^{TM}, Sonic Industries, Hatboro, PA). In terms of the mechanical index (MI), 9 MPa peak negative pressure at 3.5 MHz corresponds to an MI of 4.8. The measured waveforms with a burst length, pulse repetition rate, and peak negative pressure of 3.7 μs, 1 kHz, and 9 MPa, respectively, yielded an I_{SPTA} of 10 W cm^{-2}. It has to be noted here that the pressure amplitude used is substantially higher then the measured pressure threshold for ADV in vitro. It was not the goal of this study to find the minimum pressure for ADV in vivo.

On the contrary, 9 MPa is a very high value for cavitation-induced bioeffects. However, the very short burst duration of 3.7 μs limits the likelihood of such effects. Based on a vessel diameter of 2 mm, blood flow of 22.5 mL min^{-1}, the average velocity is 11.9 cm s^{-1}. Therefore, the mean transit time through an ultrasound beam of 1-mm diameter at the focus is 8 ms or eight firings. In a previous study the effect of the pulse repetition frequency on ADV was evaluated and found that approximately 25% of the vaporizable droplets do vaporize for a single insonification [6]. Therefore, five to six firings are required for 100% vaporization. During eight firings the local blood is exposed to a total on-time for ultrasound of 29.6 μs (3.7 μs $\times$ 8).

A pointer, which could be attached to the surface of the treatment (ADV) transducer, was used to register the position of its focus in the scan plane of the imager. The array's center frequency was 10 MHz with an aperture of 15 mm (FPA 10 MHz, GE Vingmed, Horten, Norway). At a depth of 3 to 4 cm the lateral image size of the clinical ultrasound scanner (System V, GE, Horten, Norway) was large enough to encompass both the kidney and the cross section of the renal artery. It was helpful to mount the treatment transducer's acoustic axis coplanar with the imaging plane. The focus of the treatment transducer then could be positioned inside the renal artery just before it entered the kidney and have visual feedback of the onset and progress of the treatment (image guided therapy).

Once the transducers were positioned inside the water tank, B-mode, color flow mode (CFM) and spectral Doppler (PW) of the imaging system were used to verify the anatomic position, especially in terms of cross section through the kidney. The setup required the scan plane to show the incoming renal artery as well as major arterial vessels downstream and inside the kidney in order to visually monitor and record droplet phase transition and blood flow reduction. Real-time feedback was provided by B-mode, CFM, or PW.

B. Microsphere Analysis

The gold standard for blood flow measurement was the usage of colored microspheres (Interactive Medical Technologies (IMT), Irvine CA). These spheres are injected into the left ventricle where good mixing is ensured due to the turbulent flow in the chamber. This required an arterial catheter [3 French (FR)] to be inserted into the right femoral artery and placed into the heart under X-ray guidance using a C-arm (Stenoscope GE, Cincinnati, OH). Typically, 1 mL of microsphere solution containing 1 million spheres was injected per flow measurement. The microspheres lodge in the capillaries of the downstream tissues but with negligible occlusion because of their low concentration. According to the specifications of the spheres, up to seven injections can be made without measurably changing the blood flow. This allows for the injection of up to seven different colors for measurements at independent time points. Quantitative values for flow relied on one more quantity, that being the withdrawal of blood from a major artery leaving the heart. The protocol used for sphere handling, requiring a total blood withdrawal time of 2 minutes at the rate of 1 mL/minute, was as follows:

- Withdrawal of blood for 2 minutes at a rate of 1 mL/minute from the left-side femoral artery using a syringe pump (Harvard Apparatus 22, Harvard Apparatus, Inc., South Natick, MA). This defines time zero.
- After 20 seconds microspheres solution was injected into the heart; 1 mL per 20 seconds.
- Next, 1 mL of saline was injected to flush the injection catheter; 1 mL/20 seconds.
- Then 0.3 mL of heparinized saline was injected to prevent clogging of the catheter; 0.3 mL/2 seconds.
- After a total of 2 minutes, the blood withdrawal was stopped and the collecting syringe was sealed and labeled.

These steps were repeated for several colors to evaluate the flow under various conditions. More precisely, microspheres were injected (the five steps above) 5 minutes before the left kidney was externalized and 5 minutes after externalization. Additional microsphere injections were performed 1 minute before a treatment (called "pre") and 1 minute after treatment (called "post"), in which a treatment consists of multiple droplet injections and accompanying ADV. More microsphere injections followed 30, 60, and 90 minutes after the treatment to study the recovery of the blood flow after treatment.

After the animal was sacrificed, both kidneys were surgically removed and dissected into their tissue types (cortex and medulla), and where applicable into three spatial regions (cranial, center, and caudal), as well as into three sections (dorsal, medial, and lateral). Tissues and blood samples were sent to IMT for processing.

Regional blood flow was computed from the counted microspheres in the tissue samples (N_{tissue}), the tissue weight (w_{tissue}), and the reference blood withdrawal (N_{blood}) as specified in the microsphere protocol.

$$\mathrm{RBF}\left[\frac{\mathrm{mL}}{\mathrm{min}\cdot\mathrm{g}}\right] = \frac{N_{tissue}}{w_{tissue}[\mathrm{g}]N_{blood}[\mathrm{min/mL}]}. \quad (1)$$

C. Droplet Preparation

The injected droplet emulsion was made from 75% (v/v) saline-albumin solution (5 mg/mL) and 25% (v/v) dodecafluoropentane (DDFP, C_5F_{12}, CAS #678-26-2). The mixture was sealed in an auto sampler vial (3 mL) and shaken for 30 s at 5000 cpm (MSD Wig-L-Bug, Crescent Dental Mfg. Co., Elgin, IL). A concentrated droplet emulsion with 9.5×10^9 droplets per millileter resulted (Multisizer III, Beckman Coulter Inc., Fullerton, CA, see also Fig. 2). Specifically, for this animal model, lepus albumin was used to stabilize the emulsion instead of commonly used bovine albumin to eliminate systemic reactions of the animal to the foreign protein. Moreover, the emulsion was filtered to ensure the droplets were transcapillary, i.e., the largest droplet diameter was smaller then the capillary diameter of 6 μm [7]. Filtering was done immediately before administration to the animal. Three hundred microliters stock solution was diluted into 10 mL saline, then filtered into another syringe through four membrane filter discs (25, 16, 8, and 5 μm in that order, cat numbers: 1441 325, 1443 055, 1440 042, 1106 13, Whatman, Kent, United Kingdom) that were placed inline. The size distribution of filtered and unfiltered droplets can be seen in Fig. 2. The receiving syringe was positioned vertically to allow the separation of stable and unstable droplets, the latter of which formed gas bubbles. Then, 1 mL of this solution (1.6×10^8 filtered droplets) was injected at a rate of 1 mL/min^{-1} into the arterial catheter that led into the left heart chamber.

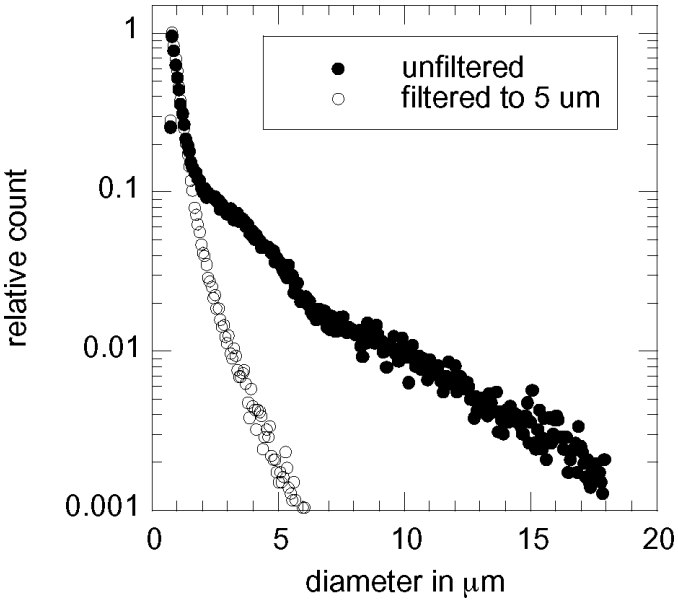

Fig. 2. Size distribution of droplets before and after filtering with membrane filters down to 5 μm pore size. Data was acquired using a Multisizer III.

D. Animal Preparation

A total of 14 rabbits were used: 11 animals for positive occlusion experiments and three animals for control experiments with no active ADV. New Zealand White female rabbits, 2 to 3 kg were used for this study. The animals initially were anesthetized with Ketamine (35 mg/kg) and Xylazine (5 mg/kg) and intubated. Fur was shaved from their abdomen and back to give acoustic access throughout the abdomen. The animal then was placed on a heated pad to prevent hypothermia throughout the experiment. Isoflurane (3% to 1%) was used as the long-term anesthetic and was administered by forced ventilation. Two arterial catheters and one venous catheter were placed in the femoral arteries and lateral ear vein, respectively. Electrocardiogram (EKG), body core temperature (rectal probe), and heart rate, and blood oxygenation (pulse oximeter) were monitored during the experiment.

The animals were euthanized after the experiment by injecting Pentobarbital (0.22 mL/kg) intravenously (IV) followed by bilateral pneumothorax. The University Committee for Use and Care of Animals approved all animal procedures.

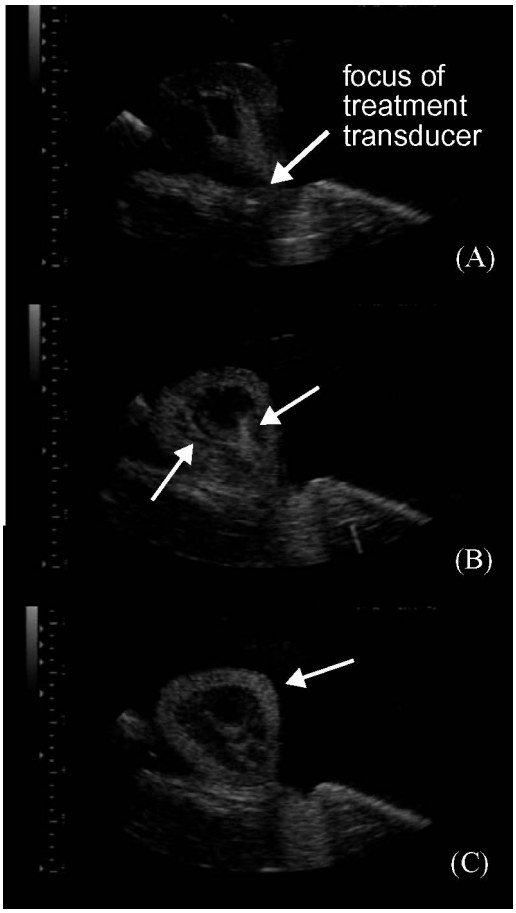

Fig. 3. B-mode image of kidney cross-section before (A), during (B), and after (C) ADV. In (B) one can see how the gas bubbles move downstream via the arterial system and lodge in the cortex (C).

III. Experimental Results

A. Ultrasonic Imaging and Doppler Flow Measurements

Fig. 3 shows image-based feedback of ADV as recorded by the imaging array. Fig. 3(A) is a baseline image before the onset of ADV. The treatment transducer is on, but no emulsion is being injected. The white arrow is pointing to the renal artery. In Fig. 3(B) one can see that droplets are converted in the renal artery, filling downstream vessels with hyper-echoic gas bubbles. This illuminates a "horizontal" vascular branch on the lower half of the interior of the kidney as well as a "vertical" vessel on the right side (see arrows). Up to three treatments were performed. Each time approximately 1.6×10^8 droplets were injected IA. In Fig. 3(C) the vascular bed (the cortex) is filled with gas bubbles.

Underlying tissues are acoustically shadowed after the target tissue is sufficiently filled with gas bubbles. Fig. 4(A) is a baseline image before ADV and Fig. 4(B) was taken after ADV. In this case, droplets were vaporized using a 10 MHz linear array imaging transducer applied to the kidney cortex. After ADV, the top cortex almost completely shadowed everything below; some structure is still visible (arrow).

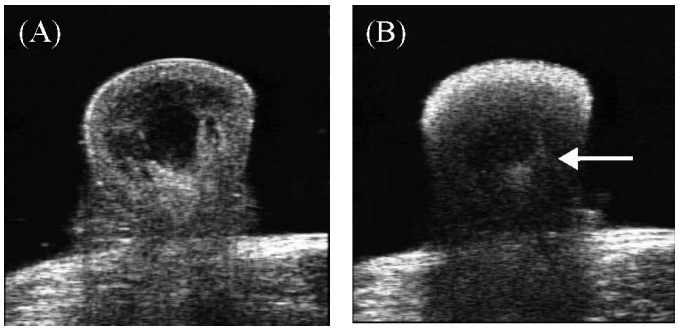

Fig. 4. Typical shadowing effect on distal tissue after ADV. Before (A) and after ADV (B).

Other feedback was acquired by means of CFM and spectral (pulse wave) Doppler (PW). Fig. 5 shows four spectral Doppler traces taken in the renal artery. Trace Fig. 5(A) was recorded before ADV, and Fig. 5(B) during ADV in which one can see the interference from the ADV field (indicated by the white arrow). Fig. 5(C) which shows after the interference indicated by the white arrow, is immediately after ADV, and Fig. 5(D) is 5 minutes after ADV. The small interference effect in Fig. 5(D) may be the result of spontaneous vaporization due to the PW field or caused by small recirculating gas bubbles. Directly after treatment, the peak flow velocity is reduced by approximately 50% as is the temporal duration of the Doppler waveform during each cardiac cycle. This indicates an overall reduction in blood flow. Fig. 6 shows the effect in CFM of the kidney vasculature. Note that there is a substantial decrease in the detectable flow when comparing before Fig. 6(A) and immediately after ADV Fig. 6(B). This reflects reduction in flow velocities in the major vessels of the kidney in response to the distal blockage of the capillary bed. However, it is also possible that acoustic shadowing and color write priority settings of CFM may also suppress the detection of any existing flow. No such effect would be present in the PW results from the renal artery.

B. Microsphere Measurements

It was necessary to use microsphere flow cytometry to quantitatively determine flow changes after treatment (ADV), as image-based flow detection was subject to changes in acoustic access. Fig. 7 shows regional results from colored microsphere tissue analysis. The kidney being dissected as described in Section II results in 12 data sets per color label for regional sampling. Regional perfusion after ADV of treated and untreated kidney are plotted as a percent change from baseline before ADV. The selected baseline is the blood flow measured after kidney externalization but prior to treatment. This ensures that the flow reduction was the result of ADV treatment rather than physical stress on the kidney from the externalization process (see Section IV).

The untreated kidney shows some change in blood flow after ADV, but remains approximately at 0% change in regional perfusion. In contrast, the left kidney regional blood

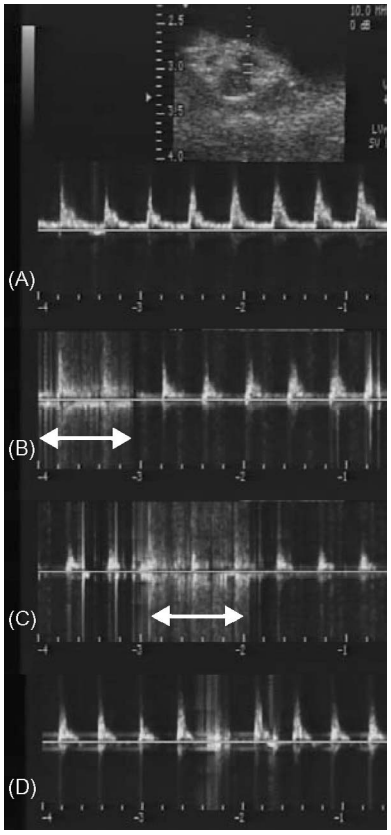

Fig. 5. Pulse wave Doppler spectrum taken in an artery inside the kidney before (A), during (B), after ADV (C), and partial recovery at 5 minutes after treatment (D). The white arrows indicate where the treatment transducer is active, and interference with the imaging system can be seen.

flow drops after ADV to −73%. This kidney was treated and, therefore, was expected to change.

It was observed that dorsal and medial cortex tended to show a lower perfusion on average after treatment compared to the lateral cortex and medulla. For the untreated kidney, tissue-by-tissue analysis does not show this separation.

Before ADV, left and right kidney perfusion is statistically identical ($p = 0.15$, using a Student's T-test assuming a two-sample unequal variance and heteroscedastic distribution); but, after ADV, left and right kidney perfusion is statistically different in all locations ($p < 0.0001$, except for one case with $p = 0.2$).

Results from colored microsphere tissue analysis show a drop in total blood flow to the treated kidney after ADV and blood flow recovery after treatment. Fig. 8 shows the blood flow reduction to the left and right kidney as a function of time.

At 0, 30, 60, and 90 minutes after ADV, the right (untreated) kidney cortex perfusion exhibits a maximum drop of −17%. But, the left (treated) kidney cortex perfusion drops right after ADV to −80% relative to its pre-ADV flow and recovers to −46% within 90 minutes. Similar trends can be seen for medullary tissue. After ADV, the left kidney medulla perfusion drops to −69% and recovers to −14% after 90 minutes. The right kidney medulla perfusion varies between −18% and +1.7%.

The ratio of cortex to medulla blood flow has been computed for the left and right kidney. After ADV, the right kidney shows a ratio of 8.2 ± 0.10, but the left kidney's ratio is $7.6 \pm .0.79$ (see Fig. 9). A ratio of 9 was found in the literature [8].

IV. Discussion and Conclusions

The ratio of cortex to medulla blood flow was used to determine how well cortex and medulla tissue was dissected separately. This was achieved to within 90% or better.

Variances were observed, not only variations in the treatment were observed, but also baseline variations between animals. Therefore, for comparison between animals, only percent blood flow reduction was presented. Significant blood flow reduction was found after ADV. Renal cortex occlusion with an average of 72% flow suppression was observed after ADV in the renal artery. Simultaneously, the blood flow in the cortex of the contralateral/untreated kidney rose to 3.6%. After 90 minutes, the capillary flow in both kidneys recovered to −45.6% and −3.15% relative to the pre-ADV baseline for treated and untreated kidney, respectively.

For individual kidneys, it has been seen that, after ADV, blood flow in the contralateral kidney may increase or decrease. Left and right kidneys are not independent systems. Autoregulation [8] controls blood flow and urine production, and it was assumed that the unilateral occlusion also caused a certain degree of flow regulation. Two possibilities are: an increase in blood flow in the untreated kidney to compensate for loss of blood flow in the treated kidney or a decrease in blood flow in the untreated kidney to balance the urinary output relative to the treated kidney.

The extent of total occlusion as well as blood flow recovery after the treatment are important measures to evaluate the potential for cancer treatment using ADV. Studies by Parkins *et al.* [11] and Chaplin and Horsman [12] acknowledge tumor treatment via occlusion. However, they found that reduction in blood flow lowers the core temperature of superficial tumors, which in turn increases the survival of tumor cells by approximately 2 orders of magnitude despite the treatment. Moreover, significant growth delays were found for occlusion times on the order of 4 hours. This would require repetitive treatments of ADV. However, the use of a kidney as a centrally vascularized tumor model is validated by Rubin and Casarett [13] who states, "The major branches from the host vessels supply the tumor via a hillus not unlike the kidney. The pattern of vascular supply is that of a branching tree with large trunks in the centre of tumor nodules, which grow by forming smaller branches."

The kidney differs from tumors with centralized vasculature in that it receives a much larger percentage of the blood flow (20% of total blood flow is directed to the kid-

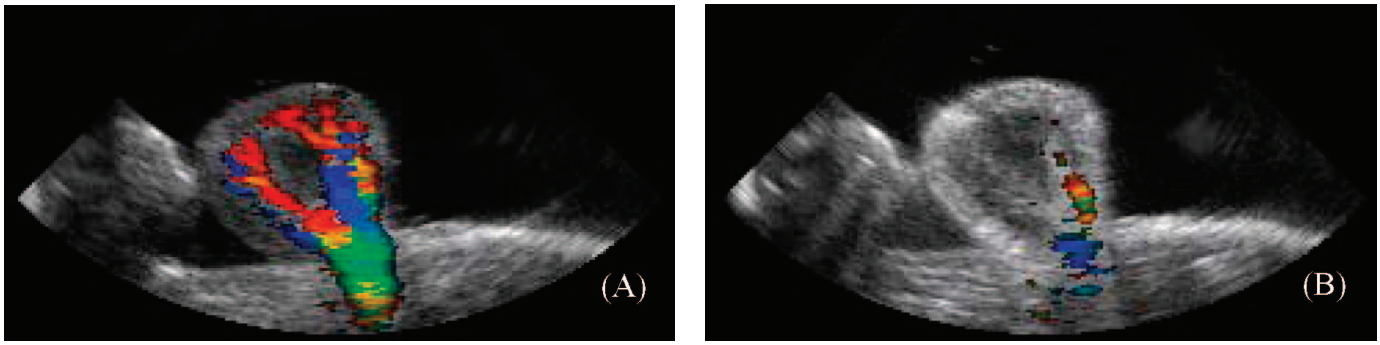

Fig. 6. Color flow mode image of the kidney before (A) and after (B) ADV. Before ADV one can see the renal artery as it enters the organ and branches through the medullary tissue toward the capillaries of the cortex. After ADV some reduction in color flow detection may be due to attenuation, but most is due to reduced flow.

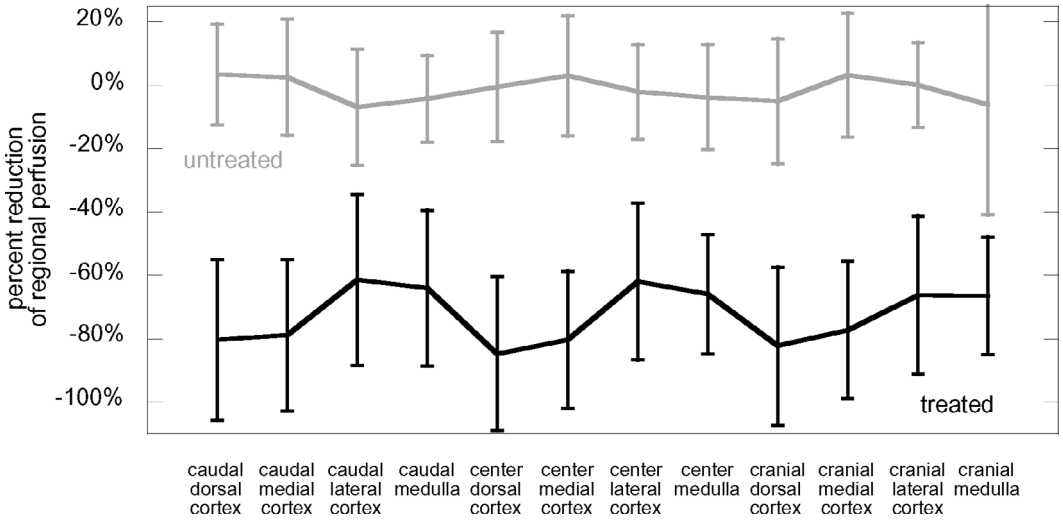

Fig. 7. Change in regional blood flow (RBF) after occlusion via ADV. Shown are results for treated and untreated kidney after ADV. The two curves show percent change in perfusion by tissue type/location. The top, gray graph is measured in the untreated kidney; the lower, solid black graph represents the treated kidney. Both graphs show error bars of single standard deviation of the mean based on statistical evaluation of seven animals.

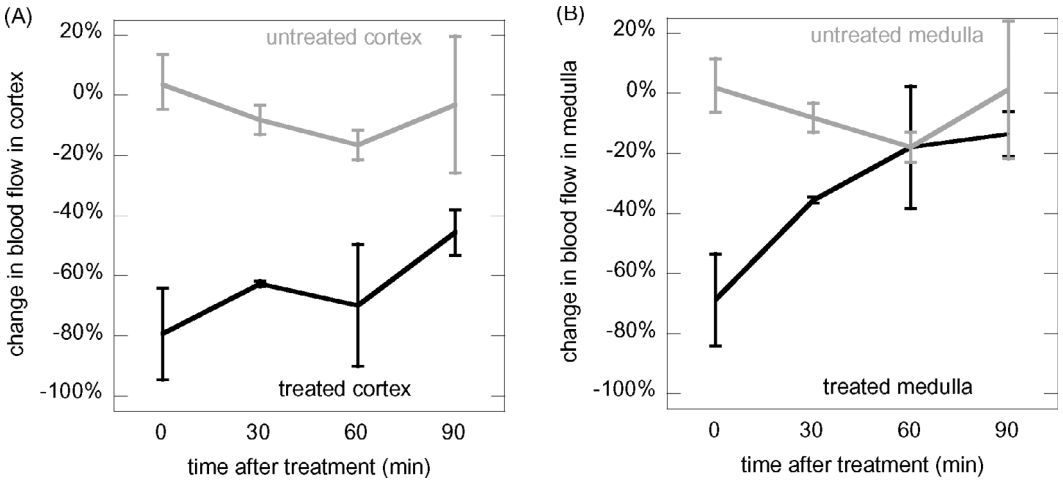

Fig. 8. Change in tissue perfusion to the kidneys after ADV. (A) Perfusion in the cortex of treated (black graph) and untreated (gray graph) kidney. (B) Perfusion in treated (black graph) and untreated (gray graph) medulla. The graphs show error bars of single standard deviation of the mean based on statistical evaluation in four animals.

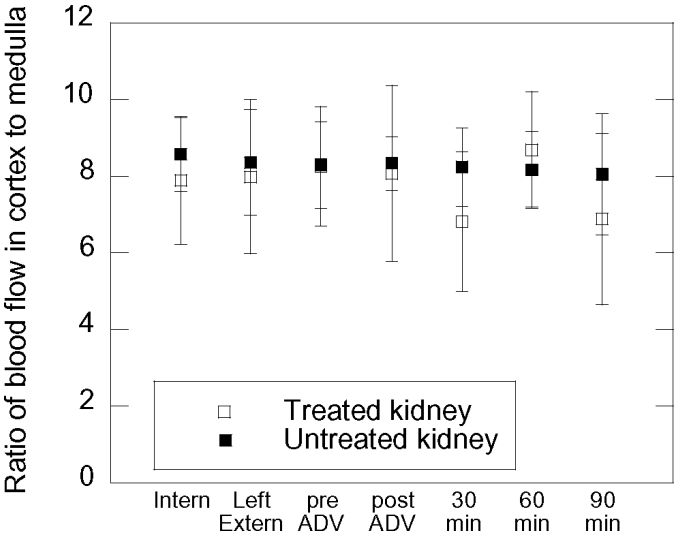

Fig. 9. Ratio of total blood flow through cortex to total blood flow through medulla, after ADV treatment of the left kidney.

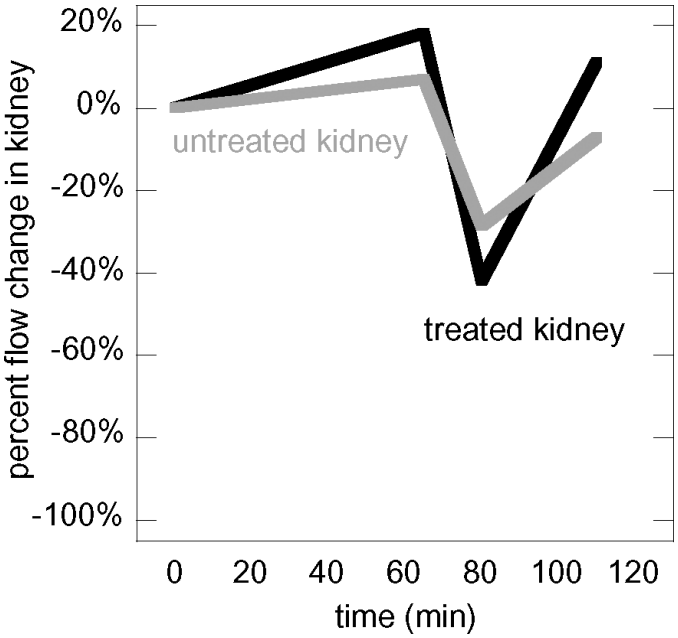

Fig. 10. Total blood flow to the left and right kidney as a function of time after left kidney externalization. This data results from 12 tissue samples in three control rabbits.

neys at any point of time). Fluid pressure of blood in the kidney is highly regulated by various chemical and mechanical mechanisms to maintain the necessary exchange to the collecting system. As these differences in the kidney presumably impede the ability to block flow, the kidney can be treated as a "worst case" tumor scenario, and successful occlusion of flow to this organ is assumed to indicate the likely ability to occlude flow to tumors. However the irregularities in tumor vasculature (i.e., shunting and pooling) will require testing on any occlusion method in tumor tissue.

A. Change in Kidney Blood Flow Due to Externalization

Three rabbits were used to evaluate the effect of externalization of the left kidney. Measurements were performed for five kidney states: while the kidneys were still inside the abdomen; after the left kidney was externalized, and after approximately 1, 1.5, and 2 hours after the kidney was externalized (see Fig. 10). For each of these rabbits, one microsphere injection was performed at one of the time points after externalization. Therefore, there are no error bars, and the total blood flow was computed by integrating the flow of all tissue samples. The left kidney is externalized, and the right kidney remains inside the rabbit's abdomen. The right kidney has not been externalized in order to minimize the overall burden on the system of the animal. The blood flow to left and right kidney changes after externalization. From the literature one can find blood flow values for an internalized kidney of 20–25 mL min^{-1} [9]. Our baseline measurements showed the same values (21 mL s^{-1}) for blood flow before any intervention or surgical procedures. Additionally, the regional blood flows for cortex and medulla were compared to values found in the literature. Cortical blood flow is about 5 mL g^{-1} min^{-1}. The blood flow is about 2.5 mL g^{-1} min^{-1} in the outer medulla and 0.6 mL g^{-1} min^{-1} in the inner medulla [10]. Microsphere results here for internal kidneys yielded 3.02 ± 0.67 (mean $\pm$ std), 1.19 ± 0.43, 3.24 ± 0.33, and 1.27 ± 0.52 mL g^{-1} min^{-1} for left cortex, left medulla, right cortex, and right medulla, respectively. These flows are lower than the literature values that may be the result of the anesthesia used.

B. Bioeffects

It has been seen that administration of DDFP-based emulsions can cause substantial bioeffects. Riess [14] reported that injection of fluorocarbon emulsions include short- and long-term effects that spontaneously resolve within 12–24 hours. Moreover, he lists animal species that are sensitive to the administration of perfluorocarbons and show "pulmonary hyperinflation". Along with pigs and monkeys, he lists rabbits as having a failure of lungs to collapse at autopsy. We observed this during the beginning of our study as well. It was reported [15] that 10% (v/v) and 60 mL kg^{-1} injection of a fluorocarbon-decalin emulsion caused hyperinflated, noncollapsible lungs, but others do not show clinical symptoms for a dose of 10% (v/v) and 20 mL kg^{-1}.

After filtering of our droplet emulsion to 99.99% less than 6 μm (see Fig. 2) and limiting the injection volume to three injections of 300 μL droplet emulsion [25% (v/v)], we have seen no adverse effects. Three injections correspond to 0.126 mL kg^{-1} ($\sim$2 kg rabbit weight) of droplet emulsion, compared to 2 mL kg^{-1} in the reported case above.

According to Riess' report [14], observations of adverse effects in administration to humans is less likely than that

for rabbits, pigs, or monkeys. Therefore, one could assume that an increased ADV treatment dose would be tolerated, thus yielding a longer-lasting effect for embolization.

C. Prospects of Cancer Treatment

Two main conclusions for cancer treatment using ADV can be drawn:

Vascular occlusion, can be used for a variety of cancer types. Millimeter-sized gelatin sponge spheres or iodized oils are used for intra-arterial embolization [16], [17]. Treated masses can be of the order of 50-mm diameter, and typically, occlusion is accompanied by deposition of a chemotherapy drug to increase local cytotoxic effects and minimize systemic effects. It is assumed that perfluorocarbon-based emulsions can be made to carry and, upon vaporization, locally deposit chemotherapy drugs. It also could be beneficial to use local deposition of chemotherapy agents directly inside of the tumor's vasculature because of the nature of cancer blood vessels. Typically, vessel walls of tumor vasculature are very permeable. It has been verified in our laboratory that at least two-component droplets of DDFP and vegetable oil can be produced and vaporized using ultrasound. To fully propose ADV as an alternative to catheter-based embolization and local drug deposition, it remains to be tested whether ADV can be functional for intravenous administration. This is feasible because the agent for occlusion is small and transpulmonary in contrast to currently used gelatin based spheres. Moreover, focused ultrasound deploys the occlusion agent where intended.

Many tumors are treated using RFA in which one or a set of spatially arranged needles are inserted percutaneously into the tumor mass. An electric current guided by the needles heats the tissue locally to exceed the thermal threshold for cell death. This effect is compromised whenever large vessels are nearby, or strong perfusion by itself acts as a heat sink and causes the in situ temperature to drop. Prior vascular occlusion could prevent this effect and benefit RFA.

D. Image-Based Versus Microsphere Feedback

It has been shown that image-based feedback for ADV has limitations that might discourage its use. However, it provides a real-time feedback with ultrasound during treatments. In the case of RFA, for example, ultrasound provides feedback for a tissue region that naturally contains a large fraction of gas during and after the treatment due to boiling. In any case, ultrasound could be used to additionally check for remaining blood flow before RFA. This is especially helpful for cancers with a defined vascular supply that can be monitored with either pulse wave Doppler or color flow.

Acknowledgment

We wish to thank Dr. Ronald Bude for assistance for catheterization of the animals and related discussions.

References

[1] O. D. Kripfgans, J. B. Fowlkes, M. Woydt, O. P. Eldevik, and P. L. Carson, "In vivo droplet vaporization for occlusion therapy and phase aberration corrections," *IEEE Trans. Ultrason., Ferroelect., Freq. Contr.*, vol. 49, no. 6, pp. 726–738, 2002.

[2] G. S. Gerber, R. Goldberg, and G. W. Chodak, "Local staging of prostate-cancer by tumor volume, prostate-specific antigen, and transrectal ultrasound," *Urology*, vol. 40, no. 4, pp. 311–316, 1992.

[3] J. M. Sabaté, A. Gómez, S. Torrubia, A. Camins, N. Roson, P. de Las Heras, and V. Villalba-Nuño, "Lymphoma of the breast: Clinical and radiologic features with pathologic correlation in 28 patients," *Breast J.*, vol. 8, no. 5, pp. 294–304, 2002.

[4] T. S. Koh, L. H. Cheong, Z. Hou, and Y. C. Soh, "A physiologic model of capillary-tissue exchange for dynamic contrast-enhanced imaging of tumor microcirculation," *IEEE Trans. Biomed. Eng.*, vol. 50, no. 2, pp. 159–167, 2003.

[5] Z. Kariya, K. Yamakado, A. Nakatuka, M. Onoda, S. Kobayasi, and K. Takeda, "Radiofrequency ablation with and without balloon occlusion of the renal artery: An experimental study in porcine kidneys," *J. Vasc. Interv. Radiol.*, vol. 14, pp. 241–245, 2003.

[6] O. D. Kripfgans, "Acoustic droplet vaporization for diagnostic and therapeutic applications)," Ph.D. dissertation, University of Michigan, Applied Physics, 2002.

[7] B. R. Gilbert, B. R. Leslie, and E. D. Vaughan, "Normal renal physiology," in *Campbell's Urology.* 6th ed. P. C. Walsh, Ed. 1992, pp. 70–90.

[8] A. Just, H. Ehmke, L. Toktomambetova, and H. R. Kirchheim, "Dynamic characteristics and underlying mechanisms of renal blood flow autoregulation in the conscious dog," *Amer. J. Physiol. Renal Physiol.*, vol. 280, no. 6, pp. F1062–F1071, 2001.

[9] F. Lyrdal and T. Olin, "Renal bloodflow and function in the rabbit after surgical trauma. I. An experimental study," *Scand. J. Urol. Nephrol.*, vol. 9, no. 2, pp. 129–141, 1975.

[10] H. Gray, P. L. Williams, and L. H. Bannister, *Gray's Anatomy: The Anatomical Basis of Medicine and Surgery.* New York: Churchill Livingstone, 1995.
Horsman

[11] C. S. Parkins, S. A. Hill, S. J. Lonergan, J. A. Chadwick, and D. J. Chaplin, "Ischemia-induced cell-death in tumors—Importance of temperature and pH," *Int. J. Radiat. Oncol.*, vol. 29, no. 3, pp. 499–503, 1994.

[12] D. J. Chaplin and M. R. Horsman, "The influence of tumor temperature on ischemia-induced cell death—Potential implications for the evaluation of vascular mediated therapies," *Radiother. Oncol.*, vol. 30, pp. 59–65, Jan. 1994.

[13] P. Rubin and G. Casarett, "Microcirculation of tumors. Part 1: Anatomy, function, and necrosis," *Clin. Radiol.*, vol. 17, pp. 220–229, 1966.

[14] J. G. Riess, "The design and development of improved fluorocarbon-based products for use in medicine and biology," *Artif. Cells Blood Sub. Immobil. Biotechnol.*, vol. 22, no. 2, pp. 215–234, 1994.

[15] L. C. Clark, R. E. Hoffmann, and S. L. Davis, "Response of the rabbit lung as a criterion of safety for fluorocarbon breathing and blood substitutes," *Biomat., Art. Cells Immob. Biotech.*, vol. 20, no. 2–4, pp. 1085–1099, 1992.

[16] T. J. Vogl, M. G. Mack, J. O. Balzer, K. Engelmann, R. Straub, K. Eichler, D. Woitaschek, and S. Zangos, "Liver metastases: Neoadjuvant downsizing with transarterial chemoembolization before laser-induced thermotherapy," *Radiology*, vol. 229, no. 2, pp. 457–464, 2003.

[17] D. O'Toole, F. Maire, and P. Ruszniewski, "Ablative therapies for liver metastases of digestive endocrine tumours," *Endocr.-Related Cancer*, vol. 10, pp. 463–468, 2003.

Oliver Daniel Kripfgans (S'00) was born in 1969 in Saarbrücken, Germany. After finishing Gymnasium, he received his Diploma in Physics from the University of Saarbrücken in 1996. During his graduate studies (1989–1996), he was a research assistant in the Department of Ultrasound at the Fraunhofer Institut for Biomedical Engineering, St. Ingbert, Germany. His work included industrial as well as biomedical ultrasound, mostly related to microbubble detection and characterization. Mr. Kripfgans is currently working as a graduate research assistant toward a Ph.D. in applied physics at the University of Michigan, Ann Arbor. His current research interests include the interaction of micro-bubbles and -droplets with ultrasound, therapeutic, and diagnostic ultrasound as well as acoustic material properties and acoustic sensors. Mr. Kripfgans is a member of the Deutsche Physikalische Gesellschaft (DAGA), the Acoustical Society of America, and has been a Student Member of the IEEE since 2000. He received the Norman H. Horwitz Award at the Young Investigators Spring Symposium of the American Association of Physicists in Medicine and Health Physics Society (AAPM, Great Lakes Chapter) and the Best Student Paper Award in Biomedical Ultrasound/Bioresponse to Vibration from the Acoustical Society of America (ASA).

Catherine M. Orifici received her B.S. degree in Engineering Science and Mechanics at Virginia Tech in 2001. The same year she started graduate school at The University of Michigan in the Department of Biomedical Engineering and in 2003 she received her M.S. degree in Biomedical Engineering. From 2001 to 2003 Ms. Orifici was working as a Graduate Student Research Assistant in the Department of Radiology. Her research interests included acoustic droplet vaporization in fluids and in gels, as well as ultrasound induced bioeffects of droplet emulsions. Currently Ms. Orifici is working as a Biologist at The National Institute of Health (NIH) in Bethesda, MD.

Paul L. Carson (M'74) received the B.S. degree from Colorado College, Colorado Springs, and the M.S. and Ph.D. degrees from the University of Arizona, Tucson, in 1969 and 1971, respectively, all in physics. From 1971 to 1981, he served in the Department of Radiology at the University of Colorado Medical Center, Denver, and since 1981, he has served as Associate Professor or Professor and as Director of Basic Radiological Sciences in the Department of Radiology, University of Michigan Health System. His responsibilities have been in research, clinical support, and teaching of radiological sciences. The research has been in diagnostic ultrasound (quantitative imaging, functional imaging, equipment performance, safety, and new or improved diagnostic and therapeutic applications) and in magnetic resonance imaging. Dr. Carson is a fellow, past vice president, and J. H. Holms Basic Science Pioneer Award Recipient of the American Institute of Ultrasound in Medicine and is a fellow and past-president of the American Association of Physicists in Medicine. He is a fellow of the Acoustical Society of America, the American College of Radiology, and the American Institute of Medical and Biomedical Engineering. He is certified in Radiological Physics and in Clinical Engineering.

Kimberly A. Ives studied Animal Science at the University of Illinois and received her B.S. in 1984. Afterwards she pursued Veterinary Medicine at the University of Illinois and received her D.V.M. in 1987. From 1982 to 1983 Dr. Ives worked as an Research Assistant at the University of Illinois in the Department of Dairy Science and from 1984 to 1987 in the Department of Veterinary Toxicology. After she received her D.V.M., she worked as a Small Animal Veterinarian at the Wise Road Animal Hospital in Schaumburg, IL and at the Allen Animal Hospital in Livonia, MI. In 1998 Dr. Ives joined the University of Michigan, where she started as a Research Associate in the Department of Internal Medicine (Electrophysiology). Currently Dr. Ives is employed in the Departments of Radiology and Biomedical Engineering at the University of Michigan. Her research interests include toxicity and ultrasound based therapy and bioeffects.

Odd Petter Eldevik, M.D., Ph.D., is Clinical Professor of Radiology, Division Director for MR, and a faculty member of the Division of Neuroradiology in the Department of Radiology, University of Michigan Health System in Ann Arbor, Michigan.

Dr. Eldevik received his M.D. from the University of Bergen, Norway in 1966 and Ph.D. in 1983 at the University of Oslo, Norway. After internships, residency in diagnostic radiology in Norway in 1968, he underwent fellowships in Neuroradiology at Ullevål Hospital (1972–1973) and a research fellowship at Medical College of Wisconsin, Milwaukee (1977–1978). He served as radiologist (overlege) at Oslo University Hospital Ullevål, Oslo, Norway, from 1979 to 1990; as Chairman for Department of Neuroradiology from 1983 to 1990; and Chairman of Department of Radiology and Medical Services from 1989 to 1990. From 1990 to 1992, he acted as visiting Associate Professor at the Department of Radiology, University of Michigan, Ann Arbor, and, from 1992 to 2000, as Associate Professor. Then, since 2000, he has acted as Clinical Professor.

Dr. Eldevik has served in many committees and in the offices of national and international professional associations, among them as Chairman for the Norwegian Association for Radiology (1983–1988) and Chairman for the Advisory Committee on Clinical Track Appointments and promotions (University of Michigan Medical School, 1999–2001).

Dr. Eldevik has more than 50 peer-reviewed publications, most in neuroradiological topics, several on safety of contrast media. He has given a similar number of invited presentations at national and international meetings.

Dr. Eldevik's focus of teaching is neuroradiological topics including MR and CT of the brain, head, and neck and spin. Research topics are in functional MR, QA, and outcome studies in neuroradiology.

Jeffery Brian Fowlkes (M'94–A'94) is an Associate Professor in the Department of Radiology and Associate Professor in the Department of Biomedical Engineering. He is currently directing and conducting research in medical ultrasound including the use of gas bubbles for diagnostic and therapeutic applications. His work includes studies of ultrasound contrast agents for monitoring tissue perfusion, acoustic droplet vaporization for bubble production in cancer therapy and phase aberration correction, and effects of gas bubbles in the use of high intensity ultrasound. Dr. Fowlkes received his B.S. degree in physics from the University of Central Arkansas in 1983, and his M.S. and Ph.D. degrees from the University of Mississippi in 1986 and 1988, respectively, both in physics.

Contributions to the scientific community by Dr. Fowlkes include educational and research efforts and organizational service. Dr. Fowlkes has served the medical ultrasonic community by his participation in the American Institute of Ultrasound in Medicine as a member of its Board of Governors, as the Chair of its Bioeffects Committee, as a member of its Technical Standards and Annual Convention Committees. He also received the AIUM Presidential Recognition Award for outstanding contributions and service to the expanding future of ultrasound in medicine. As a member of the Acoustical Society of America, Dr. Fowlkes has served on the Physical Acoustics Technical Committee and the Medical Acoustics and Bioresponse to Vibration Technical Committee and on a standards committee working group on cavitation detection and monitoring. As a Member of the IEEE, he has worked with the IEEE I&M Society Technical Committee on Imaging Systems.

In Vivo Droplet Vaporization Using Diagnostic Ultrasound - A Potential Method for Occlusion Therapy?

O.D. Kripfgans, J.B. Fowlkes, O.P. Eldevik, P.L. Carson
University of Michigan Health Systems, Department of Radiology, Ann Arbor, MI, 48109-0553, USA

M. Woydt
University of Würzburg, Neurosurgery, Joseph-Schneider-Strasse 11, 97080 Würzburg, Germany.

Abstract - The experimental objective was to determine whether a transpulmonary droplet emulsion (90% < 6 μm diameter) can be used to temporarily form large gas bubbles (> 30 μm) which would be utilized to occlude the capillary bed of tissue. Gas bubbles can be made *in vivo* to potentially block capillaries, by acoustic droplet vaporization (ADV) of injected, superheated, dodecafluoropentane (DDFP) droplets [1]. Droplets evaporate into gas bubbles when exposed to an acoustic field who's peak rarefactional pressure exceeds a well defined threshold. It has been found that I.A. as well as I.V. injections can be used to introduce the emulsion into the blood stream and subsequently perform ADV (using B- and M-mode on a clinical ultrasound scanner) at the target site. I.V. administration results in a lower gas bubble yield, possibly due to droplet filtering in the lung, dilution in the blood volume or other circulatory effects.

I. Introduction

Currently occlusive therapy is used for cancer treatment including renal and hepatocellular carcinoma. According to Sandoval et al. [2] kidney tumors were successfully embolized and showed tumor necrosis after the first embolization in 78% of the cases studied. Embolotherapy utilizes materials that can be categorized as absorbable (blood cloth, cellulose, and gelatin sponge) and non-absorbable (particulates, fluids, coils, balloons, and streamers). Particulates can be as large as 50 μm in diameter.

Intra-venous injection of a transpulmonary, inherently inert, droplet suspension would require no arterial catherization for *in situ* placement of potentially-embolic materials. Localization of the treatment would be achieved by using a focussed non-ionizing radiation source, such as sound fields produced by clinical ultrasound scanners. For tumors with well defined arterial supply vessels, those vessels could be insonified by ultrasound (squares in figure 1) to create large gas bubbles which would block the blood flow as they are too large to pass the capillary bed. For tumors with less defined or accessible supply vessels, the capillary bed itself could be treated with ultrasound and subsequent bubble formation (circle in figure 1).

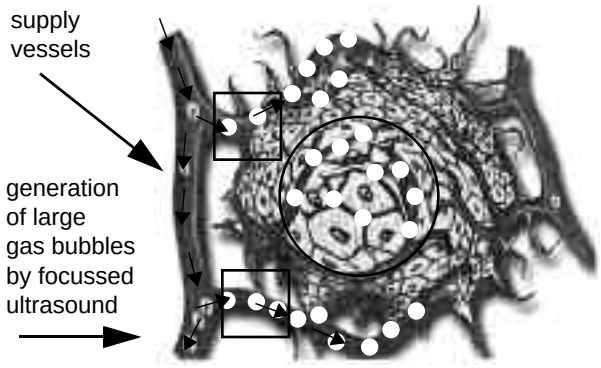

Figure 1: Focussed ultrasound could be used to generate large gas bubbles (> 30 μm diameter) from injected droplet emulsion, to locally occlude malignant tissue. Droplets could be vaporized in the supply arteries (indicated by the squares) or in the capillary bed (indicated by the circle) of the tumor.

II. Materials and Methods

In vitro experiments

The existence of an acoustic pressure threshold for ADV and it's functional dependence on the frequency of the transmitted pulse has been shown previously [1].

A matched set of transducers was used to repeat these experiments on the threshold for ADV to verify their validity under more controlled circumstances. Ultrasound images taken during ADV in flow tube experiments were used to analyze the rate of vaporization as a function of applied acoustic

pressure and frequency. The flow was imaged along the axis of the flow tube using a 10 MHz linear array scan head of a Diasonics Master Series (Diasonics VST series, Milpitas CA, USA) clinical ultrasound scanner. It has been seen that DDFP droplets boil when exposed to a certain acoustic pressure. Four transducers (Panametrics Inc., Waltham, MA, USA, types: A381S, A321S, A305S, and A308S) with center frequencies ranging from 2.25 to 7.5 MHz, 2.54 cm (1 inch) aperture and 3.81 cm (1.5 inches) focus were used to test a frequency range from 2 to 10 MHz. A more detailed description of the setup can be found in [1].

In vivo experiments

In an acute study, 10 canines anesthetized with isoflurane were used to verify acoustic droplet vaporization (ADV) *in vivo*. The droplets were made by shaking DDFP (C_5F_{12}, CAS #678-26-2) and an albumin-saline solution in a high speed vial shaker. The resulting droplet emulsion is stabilized against coalescence and 90% of the droplets are smaller than 6 μm in diameter, with a mean diameter of 3.6 μm. More details about this process can be found in [1].

A catheter line was placed in each, the left ventricle and in the left front leg for I.A. and I.V. injection, respectively. For observations of the brain, the skull was opened by a standard craniotomy. The brain was used as a model since brain tissue has low acoustic attenuation (<= 0.9 dB cm^{-1} MHz^{-1}) [5] and provides good conditions for initial tests on ADV *in vivo*. I.V. and I.A. injections were used to administer ~10^7 and ~10^6 droplets, respectively. All animal procedures were reported to and approved by the office of the University Committee on Use and Care of Animals (UCUCA) of the University of Michigan.

Colored microspheres (Interactive Medical Technologies, Ltd., Irvine, CA, NuFLOW fluorescent microspheres, 5x10^6 spheres per ml, 15 μm diameter) were used to measure the change in regional blood flow. The change in perfusion was measured by dissecting the treated volume as well as reference volumes from the brain. Both samples were approximately 10 mm by 10 mm and 3 mm thick; they were dissected from the plane covered by ultrasound. The two samples were processed to dissolve the tissue and keep the trapped microspheres. Flow cytometry yields the concentration of the spheres in tissue samples along with reference blood samples to estimate the regional blood flow. The eventual reduction in perfusion was computed by taking the ratio of the regional blood flow after ADV to the regional blood flow before ADV.

A Toshiba Power Vision 6000 clinical ultrasound scanner was used to image the brain before and after the administration of droplets. The penetration depth into the tissue was 10 mm and for focussing purposes a 10 mm stand-off pad (Parker Laboratories, Fairfield, NJ, USA; AquaFlex, Ultrasound Gel Pad) was used to set the focus to 20 mm. The acoustic output of the scanner was measured in water for M-mode at maximum acoustic output and 6 MHz center frequency using a planar hydrophone (Reference Shock Wave Hydrophone™, Sonic Industries, Hatboro, PA, USA). A 3D volume scan of the center M-mode line indicated a beam width of 1.53 mm (FWHM) was found at a depth of 20 mm. The acoustic pressure at this depth was approximately 3 MPa peak rarefactional pressure.

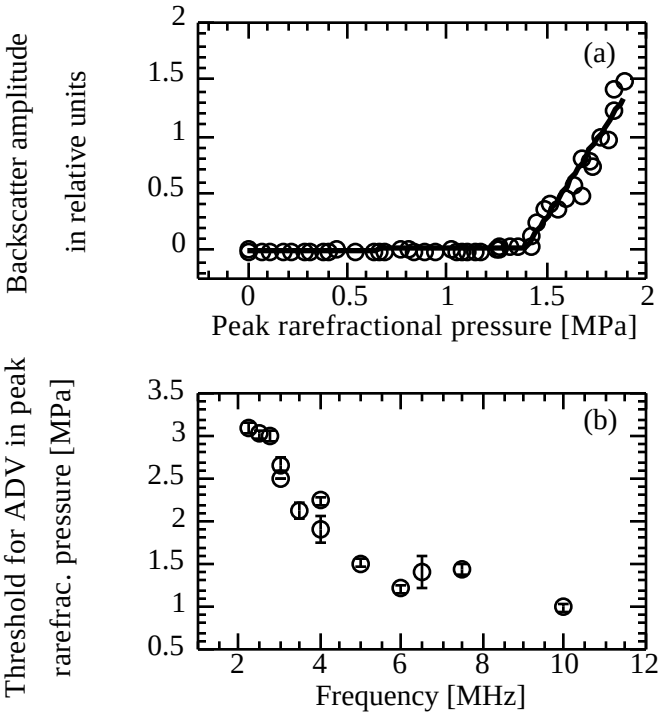

Figure 2: (a) At 7.5 MHz the threshold for acoustic vaporization of droplets is approximately 1.5 MPa PRP. At lower pressures droplets rarely, if ever, boil into gas bubbles. Therefore ultrasonic images of the area to be treated can be taken at pressures below 1.5 MPa PRP. The threshold for ADV is a function of frequency; it rises with decreasing frequency (b).

III. Results

In vitro verification of ADV

ADV has been successfully repeated and continues to exhibit a sharp threshold (figure 2a). For a transmit frequency of 7.5 MHz the pressure threshold for ADV is approximately 1.5 MPa peak rarefactional pressure (PRP). Figure 2b shows how the threshold for ADV decreases with increasing frequency from ~3 MPa PRP at 2 MHz to less than 1.5 MPa PRP at 6 MHz. Despite the frequency dependent attenuation in tissue, this trend suggests the use of higher rather than lower frequencies for ADV *in vivo*.

In vivo B-mode

As a first step, the acoustic vaporization of intra-arterial injected droplet emulsion was attempted using the Toshiba 6000 scanner at 6 MHz, MI of 0.6, imaging in B-mode. Approximately $3.3x10^6$ droplets were injected intra-arterial and subsequent insonification of a region in the white and gray matter yields a dense and spatially stationary gas bubble formation in the VOI (figure 3b). It should be noted

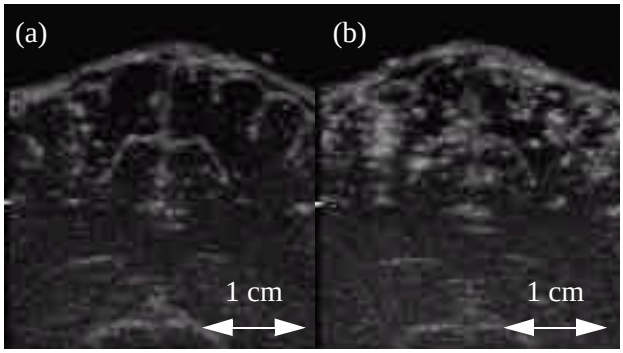

Figure 3: Gas bubble lifetime measurement in occipital region (at the back of the brain, posterior to parietal lobe). The droplets were vaporized using B-mode at 6 MHz. (a) The region before ADV, (b) some time after ADV. A 0.3 ml droplet solution was injected over 2 minutes (total of $3.3x10^6$ droplets).

that an increase in echogenicity of the monitored region was observed while injecting the droplet emulsion. First, this is due to the small, but non-zero echogenicity of the droplet emulsion itself; second, a small number of droplets may undergo spontaneous evaporation in the vasculature or at the injection site due to the pressure drop between syringe and artery.

In vivo M-mode

M-mode was used to limit ADV to one line in the scan plane or to a region which was scanned by sweeping the M-mode line across that region (see figure 4). For the case in figure 4 the perfusion on the left side of the brain was reduced by 31% relative to the untreated area on the right side of the brain. This

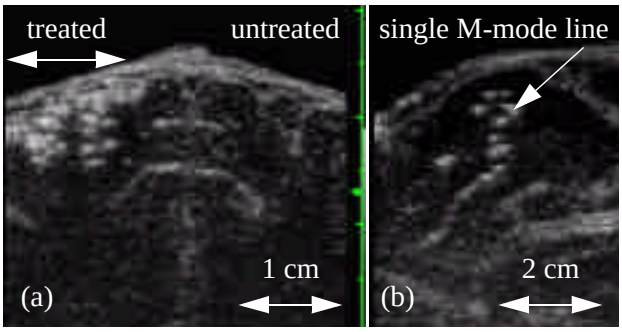

Figure 4: Tissue occlusion in the occipital lobe. Droplets were vaporized using M-mode at 6 MHz (see arrow). A 0.3 ml droplet solution was injected I.A. over 2 minutes (total of $3.3x10^6$ droplets). (a) coronal view with a swept M-mode line to cover a plane (treated area) of tissue. For the next 30 minutes this region was scanned to monitor the gas bubble life time. See figure 5 for the integrated echo of a particular region plotted as a function of time. (b) Sagittal view of single M-mode line.

region was imaged for 30 minutes after the formation of gas bubbles. Analysis of the average pixel intensity in a selected area (see figure 5) showed decay rates of the intensity in that area of approximately 0.3 dB/min. It is assumed that the decay is due to the dissolution of gas bubbles.

Acoustic imaging at low MI apparently did not evaporate injected droplets since even the intra-arterial injection of a ten-fold concentration showed very little gas bubble formation in the presence of B-mode imaging at an MI of 0.2. This is consistent with the *in vitro* results where a pressure threshold for ADV was observed (see figure 2).

Difference between I.V. and I.A.

Intra-arterial as well as intra-venous injections successfully deposited droplets in the circulatory system. However, the yield from I.A. injections is qualitatively much greater than the yield from I.V. injections. This is the case even for a ten-fold increase in the administered dose in order to compensate for the upper 10% in the droplet's size

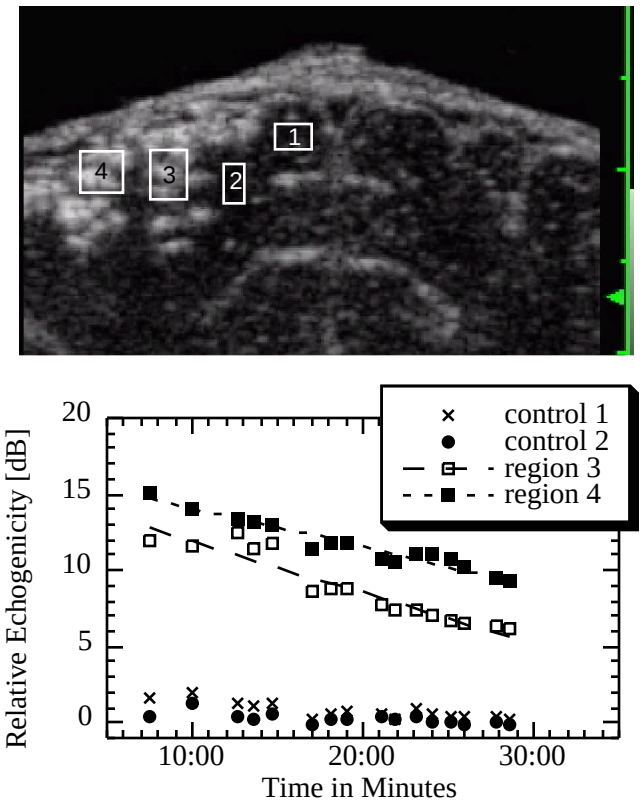

Figure 5: 'Lifetime' of gas bubbles made by ADV. The treated region is shown in figure 4. It has been reported that for *global* occlusion, a 10 minute blockage has a great likelihood to result in cell death (review paper by Lipton [3]). The echogenicity is plotted as a function of time relative to the intensity of each region before ADV.

distribution which is greater than 6 μm in diameter and therefore likely to be filtered by the lung.

IV. Conclusions and Future Work

Ultrasound at diagnostic levels and albumin stabilized DDFP droplets injected I.V. and I.A. can be employed to selectively create gas bubbles to potentially cause ischemia. If substantial occlusion is achieved to block primary and collateral flow, and the resulting ischemia is maintained for an extended period of time, this would result in ischemic necrosis. This makes ADV a possible procedure for occlusion therapy.

A potential source of error for microsphere analysis is the location and dissection of treated tissue. If the extracted source tissue block is larger than the actual treated region, the average reduction in perfusion will differ from the true reduction in the *treated* region. By treating a large and continuous volume of tissue, one could ensure the dissection of only 'occluded' tissue and measure the maximum possible effect. A second method for estimating the spatial extend of perfusion reduction is by histologic sectioning. After the injection of colored microspheres or particulate dye suspensions at high concentration one could find regions of no, or suppressed, perfusion.

The measured decay in echogenicity for gas bubbles after ADV (see figure 5) requires more careful study. A benchtop *in vitro* experiment with optical and acoustical observation of single gas bubbles would give the functional relation between decay of echogenicity and decrease in size. The knowledge of that relation would help to predict how long occlusion by ADV might be effective.

Moreover, a model for targeting the supply arteries of a specific tissue and subsequent bubble production in the vessel is necessary. A similar model, called contrast interruption, is currently under development in our laboratory [4]. This model could potentially be used to identify the supply vessels for a tumors site.

V. Acknowledgement

Work supported in part by PHS Grant No. R01 HL54201 from the National Heart, Lung and Blood Institute.

VI. Literature

[1] Kripfgans OD, Fowlkes JB, Miller DL, Eldevik OP, Carson PL. Acoustic droplet vaporization for therapeutic and diagnostic applications. Ultrasound in Med & Biol 2000; 26:1177-89.

[2] Sandoval PR, Wingartz PHF, Gonzalez HF. Renal embolization: experience in 81 patients. World Urol Update Series 1983; 11:2-7.

[3] Lipton P. Ischemic cell death in brain neurons. Physiological Reviews 1999; 79:1431-568.

[4] Fowlkes JB, Sirkin DW, Ivey JA, et al. Transcutaneous interruption of ultrasound contrast agents for blood flow evaluation. Investigative Radiology 1998; 33:893-901.

[5] Duck FA. Physical Properties of Tissue. San Diego: Academic Press; 1990.

High Speed Imaging of Acoustic Vaporization of Single Droplets

Oliver D. Kripfgans, J. Brian Fowlkes, Paul L. Carson
University of Michigan Health Systems, Department of Radiology, Ann Arbor, MI, 48109-0553, USA

Abstract - This paper will show the vaporization of single droplets by the application of single tone bursts. A high speed video system on a microscope was used to monitor droplets in a flow tube. A focused 3.5 MHz transducer was aimed at the intersection of tube and optical beam. A highly dilute droplet emulsion was injected and a special syringe setup was used to position individual droplets in the focus. Single 10 cycle bursts were sufficient to phase transition droplets. During the acoustic irradiation, the droplets showed dipole type oscillations along the acoustic axis (average amplitude 1.3 um, independent of droplet diameter). The onset of vaporization was monitored as either spot-like within the droplet or homogeneous through-out the droplet's imaged cross-section. The spot-like centers of nucleation were solely observed along the direction of oscillation. Smaller droplets required more acoustic energy for vaporization than larger droplets, which is consistent with earlier experiments on emulsions. Simulations of the free field scattering theory of rigid spheres have been found to be only a small fraction of the dipole motion in the experimental observations.

I. Introduction

It has been observed in the past that micrometer sized droplets in emulsions can be vaporized into gas bubbles by the application of tone bursts in the frequency and power range of diagnostic ultrasound [1]. This phenomenon is referred to as Acoustic Droplet Vaporization (ADV).

As a liquid agent up to 97% of the particles are smaller than 10 um, with an average diameter of 3 um. As droplets the particles are mostly transpulmonary and can be circulated through the body with the blood stream. Exposure to ultrasound creates 20 to 80 um diameter gas bubbles that can no longer pass the capillary bed and subsequently become trapped in vasculature. Two medical applications are currently under investigation which use this droplet emulsion and the vaporization thereof.

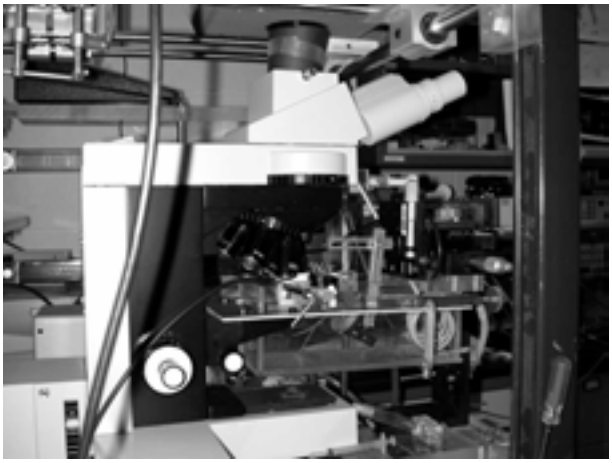

Fig. 1: A water tank is mounted under a microscope to image single droplets as they are being vaporized using a single ultrasound tone burst. To capture sub microsecond video frames, a high speed video system is attached to the microscope.

This is the direct intention for the first application. In the vessels upstream to a region of cancer tissue, gas bubbles are created which will subsequently block the blood flow to that region. For this therapeutic application a large number density of droplets/gas bubbles is needed, whereas the usage of a very sparse droplet population can be used to generate reference point beacons for image corrections. In that case the reflection of a single gas bubble provides a reference spherical wave of uniform phase and any phase aberration across the imaging array resulting from inhomogeneties in speed of sound along the wave's path can be corrected.

This paper will show the experimental results of the vaporization of single albumin stabilized droplets as they are exposed to single acoustic tone bursts. A better understanding of the physical effect behind ADV is the primary goal of this work.

II. Materials and Methods

A high speed video system with 200 ns exposure time per full-frame (576 x 385 pixel) and a

streak image with 17 ns per streak line was used to capture the vaporization optically. Second, an optical microscope with the video system connected to the camera port was used to monitor the droplets in a flow tube beneath the 100x microscope objective achieving a resolution of 0.46 um per pixel. The light of a 2.5 kW Argon flash light was guided into the optical path, facing the objective (see Fig. 2 and 3). A polyethylene tube (200 um inner diameter, 50 um wall thickness) was mounted in a small water tank with degassed water. A single-element focused transducer with a center frequency of 3.5 MHz was aimed at the intersection of the tube and the optical beam (see Fig. 3). A highly dilute droplet emulsion was injected into the flow tube and a special syringe setup was used to position individual droplets in the focus.

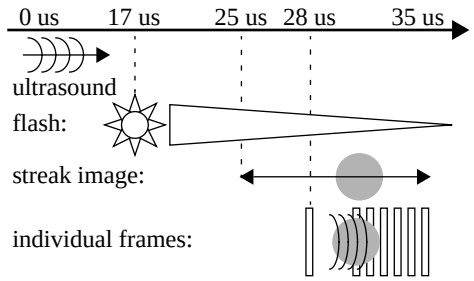

Fig. 2: Timing diagram for transmitted ultrasound burst, light pulse, acquired streak image, and individual frames. The launch of the acoustic tone burst is time zero. It triggers the flash/strobe light with a 17 us delay. Eight microseconds later, at 25 us, the streak image starts recording for 10 us and at 28 us the first full frame picture is taken. The remaining 6 images are taken at various time points to investigate either the translation or the vaporization process.

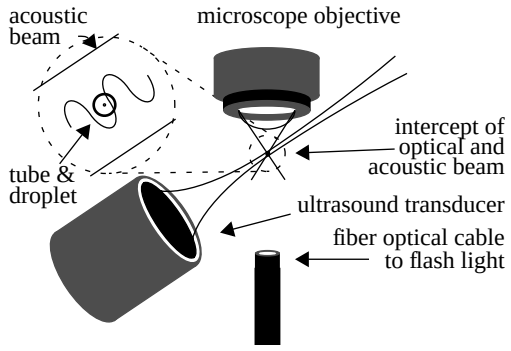

Fig. 3: The 3.5 MHz transducer has an aperture of 25.4 mm and a beam diameter of 0.96 mm. The polyethylene flow tube has a 200 um inner diameter and 50 um wall thickness. For comparison, a 3.5 MHz two cycle tone burst is shown in the inset.

III. Results

Experimental results

Dipole type oscillations - Single sinusoidal tone bursts (10 cycles at 3-4 MHz) were sufficient to phase transition individual droplets. High speed video images are shown in Fig. 4 and Fig. 5. The droplets show a translatory, dipole type motion with the same frequency and duration as the transmitted acoustic tone burst. An edge detection algorithm was used to find and analyze the observed translatory motion in the streak image. Measurements at 3 and 4 MHz where performed on droplets in the size range from 7 to 27 um diameter. At threshold, i.e. at the acoustic pressure threshold where the droplet vaporizes, an average displacement of 2.6 ±0.38 um peak to peak was measured independent of the droplet's size and the frequency used (see Fig. 6). Due to the image resolution of 0.46 um per pixel an error of at least 20% must be expected.

Nucleation site - The onset of vaporization was monitored as either spot-like and subsequently expanding centers of nucleation inside the droplet or as homogeneous throughout the droplet's imaged cross-section. Spot-like centers of nucleation were solely observed along the direction of motion (Fig. 5).

Acoustic threshold - It has been observed that smaller droplets require more acoustic energy to be vaporized than larger droplets (10 to 20 um diameter yielded thresholds of 8 to 6 MPa peak to peak respectively for 10 cycles at 3 MHz, see Fig. 7), which is consistent with earlier experiments where the pressure threshold for vaporization of filtered and unfiltered emulsions was measured [2]. Droplets were vaporized using either 3 MHz or 4 MHz tone bursts of 10 cycles. Earlier free field experiments on emulsions showed a decrease in threshold for ADV with increasing frequency, which is contradictory to the current experiments. However, this may be caused by the rather complex acoustic field resulting from the presence of the flow tube and its location just beneath the microscope objective, favoring 3 MHz over 4 MHz. This does not affect the dependence of the pressure needed for ADV on the droplet's size.

Theoretical results

Simulations on the free field scattering theory of rigid spheres have been compared to the dipole type oscillations seen in the experiment. Results showed dipole like translatory motion of droplets, however,

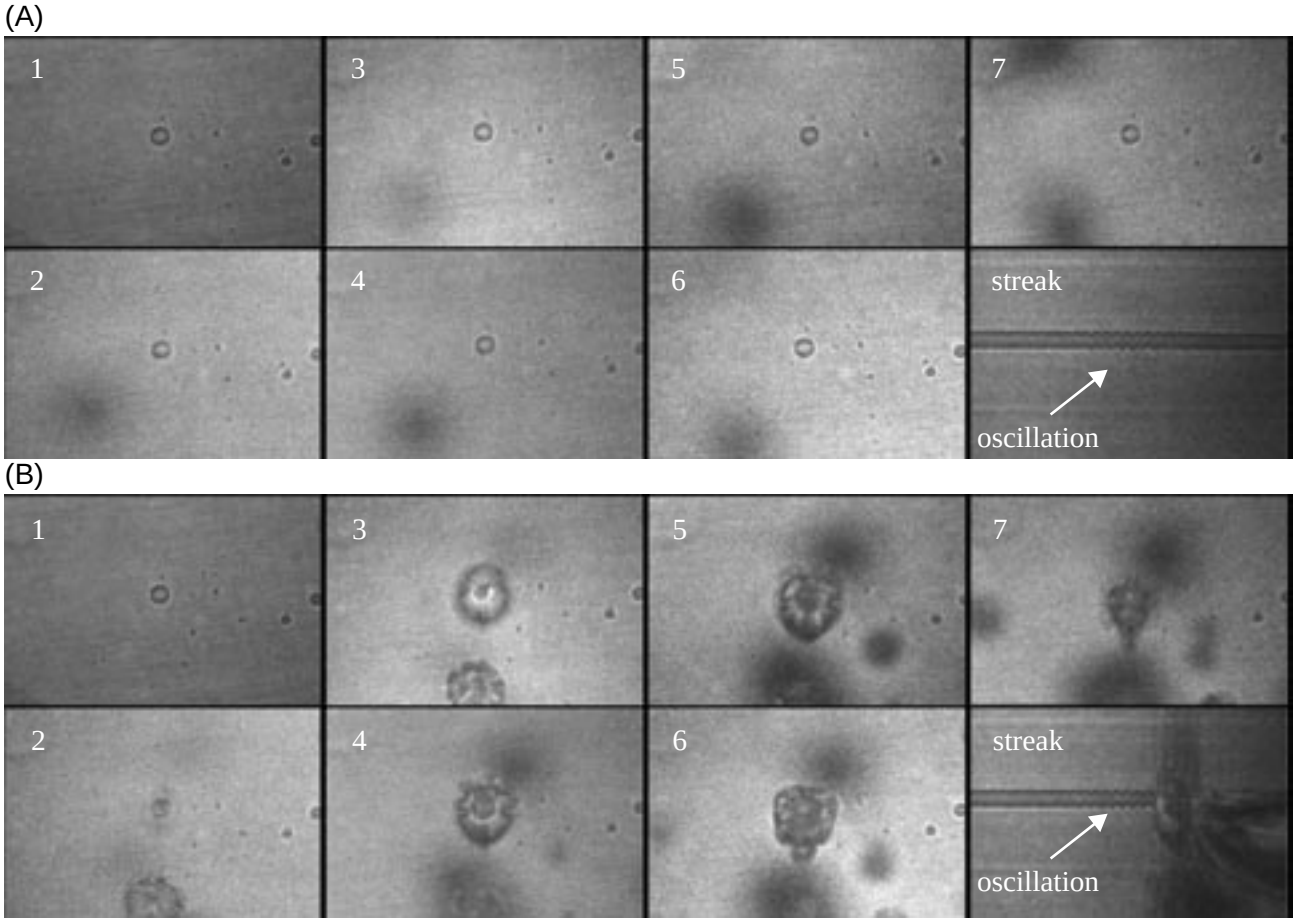

Fig. 4: Acoustic vaporization of an 18 um diameter droplet. Two sequences are shown. (A) Images 1 to 7 are full frame pictures of the droplet in the flow tube. The 8th frame is a streak image. The acoustic pressure in the first sequence is not sufficient to vaporize the droplet. In the center of the streak image one can see a translatory motion of the droplet for the duration of the 10 cycle, 3 MHz tone burst. (B) Increasing the acoustic pressure to 6.5 MPa peak-peak leads to the vaporization of the droplet after 8 cycles.

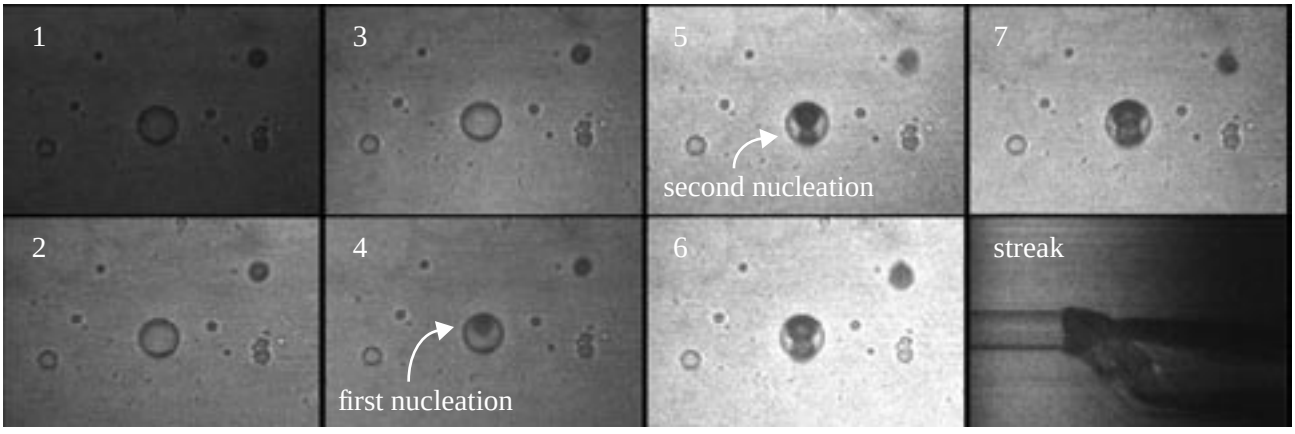

Fig. 5: Frame 4 of the sequence shows the first nucleation point of the droplet's vaporization, and frame 5 shows another nucleation site. The frames were placed back to back with 100 ns duration. For this vaporization a 10 MHz and 30 cycles tone burst at 9 MPa was used.

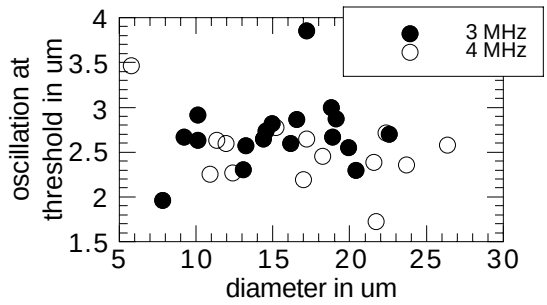

Fig. 6: Droplets of various diameters were analyzed for the magnitude of dipole oscillation at the threshold of vaporization. The peak to peak amplitude was found to be ~2.6 um, independent of the droplet's size.

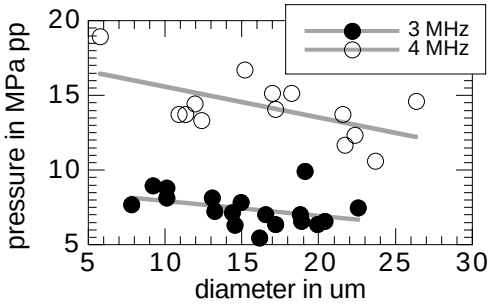

Fig. 7: The pressure threshold for ADV was evaluated as a function of droplet diameter. In general smaller droplets required higher pressures to be vaporized.

the magnitude of these oscillations was computed to 1/37 of those observed in the experiment.

The droplets were modeled as solid spheres of dodecafluropentane (Z=0.7 MRayl, c=471 m s^{-1}, and ρ=1660 kg m^{-3}), neglecting the albumin shell which stabilizes them against coalescence. A rigid sphere model and its solutions [3] as given in equation 1 was used to predict the translatory motion of droplets as observed in the experiment.

$$p_a(t,\theta) = \frac{Ae^{-I\omega t}}{(ka)^2}\sum_{m=0}^{\infty}\frac{2m+1}{B_m}P_m(\cos\theta)e^{-I\left(\delta_m-\frac{1}{2}\pi m\right)}$$

$$\Sigma_\theta = \frac{2\pi}{N}\sum_{n=0}^{N-1}\cos\left(\frac{2\pi n}{N}\right)\cdot p_a\left(t,\cos\left(\frac{2\pi n}{N}\right)\right) \quad (1)$$

$$s(t) = \mathrm{Re}\left(\frac{\Sigma_\theta}{-I\omega c\rho}\right)$$

In this simple, linear approach a droplet's displacement can be computed from the integrated velocity, which is derived from the sound pressure function. The following parameters were used to predict the droplet displacement in a given sound field: 18 um droplet diameter, 3 MHz tone burst, and 6.7 MPa peak-peak sound pressure. A total displacement of 70 nm results.

IV. Summary and Conclusion

The vaporization of single droplets has been observed. An acoustic pressure threshold which decreases with droplet size has been directly confirmed to earlier measurements on filtered emulsions. High spatial and temporal resolution revealed a dipole type translation of the monitored droplet. This translation was 2.6 um peak to peak, independent of the droplet's size. The theoretical model of a rigid sphere in an acoustic field yielded 0.07 um peak to peak, a very small fraction of the experimental value. This huge discrepancy suggests that some other mechanism must be involved in the apparent droplet oscillation. One more possible explanation for it is a displacement of the flow tube in the acoustic field, i.e. a moving tube will also move the contained droplet. Unfortunately this was not verified in the actual experiment.

V. Acknowledgement

Supported in part by PHS Grant No. R01HL54201 and US Army Grant No. DAMD17-00-1-0344.

VI. Literature

[1] Kripfgans OD, Fowlkes JB, Miller DL, Eldevik OP, Carson PL. Acoustic droplet vaporization for therapeutic and diagnostic applications. Ultrasound in Med & Biol 2000; 26:1177-89.

[2] Kripfgans OD, Fowlkes JB, Woydt M, Psychoudakis DA, Carson PL. In Vivo Droplet Vaporization for Occlusion Therapy and Phase Aberration Corrections. submitted to IEEE UFFC

[3] Philip M. Morse and K. Uno Ingard. "Theoretical Acoustics" Princeton University Press 1968.

On the Mechanism of Acoustic Droplet Vaporization

Oliver D. Kripfgans, Paul L. Carson, J. Brian Fowlkes
University of Michigan Health Systems, Department of Radiology, Ann Arbor, MI, 48109-0553, USA

Abstract - It has been observed in the past that micrometer sized droplets can be vaporized into gas bubbles by the application of diagnostic ultrasound [1]. This paper will discuss the possible underlying mechanism of acoustic droplet vaporization (ADV) including acoustic cavitation, acoustic heating, shape oscillations during acoustic irradiation, and hydrodynamic cavitation. Experiments were performed on droplet emulsions as well as on single droplets. The vaporization of emulsions was quantified based on gas bubbles generated in a flow tube using a 10 MHz linear imaging array. Single droplets were monitored optically under a microscope and a high speed video system. Details on the individual setups can be found in [1]. The frequency dependence of ADV as well as trials with degassed water (40% of saturation) imply that acoustic cavitation is not the mechanism for ADV. Acoustic heating was investigated by exposing the droplet emulsion to repetitive tone bursts (50 Hz to 5 kHz). No significant change in pressure threshold for ADV was observed, however the yield of gas bubbles was used to calculate the single pulse conversion efficiency of ADV to 26%. Droplet shape oscillations causing a non-uniform Laplace pressure, were found to be 15% or less of the droplet diameter. They could be observed at the beginning and at the end of the acoustic irradiation. Observed was a dipole-type motion (1.3 um amplitude) of irradiated droplets as well as the spot-like onset of vaporization on the axis of oscillation close to a pole of the droplet. It is concluded that because of the high Reynolds number during ADV ($4\text{-}5\text{x}10^5$), the mechanism of vaporization might be based on hydrodynamic effects.

I. Introduction

It has been observed in the past that micrometer sized droplets of perfluorocarbon liquids in emulsions can be vaporized into gas bubbles by the application of tone bursts in the frequency and power range of diagnostic ultrasound [2-5]. We refer to this phenomenon as Acoustic Droplet Vaporization (ADV). These emulsions can be produced where up to 97% of the particles are smaller than 10 um in diameter, with an average diameter of 3 um. As such particles are mostly transpulmonary they can be circulated through the body in the blood stream. Exposure to ultrasound creates 20 to 80 um gas bubbles that can no longer pass the capillaries and subsequently become trapped for some time in the vasculature. Possible medical and other applications thereof were discussed in [1]. This paper will show the experimental results of the vaporization of single albumin stabilized droplets as they are exposed to single acoustic tone bursts. Possible mechanisms for ADV will be hypothesized and discussed using experimental results as well as findings from the literature. These include (a) acoustic and hydrodynamic cavitation which could potentially nucleate the evaporation of the superheated droplet; and (b) deformation of the droplet which could lead to rupturing of the shell, including redistribution of albumin on the droplet's surface [6, 7], and/or a non-uniform Laplace pressure on the sphere.

Cavitation has been the topic of many investigations and the physical mechanisms by which gas bubbles are created using ultrasound are manyfold. Apfel used the crevice-mote model [8] and even though the model is very simplified in the description, one can understand how changes in the gas content or the ambient static pressure of the liquid can lower or raise the threshold for nucleation of gas bubbles from crevices. Furthermore it has been expected that acoustic waves increase the sensitivity of superheated droplet suspensions to vaporization [3].

There are several scenarios under which hydrodynamic cavitation might occur, such as cavitation on ship propellers and venturi-liners [9-11]. In a general definition [11] cavitation is defined as a process in which micro gas bubbles are created as a consequence of a pressure reduction. Observations have shown cavitation in small water tunnel experiments using flow of 15 to 45 m s^{-1} past simple geometries [10, 12].

One of the classic acoustic experiments

involving drops or droplets is acoustic levitation [13-15]. Shi and Apfel [16], for example levitated a 1.18 mm radius water drop in air at 28 kHz and up to 3 kPa sound pressure (*ka*=0.14). During the experiment they observed shape oscillations with aspect ratios of up to 2.

II. Materials and Methods

An Imacon 468 high speed video system (DRS Technologies, DRS Hadland, Inc. Cupertino, CA, USA) was used to optically image the process of ADV. Full-frame pictures were taken with an exposure time of 100-200 ns and 17.4 ns per streak line. Since this ADV occurs at a micron scale, an optical microscope (JenaVAL, Carl Zeiss Jena GmbH, Jena, Germany) was connected to the video system.

The acoustic exposure occurred in a tank with degassed water. A polyethylene tube (200 um inner diameter, 50 um wall thickness) was mounted in the focus of a single-element ultrasound transducer and the optical beam. The calibrated ultrasound transducer was driven by an RF gated amplifier (model 350, Matec, Northboro, MA, USA) and controlled by an HP3314 a multipurpose function generator (Agilent, Palo Alto, CA, USA). Rf-signals were monitored using a 300 MHz LeCroy 9310L oscilloscope (LeCroy Corp., Chestnut Ridge, NY, USA).

Droplet emulsions were made from 75 vol-% saline-albumin solution and 25 vol-% dodecafluropentane (DDFP, C_5F_{12}, CAS #678-26-2). A highly concentrated droplet emulsion with $9.5x10^9$ droplets per mL resulted. This emulsion was diluted (1:10,000) and small volumes of it were injected into the flow tube. For each picture taken an individual droplet was positioned in the acoustical and optical focus. The first image was taken before the sound wave reached the tube. Subsequent frames were either placed back-to-back in order to monitor the process of ADV or were separated by several hundred nanoseconds to monitor the droplet during the insonification, before vaporization started. Each droplet was exposed to a series of acoustic tone bursts of increasing acoustic power. For each power level a set of seven full frames and one streak image was acquired. The acoustic intensity was increased until the droplet vaporized. Hand tracing of the streak image was used to reconstruct any possible center of mass or shape oscillation of the droplet.

III. Results and Discussion

Acoustic cavitation is one of the four mechanisms which were under investigation to explain how ADV might work. For transient cavitation in the presence of 0.8 um diameter polystyrene spheres, an increase in pressure threshold for cavitation from 11 bars to 12.3 bars (10.6%) was observed when the dissolved gas content was lowered from 87% to 50% [17]. In this case the expected threshold for ADV would be 850 kPa, which is approximately 2 standard deviations away from the measured value of 947 ±64 kPa P_ from above. It is therefore concluded that, based on a 2 standard deviation difference, transient cavitation is probably not the mechanism of ADV.

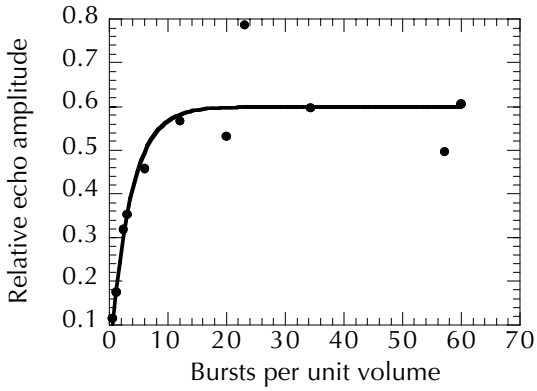

Fig. 1: The efficiency of ADV is evaluated by fitting the relative echo amplitude to the number of bursts each unit volume of droplets is exposed to.

Effects of repetitive pulses were measured to test if *acoustic heating* changes ADV. Repetitive pulsing has a special significance since it bears a direct time constant which is coupled to the flow rate, when working on ADV of emulsions flowing through a tube. Two ways in which this change might manifest itself are anticipated; (a) the fraction of droplets which will be vaporized per unit time, and (b) the pressure threshold that has to be overcome to start ADV might shift. Five-cycle, 4 MHz center frequency tone bursts were transmitted with pulse repetition periods (PRPs) between 0.2 ms and 20 ms. An exponential fit of the relative echogenicity as a function of exposures per unit volume of droplet emulsion in the focus yields the efficiency when the pulse repetition period is normalized by the beam transit time.

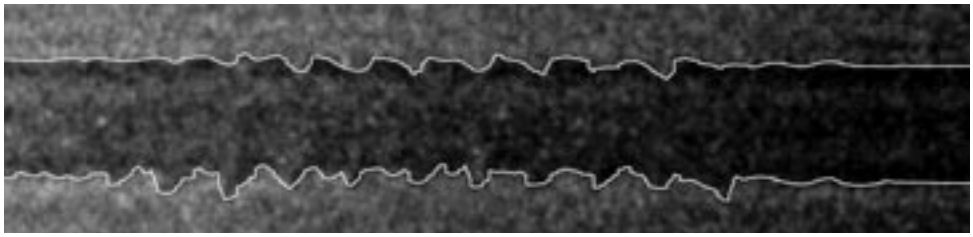

Fig. 2: Hand-traced streak line of a 16 um diameter droplet. One can see the onset of oscillation at the bottom trace, before onset occurs in the top trace.

$$REA = m_1(1 - e^{-m_2 N}) \quad (1)$$

where m_1 and m_2 were evaluated from the experimental data as 0.60 and 0.29 (R^2=0.87). The resulting rate of ADV or conversion efficiency is then 26%. This rate is based on the subset of droplets that *is* convertible. An analysis of the second effect, a shift in the pressure threshold for ADV due to a change in PRF, was performed next. Over the two-order of magnitude change in PRF the threshold for ADV changed only ~100 kPa or 11%. The experimental pressure step size was 20 kPa which should not be the reason for a limiting resolution.

Other parameters which contribute to heating include burst length, ambient temperature, and ambient viscosity. Current results of the PRF study do not support heating as a mechanism for initiation of ADV. However more experiments would be required to definitely determine that heating is not involved.

Another effect of the acoustic field could be the production of cavitation events in the medium which could trigger ADV. This will be examined next. Full frame images as well as streak images were analyzed for the droplet's action prior to and at the time of vaporization. Furthermore, droplet deformation was simulated using a droplet levitation theory [15]. Center of mass as well as thickness oscillation was observed during acoustic irradiation (Fig. 2 and 3). Displacement amplitudes were increasing with acoustic amplitude and did not exceed an average of 2.3 um peak to peak (Fig. 4). The observed droplet vaporized when exposed to sound pressure higher than such resulting in 2.3 um displacement. This threshold was observed to be independent of droplet size and can be also seen as a maximum displacement velocity (Fig. 5).

Spot-like onset of vaporization was observed during the dipole-type motion of droplets. This onset was solely seen on the axis of oscillation close to a pole of the droplet. The nucleation did not coincide

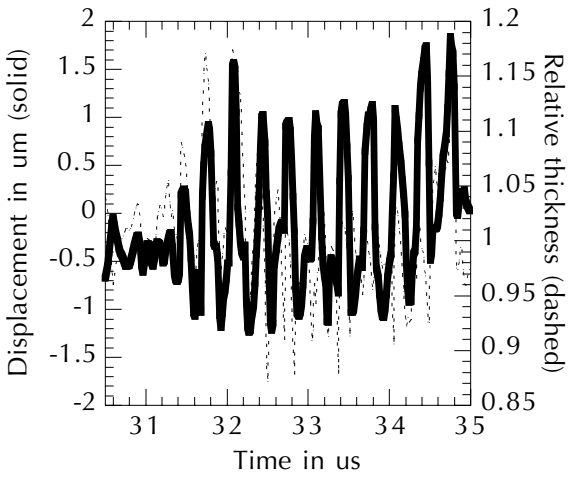

Fig. 3: Dipole (displacement) and thickness oscillation of a 16 um diameter droplet (thick and dashed lines, respectively). The spectral amplitude of the displacement is 40 dB above the noise and 13 dB above the image resolution. The thickness oscillation is 7 dB above the noise and of the same order as the image resolution. However, in general, it has been observed that the initial thickness oscillation does show a spectral response at 3 MHz.

with the occurrence of the shape oscillations. Based on these observations it is concluded that hydrodynamic effects might be the base for ADV.

IV. Acknowledgement

Supported in part by PHS Grant No. R01HL54201 and US Army Grant No. DAMD17-00-1-0344.

V. Literature

[1] O. D. Kripfgans, "Acoustic droplet vaporization for diagnostic and therapeutic applications," Dissertation in Applied Physics. Ann Arbor: University of Michigan, 2002, pp. 153.

[2] Kripfgans, O. D., J. B. Fowlkes, D. L. Miller, O. P. Eldevik, and P. L. Carson, "Acoustic droplet

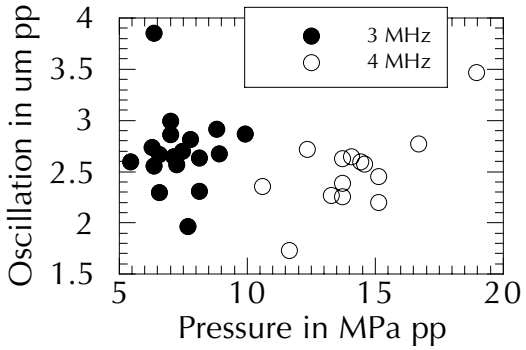

Fig. 4: Amplitude of oscillation of individual droplets as a function of acoustic peak-to-peak pressure. Shown are the results for experiments at 3 and 4 MHz. Peak-to-peak amplitude of oscillation *at threshold for ADV* is a function of applied pressure and droplet size; data points represent distinct droplets of various diameters.

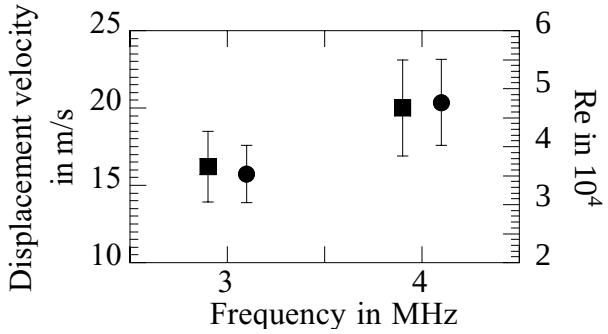

Fig. 5: Droplets of various diameters were analyzed for the magnitude of dipole oscillation at the threshold of vaporization. The average displacement amplitude at a given frequency was used to compute the average velocity (circles) at which the droplet was assumed to be moving relative to the host fluid. Additionally the corresponding Reynolds number was computed (squares). The error bars are based on the single standard deviation of the displacement amplitude.

vaporization for therapeutic and diagnostic applications," Ultrasound in Med. & Biol., vol. 26, pp. 1177-1189, 9, 2000.

[3] Apfel, R. Nucl. Instrum. Methods, 162, 603-608 (1979)

[4] Apfel, R. E. (1998). Activatable infusable dispersions containing drops of a superheated liquid for methods of therapy and diagnosis. US, Apfel Enterprises, Inc.

[5] Kripfgans O. D., Fowlkes J. B., Woydt M., Eldevik P. O., Carson P. L. In Vivo Droplet Vaporization for Occlusion Therapy and Phase Aberration Corrections. IEEE Transactions Ultrasonics, Ferroelectrics, and Frequency Control 2002; Vol. 49, No. 5

[6] Leppinen, D. M., M. Rensizbulut, et al. (1996). "The Effects of Surfactants on Droplet Behavior at Intermediate Reynolds Numbers - I. The Numerical Model and Steady-State Results." Chemical Engineering Science 51(3): 479-489.

[7] Leppinen, D. M., M. Rensizbulut, et al. (1996). "The Effects of Surfactants on Droplet Behavior at Intermediate Reynolds Numbers - II. Transient Deformation and Evaporation." Chemical Engineering Science 51(3): 491-501.

[8] Apfel, R. E. (1997). "Sonic effervescence: A tutorial on acoustic cavitation." J Acoust Soc Am. 101(3).

[9] Strasberg, M. "Propeller Cavitation Noise...", ASME Symposium on "Noise and Fluids Engineering" Nov. 1977, pp. 89-99

[10] Hutton, S., P. 1972 Inaugural Lecture University of Southampton

[11] Trevena, D. H. (1984). "Cavitation and the Generation of Tension in Liquids." Journal of Physics D-Applied Physics 17(11): 2139-2164.

[12] Selim S.M.A., 1981, P C Cavitation Erosi, P15

[13] Tian, Y. R., R. G. Holt, et al. (1993). "Deformation and location of an acoustically levitated liquid-drop." J Acoust Soc Am 93(6): 3096-3104.

[14] Feng, Z. C. and Y. H. Su. 1997. "Numerical simulations of the translational and shape oscillations of a liquid drop in an acoustic field." Phys. Fluids 9:519-529.

[15] Lee, C. P., A. V. Anilkumar, et al. (1991). "Static shape and instability of an acoustic levitated liquid drop." Physics of Fluids A3(11): 2497-2516.

[16] Shi, W. T. and R. E. Apfel (1996). "Deformation and position of acoustically levitated liquid drops." J. Acoust. Soc. Am. 99(4): 1977-1984.

[17] Roy, R. A., S. I. Madanshetty, et al. (1990). "An acoustic backscattering technique for the detection of transient cavitation produced by microsecond pulses of ultrasound." J. Acoust. Soc. Am. 87(6): 2451-2458.

KIDNEY BLOOD FLOW OCCLUSION BY ACOUSTIC DROPLET VAPORIZATION

O. D. KRIPFGANS[1], C. M. ORIFICI, P. L. CARSON, and J. B. FOWLKES
University of Michigan Health Systems, Department of Radiology, Ann Arbor, MI, 48109-0553, USA

Abstract - Acoustic Droplet Vaporization (ADV) has been introduced with the potential application of tumor treatment via occlusion and subsequent necrotic ischemia in the targeted region. In this study an entire organ was the target for occlusion. Lepus kidneys were chosen for bubble production and subsequent vascular occlusion of the organ. The left kidney was externalized and an imaging array plus a single element transducer were positioned with direct access to the kidney's vasculature and renal artery. Filtered droplet emulsions (diameter <5 um) were injected during insonification of the renal artery and the extent of blood flow reduction by ADV was compared to the untreated right side kidney. Blood flow before and after each treatment was measured using fluorescently stained PVC spheres (diameter 15 um) injected intra-arterially (IA) into the heart's left ventricle. Flow cytometry analysis of kidney tissue samples allowed the estimation of regional blood flow inside the tissue samples. Bubble production was possible for IV as well as IA administered emulsions. A maximum regional blood flow reduction of >95% (91% for total organ) was found for occlusion produced by bubbles from ADV of IA injected droplet emulsions. Hyperechogenicity from ADV of IA injections was monitored for approximately one hour.

I. INTRODUCTION

Earlier *in vivo* experiments in canines, as reported in a previous paper [1], showed that Acoustic Droplet Vaporization (ADV) could be used to reduce the blood flow in brain tissue. In that study, for the first time, ADV was repeated capable of causing a quantitative blood flow reduction to an average of 66%. Since that report we have concentrated on improving the level of blood flow reduction and understanding the requisite conditions to optimize the process.

Acoustic targeting and bolus injection of the droplet emulsion can be used to limit the ADV induced blood flow occlusion to a selected target site. Special attention has to be paid to the available acoustic access at the selected transducer frequency and aperture. Additionally the method of blood flow measurement as a feedback of the effectiveness of ADV is important.

The objective of the following work was to test whether is was possible to substantially reduce the vascular flow in an organ which is strongly perfused. Moreover, it should be investigated as to how long the flow could be interrupted and what systemic effects could be observed.

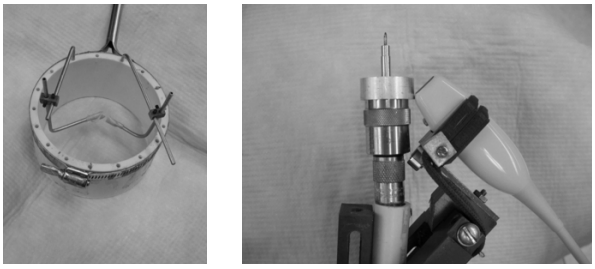

Fig. 1: Top: 'Local' standoff water tank to warrant acoustic access to the externalized kidney. Bottom: Single element (f#=1.5) therapy transducer with focus pointer plus attached imaging array.

II. MATERIALS AND METHODS

General experimental setup

Rabbits were used as our animal model. The target organ for occlusion was the kidney. For each rabbit, the left kidney was externalized and a water bath made from a section of PVC tubing (5 cm tall and 12 cm diameter, see Figure 1 left) was positioned over the externalized kidney and glued to the skin. This type of attachment creates a water bath without an interface layer between the transducer and the target tissue. Metal cradles attached to the water bath were used to secure the kidney in position and a specially machined transducer arm held a focused phased array imager and a treatment transducer. This treat-

1.E-mail: greentom@umich.edu

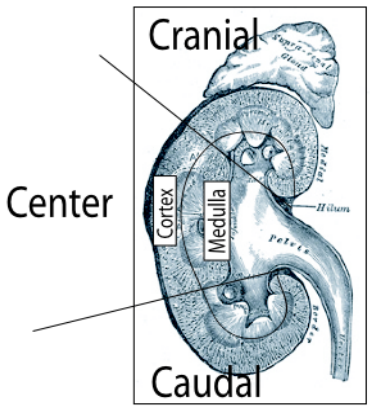

Fig. 2: Illustrated are three spatial cuts that were made when dissecting kidneys after ADV treatment. Kidney schematics modified from [2].

ment transducer was a single PZT element (A381S, Panametrics, Waltham, MA) with a 3.5 MHz center frequency, 25.4 mm aperture, and 37.5 mm focal length. A system of two function generators and an amplifier were used to drive the single element transducer. One function generator provided the short tone burst signal, which was subsequently transmitted by the transducer and the second function generator provided a gating signal for the power amplifier, which was driving the ADV transducer. Typically input amplitudes of 300 Vpp were used with a pulse duration of 13 cycles at 3.5 MHz, i.e. 3.7 us. Acoustic pressure measured at lower applied voltages were extrapolated to indicate peak rarefactional pressures exceeding 2 MPa.

A pointer was used to register the position of the treatment transducer's focus in the scan plane of the imager (GE System V with a 10 MHz phased array, 15 mm aperture). Once the transducers were placed inside the water tank, we used B-Mode, Color Flow Mode (CFM) and Spectral Doppler (PW) of the imaging system to verify the current anatomic position, especially in terms of cross-section through the kidney. We required the scan plane the show the incoming renal artery as well as major arterial vessels downstream and inside the kidney. Thus the phase transition and the path of the gas bubbles into the kidney could be monitored and afterwards measured. Feedback was provided by B-Mode, CFM, or PW.

Our gold standard for blood flow measurement was the usage of colored microspheres (Interactive Medical Technologies IMT, Irvine CA). These spheres are injected into the left ventricle, where good mixing is ensured due to the turbulent flow in the chamber. When injected, the microspheres are terminal in the capillaries of the downstream tissues but with sufficiently low concentrations to produce occlusion.

The injected droplet emulsion was made in our laboratory under guidelines previously published. [1] Specifically for this animal model, leporine albumin was used to stabilize the emulsion instead of bovine albumin to eliminate systemic reactions of the animal to the foreign protein.

Animal preparation

Fourteen New Zealand white female rabbits, 2 to 3 kg were use for this study. The animals were initially anesthetized with Ketamine (35 mg/kg) and Xylazine (5 mg/kg) and intubated. Fur was shaved from their abdomen and back and depilatory cream was applied to remove any residual hair and give acoustic access through out the abdomen and parts of the back. The animal was then placed on a heated pad to prevent heat loss through out the experiment. Isoflurane (1-3%) was used as the long term anesthetic and was administered by ventilation. Two arterial catheters and one venous catheter were placed in the femoral arteries and ear vein, respectively. EKG, body core temperature (rectal probe), as well as heart rate and blood oxygenation (pulse oximeter) were monitored through out the experiment.

The animals were euthanized after the experiment by injecting pentobarbital IV followed by bilateral pneumothorax. Both kidneys were surgically removed and dissected (see Figure 2) into cranial, center, and caudal and each of these three sections was divided into cortex and medulla. The University Committee for Use and Care of Animals approved all animal procedures.

III. Experimental Results

Figure 3 shows the appearance of ADV as recorded by the imaging array. Figure 3A is a baseline image before the onset of ADV. The ADV transducer is on, but no emulsion is being injected. Radial streak lines visible at the top of the image are due to interference with the acoustic field from the ADV transducer. The white arrow is pointing to the renal artery. In (B) one can see a ‘horizontal’ vascular branch on the lower half of the interior of the kidney as well as a

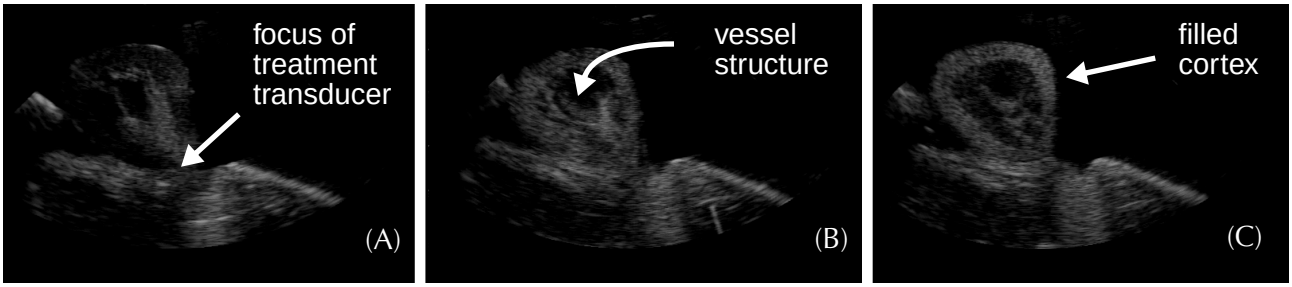

Fig. 3: B-mode image of kidney cross-section before (A), during (B), and after (C) ADV. In (B) one can see how the gas bubbles move downstream via the arterial system and launch in the cortex (C).

'vertical' vessel on the right side. These vessels are filled with hyper-echoic gas bubbles. In (C) the vascular bed (the cortex) is filled with gas bubbles.

Underlying tissues are acoustically shadowed after the target tissue is sufficiently filled with gas bubbles. Figure 4 (left) is a baseline image before ADV whereas the right side was taken afterwards. In this case, droplets were vaporized using a 10 MHz linear array imaging transducer. After ADV the top cortex completely shadows everything below.

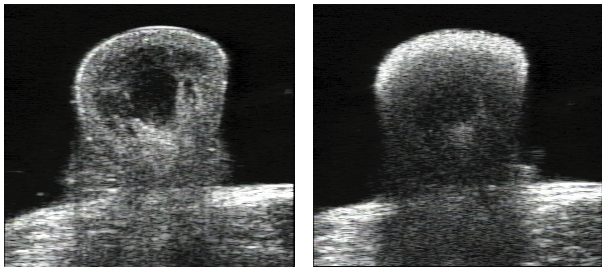

Fig. 4: Typical shadowing effect to distant tissue (bottom) after ADV of the kidney cortex (top). Left side shows the kidney before ADV, right side afterwards.

Additional feedback on the ADV process was acquired by means of color flow mode (CFM) and Spectral Doppler (PW). Traces were recorded before, during, and after ADV. Directly after ADV the peak flow velocity was reduced by approximately 50% as well as a decrease in the temporal duration of the Doppler waveform during each cardiac cycle indicating an overall reduction in blood flow. Similar results were seen in Color Flow mode. We noted a substantial decrease in the detectable flow after ADV. This reflects reduction in flow velocities in the major vessels of the kidney in response to the distal blockage of the capillary bed. These observations were made at locations that were not apparently shadowed by the bubbles production.

Quantitative blood flow measurements based on colored microsphere analysis were used to measure reduction in tissue perfusion. The following graphs show blood flow for cortex and medulla of the whole kidney. For example mean and standard deviation for cortex were computed by pooling results from several experiments (animals) each having the 9 cortex data points in individual kidneys.

The time courses of the perfusion of the cortex of treated and untreated kidneys are shown in Figure 5. The left and right columns of the figure present treated and untreated kidneys, respectively. Each graph shows five data points. At first the kidney is inside the animal. This state is labeled 'intern'. Then the left kidney is externalized, hence the label 'extern' on the abscissa. All values are shown as %-changes from a baseline, which has been chosen to be the measured blood flow for 'extern'. Relative values are plotted in order to compensate for flow variations between animals.

Externalizing the left kidney reduces the blood flow to both the external as well as to the internal kidney. P-values computed for the two populations, internal versus external, of each kidney are: $p<0.0005$ and $p<0.0005$, for left and right cortex, respectively.

Treatment with ADV on the external/left kidney was performed next. In Figure 5 one can see how ADV affects the cortex of the external kidney. The blood flow in cortex falls to -91% after the treatment. The p-value for the correlation between baseline and ADV is: $p<0.0005$. At the same time, blood flow through the internal/right kidney remains constant with a p-value of: $p=0.227$. Moreover the correlation between treated and untreated kidney has been evaluated by means of the p-value for testing the blood flow

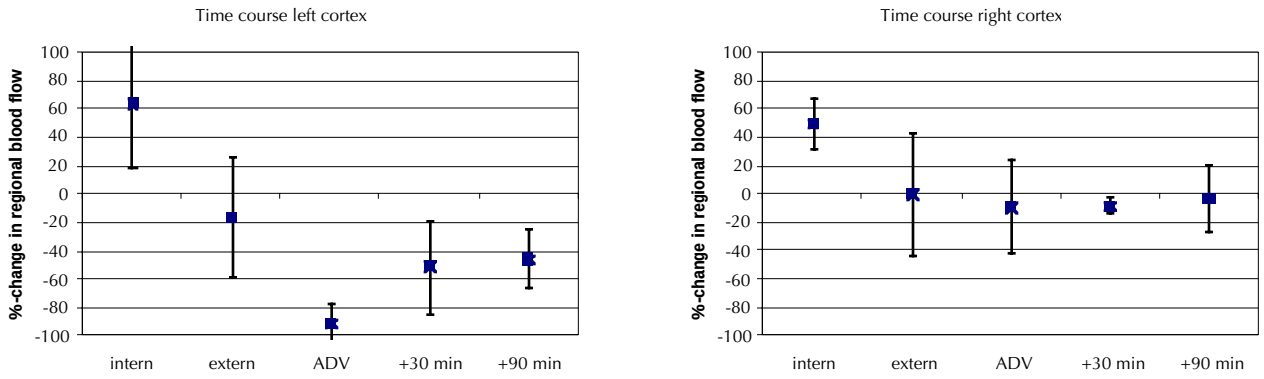

Fig. 5: The %-change of blood flow in kidney is shown for externalizing the kidney, for ADV treatment, and for blood flow recovery after ADV. Internal/left and external/right kidney are shown on the left and right side, respectively. Externalization of the left kidney caused a drop in blood flow in both kidneys. After treatment with ADV to cause occlusion, the left/external kidney shows a drop in blood flow, from which it mostly recovers 90 minutes after the treatment. The blood flow in the internal kidney remains mostly constant.

through them being significantly different, $p<0.0005$.

After it has been seen that the blood flow could be suppressed by ADV, the next question was how this suppression would change with time. One of the characteristics of occlusion therapy by ADV is that the flow suppression is of a temporal nature as opposed to coils or other solid materials that are currently used in occlusion therapy, which are permanent. Figure 5 shows how the vasculature in the cortex recovers from the occlusion after treatment. On the right side of the graphs in Figure 5, one can see the RBF value for cortex 30 and 90 minutes after the treatment. For the cortex in the treated kidney, the blood flow recovers from an average of -91% to -51% occlusion at 30 minutes after treatment. At the same time cortex in the untreated kidney remains at constant blood flow ($p=0.0984$). One hour later, i.e. 90 minutes after ADV, the cortex of the treated kidney recovers to -46%.

IV. Summary and Conclusion

Renal occlusion to an average of 91% flow suppression in the renal cortex has been observed after Acoustic Droplet Vaporization in the renal artery. At the same time the blood flow in the cortex of the contra-lateral/untreated kidney lowered by only 9% (statistically not significant). After 90 minutes the capillary flow in both kidneys recovered to 46% and 3% below baseline for treated and untreated kidney respectively.

For individual kidneys it has been seen that after ADV, blood flow in the contra-lateral kidney may increase or decrease. Left and right kidneys are not independent systems. Autoregulation [3] controls blood flow and urine production and we assume that the unilateral occlusion also caused a certain degree of regulation response. Two possibilities are (a) increase in blood flow in the untreated kidney to compensate for loss of blood flow in the treated kidney and (b) decrease in blood flow in the untreated kidney to balance the urinary output relative to the treated kidney.

V. Acknowledgement

Supported in part by PHS Grant No. R01 EB00281-07 and US Army Grant No. DAMD17-00-1-0344.

VI. Literature

[1] Kripfgans, O. D., Fowlkes, J. B., Woydt, M., Eldevik, O. P., & Carson, P. L. (2002). In Vivo Droplet Vaporization for Occlusion Therapy and Phase Aberration Corrections. IEEE Trans. on Ultrasonics, Ferroelectrics, and Frequency Control, 49(6), 726-38.

[2] Gray, H., Williams, P. L., & Bannister, L. H. (1995). Gray's anatomy: the anatomical basis of medicine and surgery. New York: Churchill Livingstone.

[3] Just, A., Ehmke, H., Toktomambetova, L., & Kirchheim, H. R. (2001). Dynamic characteristics and underlying mechanisms of renal blood flow autoregulation in the conscious dog. American Journal of Physiology-Renal Physiology, 280(6), F1062-F1071.

MICROBUBBLES FOR ULTRASOUND DIAGNOSIS AND THERAPY

JB Fowlkes*†, OD Kripfgans*, PL Carson*†
*Department of Radiology, University of Michigan Health Systems
Kresge III, R3315, 200 Zina Pitcher Place, Ann Arbor, MI 48109-0553
†Department of Biomedical Engineering, University of Michigan

Abstract – Methods for the local production of microbubbles *in vivo* are being developed for applications in both diagnostic and therapeutic ultrasound. The techniques involve the use of superheated perfluorocarbon droplets that can be vaporized by the application on focused ultrasound. This provides localization of the resulting gas bubbles and control over the number density and size of bubbles being released. For therapeutic ultrasound, large gas bubbles are produced in numbers sufficient to restrict blood flow or the bubbles can act as nuclei for cavitation-based tissue disruption. In lower number density, the bubbles provide targets with ideal properties for aberration correction [1], which can be used to improve both therapeutic and diagnostic fields.

INTRODUCTION

Stable perfluorocarbon emulsions have been used in the past as ultrasound contrast agents [2] and there is a renewed interest in stable liquid formulations that include targeting [3]. It is also known that perfluorocarbon liquid droplets can be produced that will almost never vaporize at temperatures moderately above the boiling point of the bulk fluid [4]. These "superheated" droplets are then subject to sudden vaporization when perturbed by any number of forces including ultrasound. In fact, a previously considered ultrasound contrast agent used this mechanism to store small droplets that could then be activated mechanically to produce the gas bubble [5]. Superheated perfluorocarbon droplets have also been used as radiation detectors [6] and medical applications using local vaporization have recently been investigated more extensively [7]. The conditions under which Acoustic Droplet Vaporization (ADV) can be achieved have also been studied [8, 9] but the exact mechanisms that lead to the bubble formation are not yet known. Some interesting potential applications of ADV may lead to effective uses in ultrasound therapy and diagnosis. A few of these will be explored here.

DROPLET FORMULATION

Perfluorocarbon droplets can be formulated in much the same way as ultrasound contrast agents using shell materials such as albumin or lipids. The shells provide a means to prevent coalescence of the droplets and the surface tension at the droplets interface is likely affected by the presence of the shell materials. A droplets emulsion using an albumin shell can be produced following previously described methods [7], in which dodecafluoropentane (DDFP, C_5F_{12}, with a boiling point of 29ºC) is mixed in an albumin-saline solution and shaken at high speed. The resulting size distribution is shown in Figure 1. These droplets remain stable in storage for several weeks and can be superheated to as much as 60ºC if otherwise unperturbed. However, relatively low amplitude ultrasound will cause the droplets to vaporize at 37ºC, which makes them suitable for *in vivo*

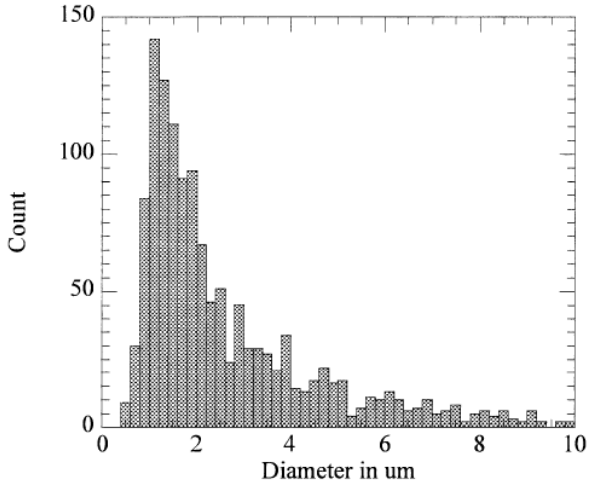

Figure 1 - Size distribution of DDFP droplets produced with an albumin shell to prevent coalescence. [From reference 7]

applications. Droplet produced with albumin or other shells have the potential to be targeted in the same fashion as ultrasound contrast agents. This substantially increases the potential utility of these agents, particularly if they can be made sufficiently small to escape the vascular system. These areas are currently being further investigated.

ACOUSTIC DROPLET VAPORIZATION (ADV)

The application of ultrasound to cause vaporization of the droplet (ADV) can be studied in a variety of environments. We have examined ADV in tubes with flowing and static fluid [8] where the latter of these methods allowed for the observation of the individual droplet vaporizations. For ADV in saline, the requisite rarefactional pressure at 7.6 MHz using a 5-cycle tone burst and a PRF of 5 kHz is only 0.7 MPa. This relatively low threshold allows for ADV, *in vivo* [8]. In addition, others have measured the threshold for ADV [9] using different acoustic parameters and also found the threshold for droplet vaporization to be quite low. The mechanism for vaporization in each case is not yet verified but some high-speed photography of the process has revealed some interesting effects on the droplets. Since ADV occurs at a micron scale, an optical microscope (JenaVAL, Carl Zeiss Jena GmbH, Jena, Germany) must be connected to a high-speed video system to record the process. An Imacon 468 high-speed video system (DRS Technologies, DRS Hadland, Inc. Cupertino, CA, USA) was used. Full-frame pictures were taken with frame rates of 5-10 MHz. In streak mode, a vertical central line of an image was captured at 57.6 MHz. In this case, the droplets were suspended in a polyethylene tube (200 um inner diameter, 50 um wall thickness) containing saline.

Figure 2 shows the effects of the acoustic field on an individual droplet. These photographs show a droplet undergoing ADV. In the final frame of the eight frame sequence is the streak image that follows the central line through the droplet. Figure 3 is a magnified view of a streak image for a droplet before ADV occurs. Note that the droplet is oscillating in a dipole fashion here. An oscillation of this mode would be enhanced at higher frequencies as the droplet becomes larger in comparison to the ultrasound wavelenth. This could explain the inverse frequency behavior seen in earlier experiments [7-8].

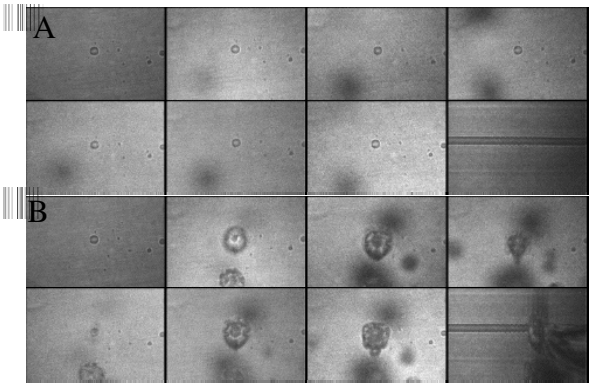

Figure 2 - Acoustic vaporization of an 18 μm diameter droplet. Two sequences are shown. (A) Images 1 to 7 are full frame pictures of the droplet in the tube. The 8th frame is a streak image. The acoustic pressure in the first sequence is not sufficient to vaporize the droplet. In the center of the streak image, one can see a translatory motion of the droplet for the duration of the 10 cycle, 3 MHz tone burst. (B) Increasing the acoustic pressure to 6.5 MPa peak-peak (which is P-=2.6 MPa) leads to the vaporization of the droplet after 8 cycles.

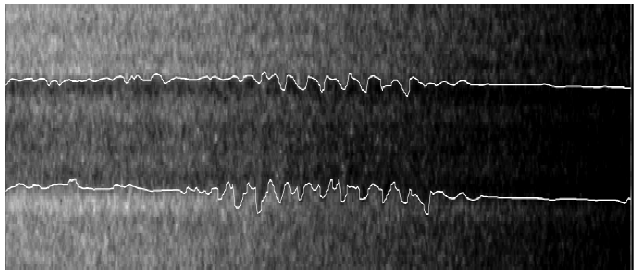

Figure 3 - Expanded view of the eighth frame in Fig. 2A. Hand-traced streak line of a 16 um diameter droplet. One can see the onset of oscillation at the bottom trace, before onset occurs in the top trace.

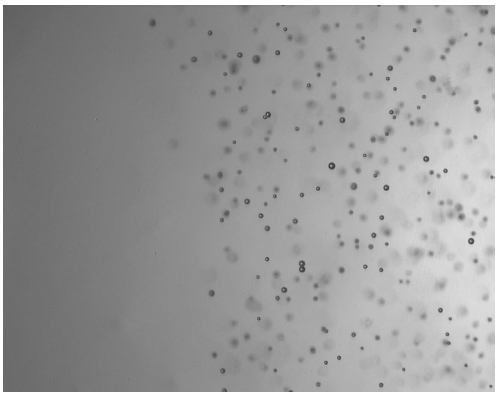

Figure 4 - Acrylamide gel blocks containing high concentration of perfluorocarbon droplets. Right side of gel exposed to 10 MHz linear array, MI 1.2, resulting in ADV and microbubble formation. 4.5 x 3.5 mm.

We have also suspended the droplets in acrylamide gels to determine the influence of the gel matrix and the effects of re-condensation [10]. The gels were made from 15%, 10%, and 6% concentrations of bis-acrylamide (BA). All chemicals are from Sigma Chemicals (St. Louis, MO); solutions are by volume. The pre-gelled solution was poured into a mold and degassed in a vacuum chamber. Next, the DDFP droplets were added to the solution (from a stock solution of 10^7 droplets per ml [8]), followed by the two cross-linking agents TEMED and APS at concentrations of 1 and 5 µl of each per ml gel.

When the droplets are placed in the acrylamide gel, ADV is still effective in producing bubbles. Figure 4 shows the result of exposing only half the gel to ultrasound. The resulting gas bubbles are seen on the exposed right side. When subsequently refrigerated these gas bubbles disappear and can then be reformed later by warming the gel back to room temperature and exposing to ultrasound. The process may not be completely reversable depending on the duration of time the DDFP bubbles are present. The bubbles begin as pure DDFP but the constituent gases of air will diffuse into the bubble over time and the DDFP diffuses more slowly into the gel. This results in an increased bubble size over that associated with just the volume of DDFP. In addition, depending on stiffness, the gel may structurally fail and the resulting bubble may not be spherical at the first or later vaporization cycles. However, if the bubble remains small compared to the wavelength such shape variations may not be critical to its uses such as providing a point target for aberation corrections and evaluation of ultrasound system point response function.

IN VIVO OBSERVATIONS OF ADV

The important aspect of the ADV process is that it can be achieved *in vivo*. In a series of initial animal studies [8], we demonstrated that ADV was possible and that the bubbles produced persisted for >30 minutes. Subsequently, more detailed investigations with high concentrations have measured the actual level of vascular occlusion. (All procedures were approved by our university committee for use and care of animals.) The target organ for occlusion was the kidney in rabbit. To create a water path to the target tissue, the left kidney was externalized and a water bath made from a section of PVC tubing (5 cm tall and 12 cm diameter) was positioned over the externalized kidney and glued to the skin using medical adhesive. A mechanical arm held a focused phased array imager and a single PZT element with a 3.5 MHz center frequency, 25.4 mm aperture, and 37.5 mm

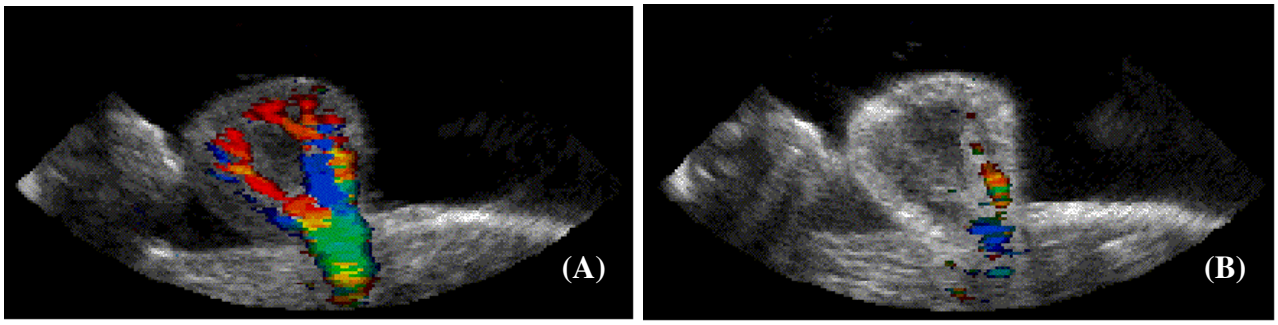

Figure 5 - Color flow mode of the kidney before and after ADV. One can see the renal artery as it enters the organ and branches through the medullary tissue to the capillaries of the cortex.

focal length (A381S, Panametrics, Waltham, MA). The single element transducer was driven with a pulse duration of 13 cycles at 3.5 MHz and the pulse repetition interval was 1 ms. Acoustic pressures were at least 2 MPa peak negative, which provided the requisite acoustic field for vaporization. The injected droplet emulsion was made in our laboratory as previously published [7-8] but with lepus albumin instead of bovine albumin to eliminate systemic reactions. To ensure the emulsion was transpulmonary, it was also filtered using a set of four membrane filter discs (25, 16, 8, and 5 μm in that order, cat numbers: 1441 325, 1443 055, 1440 042, 1106 13, Whatman, Kent, United Kingdom) which were placed back to back. Droplets were injected at a rate of 1 mL/min.

The occlusion of tissue *in vivo* was demonstrated both by changes in Doppler ultrasound images in the rabbit kidney (Figure 5) or use of a standard microsphere method to measure actual perfusion changes (Figure 6). In either case, microbubble formation in the renal artery by ADV caused a dramatic change in blood flow as would be expected from these larger gas bubbles.

The individual bubbles are easily seen in ultrasound imaging and should also act as point targets for aberration correction if produced in low number density. Theoretical investigations of the scattering from such bubbles indicate that bubbles as large as 40 micron diameter still provide a nominally spherical angular scattering pattern at frequencies up to 12 MHz and f No.'s as low as 1.

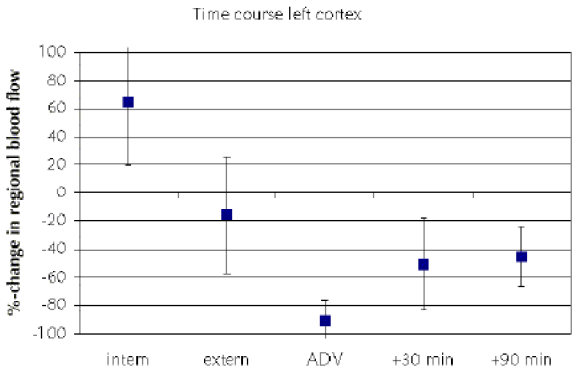

Figure 6 - The %-change of blood flow in the kidney cortex is shown for externalizing the kidney, for ADV treatment, and for blood flow recovery after ADV. Externalization of the left kidney caused a drop in blood flow in both kidneys. After treatment with ADV to cause occlusion, the left/external kidney showed a drop in blood flow, from which it mostly recovered 90 minutes after the treatment.

CONCLUSIONS

Perfluorocarbon droplets can be produced that are superheated at body temperature and can be vaporized by the application of ultrasound. There are a number of potential applications for such droplets including tissue occlusion and use as targets to correct aberrations caused by overlying tissue. Each of these could have a significant impact on therapeutic ultrasound.

ACKNOWLEDGEMENTS

Research supported in part by PHS grant EB00281 and US Army Grant No. DAMD17-00-1-0344. Special thanks to Kimberly Ives, DVM for her assistance in animal research.

REFERENCES

[1]Psychoudakis D, et al. , Microbubbles as Point Targets for Phase Aberration Correction, AIUM 46th Annual Convention, Nashville, March 10-13, J. Ultras. Med., 21, S21, 2002

[2] Mattrey RF, et al., Perfluoroctylbromide:a liver/spleen-specific and tumor-imaging ultrasound contrast material. Radiology, 145, 759-62, 1982.

[3] Lanza GW, et al., A novel site-targeted ultrasonic contrast agent with broad biomedical application Circulation, 94, 3334-40, 1996.

[4] Apfel RE, Activatable infusable dispersions containing drops of a superheated liquid for methods of therapy and diagnosisUS Patent 5,840,276, 1998.

[5] Correas JM and Quay SC, EchoGen Emulsion: a new ultrasound contrast agent based on phase shift colloids, Clin Radiol, 51 (S1), 11-14, 1996.

[6] Apfel RE and Lo YC, Practical neutron dosimetry with superheated drops. Health Phys, 56, 79-83, 1989.

[7]Kripfgans OD, et al., Generation and vaporization of Micrometer-Sized Droplets for therapeutic and diagnostic applications: Preliminary results, Ultrasound Med. Biol., 26 (7), 1177-1189, 2000.

[8]Kripfgans OD, et al., *In vivo* droplet vaporization for occlusion therapy and phase aberration correction, IEEE Trans. Ultras. Ferroel. Frequency Control, 49/6, 726-738, 2002

[9] Giesecke T and Hynynen K, Ultrasound-mediated cavitation thresholds of liquid perfluorocarbon droplets *in vitro*, Ultras Med Biol, 29, 1359-65, 2003.

[10] Orifici, et al., An ultrasound test object utilizing acoustic droplet vaporization (ADV) to produce distributed point target scatterers Med Phys, 29, 1292-2, 2002.